Published by Institute of Physics Publishing for SISSA

Received: *May 15, 2007*
Revised: *September 14, 2007*
Accepted: *September 25, 2007*
Published: *October 22, 2007*

Wilson loops in 2D noncommutative euclidean gauge theory: 2. $1/\theta$ expansion

Jan Ambjørn,[ac] **Andrei Dubin**[b] **and Yuri Makeenko**[ab]

[a] *The Niels Bohr Institute, Blegdamsvej 17, 2100 Copenhagen Ø, Denmark*
[b] *Institute of Theoretical and Experimental Physics, B. Cheremushkinskaya 25, 117259 Moscow, Russia*
[c] *Institute for Theoretical Physics, Utrecht University, Leuvenlaan 4, NL-3584 CE Utrecht, The Netherlands*
E-mail: ambjorn@nbi.dk, dubin@itep.ru, makeenko@itep.ru

Abstract: We analyze the $1/\theta$ and $1/N$ expansions of the Wilson loop averages $< W(C) >_{U_\theta(N)}$ in the two-dimensional noncommutative $U_\theta(N)$ gauge theory with the parameter of noncommutativity θ. For a generic rectangular contour C, a concise integral representation is derived (non-perturbatively both in the coupling constant g^2 and in θ) for the next-to-leading term of the $1/N$ expansion. In turn, in the limit when θ is much larger than the area $A(C)$ of the surface bounded by C, the large θ asymptote of this representation is argued to yield the next-to-leading term of the $1/\theta$ series. For both of the expansions, the next-to-leading contribution exhibits only a *power-like* decay for areas $A(C) >> \sigma^{-1}$ (but $A(C) << \theta$) much larger than the inverse of the string tension σ defining the range of the exponential decay of the leading term. Consequently, for large θ, it hinders a direct stringy interpretation of the subleading terms of the $1/N$ expansion in the spirit of Gross-Taylor proposal for the $\theta = 0$ commutative $D = 2$ gauge theory.

Keywords: Nonperturbative Effects, 1/N Expansion, Field Theories in Lower Dimensions.

JHEP10(2007)079

Contents

1. Introduction

In short, given a commutative field theory defined in the Euclidean space $\mathbf{R}^D$ by the action $S = \int d^D x\ \mathcal{L}(\phi(x))$, the corresponding noncommutative theory is implemented replacing the products of the fields $\phi(\mathbf{x})$ by the so-called star-products introduced according to the rule[1]

$$(f_1 \star f_2)(\mathbf{x}) \equiv exp\left(-\frac{i}{2}\theta_{\mu\nu}\partial_\mu^y \partial_\nu^z\right)\ f_1(\mathbf{y})\ f_2(\mathbf{z})\Big|_{y=z=x}, \tag{1.1}$$

where the parameter of noncommutativity $\theta_{\mu\nu}$, entering the commutation relation $[x_\mu, x_\nu] = -i\theta_{\mu\nu}$ satisfied by D noncommuting coordinates, is real and antisymmetric. In particular, the action of the standard $D-$dimensional $U(N)$ Yang-Mills theory is superseded by

$$S = \frac{1}{4g^2}\int d^D x\ tr\left(\mathcal{F}_{\mu\nu}^2(\mathbf{x})\right) \quad ; \quad \mathcal{F}_{\mu\nu} = \partial_\mu \mathcal{A}_\nu + \partial_\nu \mathcal{A}_\mu - i(\mathcal{A}_\mu \star \mathcal{A}_\nu - \mathcal{A}_\nu \star \mathcal{A}_\mu), \tag{1.2}$$

where $\mathcal{A}_\mu \equiv \mathcal{A}_\mu^a t^a$ with $tr(t^a t^b) = \delta^{ab}$, and $\theta_{21} = -\theta_{12} = \theta$ in the $D = 2$ case in question.

The noncommutative two-dimensional $U_\theta(N)$ system (1.2) provides the simplest example of the noncommutative gauge theory. As well as in the $\theta = 0$ case, investigation of non-perturbative effects in a low-dimensional model is expected to prepare us for the analysis of a more complicated four-dimensional quantum dynamics. An incomplete list of papers, devoted to this direction of research, is presented in references [3]–[23].

The aim of the present work is to extend the perturbative analysis of our previous publication [14] and examine, non-perturbatively in the coupling constant g^2, the two

[1] For a review see [1, 2] and references therein.

alternative expansions of the Wilson loop-average $< W(C) >_{U_\theta(N)}$ in the $D = 2$ $U_\theta(N)$ theory on a plane. The first one is the $1/\theta$ series

$$< W(C) >_{U_\theta(N)} = \sum_{k=0}^{\infty} \theta^{-k} < \mathcal{W}(C) >_N^{(k)} \tag{1.3}$$

that is to be compared with the more familiar 't Hooft $1/N$ topological expansion

$$< W(C) >_{U_\theta(N)} = \sum_{G=0}^{\infty} N^{-2G} < W(C) >_{U_\theta(N)}^{(G)}, \tag{1.4}$$

where G can be identified with the genus of the auxiliary surface canonically associated with any given diagram of the weak-coupling series of the $N-$independent quantity $< W(C) >_{U_\theta(N)}^{(G)} = < W(C) >_{U_\theta(1)}^{(G)}$. Also, the contour C is always restricted to be closed.

The $\theta \to \infty$ limit of the $U_\theta(N)$ theory is known [24] to retain the same set of the planar diagrams (described by the same amplitudes) as the $N \to \infty$ limit does so that the leading terms of both of the above expansions coincide,

$$< W(C) >_{U_\theta(N)}^{(0)} = < \mathcal{W}(C) >_N^{(0)}, \tag{1.5}$$

provided the appropriate identification of the coupling constants. As the $G = 0$ term of eq. (1.4) is $\theta-$*independent*, it therefore reduces to the corresponding average in the commutative variant of the gauge theory. In consequence, the leading term of the series (1.3) reduces,

$$< \mathcal{W}(C) >_N^{(0)} = < W(C) >_{U(N)}^{(0)} \quad , \quad < \mathcal{W}(\Box) >_N^{(0)} = exp[-\sigma A(\Box)], \tag{1.6}$$

to $G = 0$ term of the $\theta = 0$ expansion (1.4) of the average $< W(C) >_{U(N)}$ in the ordinary commutative $U(N)$ gauge theory. In particular, it fits in the simple Nambu-Goto pattern for an arbitrary non-self-intersecting contour C.

In this paper, for an arbitrary rectangular contour $C = \Box$, we evaluate the next-to-leading term $< W(C) >_{U_\theta(1)}^{(1)} /N^2$ of the topological expansion (1.4) and argue that its large θ asymptote exactly reproduces,

$$< \mathcal{W}(C) >_N^{(2)} = \frac{1}{N^2} \lim_{\theta\to\infty} \theta^2 < W(C) >_{U_\theta(1)}^{(1)}, \tag{1.7}$$

the $k = 2$ term of the $1/\theta$ series (1.3) (while $< \mathcal{W}(C) >_N^{(1)} = 0$). The proof of the relation (1.7) will be presented in a separate publication [25]. As for the computation of $< \mathcal{W}(C) >_N^{(2)}$, for this purpose we perform a resummation of the genus-one diagrams for a generic $C = \Box$, that is facilitated by the choice of the axial gauge where, at the level of the $D = 2$ action (1.2), only tree-graphs (without self-interaction vertices) are left. Nevertheless, the problem remains to be nontrivial: due to the noncommutative implementation [26]–[35] of the Wilson loop, an infinite number of different connected $G = 1$ diagrams contributes to the average $< W(C) >_{U_\theta(N)}$ even in the case of a non-self-intersecting contour C that is in contradistinction with the commutative case, where

$< W(\Box) >_{U(N)} = < W(\Box) >^{(0)}_{U(N)}$. To deal with this problem, we propose a specific method of resummation.

Application of the method allows to unambiguously split the whole set of the relevant perturbative $G = 1$ diagrams into the three subsets. Being parameterized by the two integer numbers r and v with $0 \leq r \leq v \leq 1$, each subset can be obtained starting with the corresponding protograph (with $2 + r - v$ lines) and then dressing it through the addition of extra lines in compliance with certain algorithm. For a rectangle $C = \Box$, it yields an integral representation of the $G = 1$ term of the $1/N$ expansion in the form

$$< W(\Box) >^{(1)}_{U_\theta(1)} \;=\; \frac{1}{(2\pi\sigma\theta)^2} \sum_{0\leq r\leq v\leq 1} h_{rv} \mathcal{Z}_{rv}(\bar{A}, \bar{\theta}^{-1}) \,, \tag{1.8}$$

where $\mathcal{Z}_{rv}(\bar{A}, \bar{\theta}^{-1})$ denotes the effective amplitude which, after multiplication by the factor $h_{rv} = 2 + r - v$ separated for a later convenience, accumulates the entire $rv-$subset of the perturbative amplitudes. Besides a dependence on $\bar{\theta} = \sigma\theta$, $\mathcal{Z}_{rv}(\cdot)$ depends only on the dimensionless area $\bar{A} = \sigma RT$ of $C = \Box$ rather than separately on the lengths T and R of the temporal and spatial sides of $\Box$.

Correspondingly, in the large θ limit,

$$\theta >> A(C) \,, \tag{1.9}$$

the $N = 1$ relation (1.7) can be rewritten as

$$< \mathcal{W}(\Box) >^{(2)}_{1} = \frac{1}{(2\pi\sigma)^2} \sum_{0\leq r\leq v\leq 1} h_{rv} \mathcal{Z}_{rv}(\bar{A}, 0) \,, \tag{1.10}$$

where $\mathcal{Z}_{rv}(\bar{A}, 0)$ is obtained from $\mathcal{Z}_{rv}(\bar{A}, \bar{\theta}^{-1})$ (which, as a multiple integral, is *continuous* in $\bar{\theta}^{-1}$ in a vicinity of $\bar{\theta}^{-1} = 0$) simply replacing[2] $\bar{\theta}^{-1}$ by zero in the corresponding integrand. Then, performing the Laplace transformation with respect to $\bar{A}$, the image $\tilde{\mathcal{Z}}_{rv}(\beta, 0)$ of the large θ asymptote $\mathcal{Z}_{rv}(\bar{A}, 0)$ assumes the concise form

$$\tilde{\mathcal{Z}}_{rv}(\beta, 0) = \frac{1}{(\beta+1)^2} \int\limits_{-\infty}^{+\infty} d\bar{\zeta} d\bar{\eta} \; \frac{\mathcal{K}_{rv}(\bar{\zeta}, \bar{\eta})}{(\beta + |1 - \bar{\zeta}|)^{h_{rv}-1} \; (\beta + |1 + \bar{\eta}|) \; (\beta + |1 + \bar{\eta} - \bar{\zeta}|)} \,, \tag{1.11}$$

where

$$\mathcal{K}_{rv}(\bar{\zeta}, \bar{\eta}) = \sum_{e_3=-r}^{0} \sum_{e_1=-1}^{v-r} \sum_{e_2=v}^{1} (-1)^{v+\sum_{k=1}^{3} e_k} \; 2^{(v-r)(1-|e_1|)} |e_1 + \bar{\zeta}| \; |e_2 + \bar{\eta}|^{1-v} \; |e_3 + \bar{\zeta}|^r \;. \tag{1.12}$$

The integral representation (1.11) is the main result of the paper.

Building on the latter representation, one concludes that the pattern of the $\theta \neq 0$ expansion (1.4) shows, especially in the limit (1.9), a number of features which are in sharp

[2]The peculiarity of this replacement is that it can *not* be applied directly to the perturbative amplitudes describing individual Feynman diagrams. It matches the observation [14] that the large θ asymptote of the leading perturbative contribution to $< W(C) >^{(1)}_{U_\theta(1)}$ scales as θ^0 rather than as θ^{-2}. In turn, it implies a non-triviality of the relation (1.7).

contrast with the $1/N$ expansion of the average in the $\theta = 0$ case. Indeed, in the latter case, the Nambu-Goto pattern (1.6) provides the exact result $< W(\Box) >_{U(N)} = < W(\Box) >^{(0)}_{U(N)}$ for an arbitrary non-self-intersecting loop C, and the corresponding subleading terms are vanishing: $< W(C) >^{(G)}_{U(N)} = 0$ for $G \geq 1$. Furthermore, for self-intersecting contours C, nonvanishing subleading $G \geq 1$ terms $< W(C) >^{(G)}_{U(N)}$ all possess [36] the area-law asymptote like in eq. (1.6) in the limit $\bar{A} \to \infty$.

When $\theta \neq 0$, even for a rectangular loop C, the pattern of $< W(C) >_{U_\theta(N)}$ is characterized by an infinite $1/N-$series, each $G \geq 1$ term of which nontrivially depends both on $\bar{\theta}$ and on $\bar{A}(C)$. In addition, we present simple arguments that, in contradistinction with eq. (1.6), the asymptote (1.10) of the next-to-leading term exhibits a power-like (rather than exponential) decay for areas $\sigma^{-1} << A(\Box) << \theta$ much larger than the string tension σ. This asymptote is evaluated in [25] with the result

$$\frac{1}{N^2} < W(\Box) >^{(1)}_{U_\theta(1)} \quad \longrightarrow \quad \frac{4}{\pi^2 \left(\sigma\theta N\right)^2} \, \frac{ln(\sigma A)}{\sigma A} \quad , \qquad \sigma\theta, \, \sigma A \, \longrightarrow \, \infty \, , \tag{1.13}$$

that can be traced back to the (infinite, in the limit $\theta \to \infty$) *nonlocality* of the star-product (1.1) emphasized in the discussion [37] of the UV/IR mixing. Due to the generality of the reasoning, all the subleading $G \geq 1$ coefficients $< W(C) >^{(G)}_{U_\theta(1)}$ are as well expected to show, irrespectively of the form of C, a power-like decay for $\sigma^{-1} << A(C) << \theta$. In particular, it precludes a straightforward stringy interpretation of the subleading terms of the expansion (1.4) in the spirit of Gross-Taylor proposal [38] for the $\theta = 0$ commutative $D = 2$ gauge theory.

In section 2, we put forward a concise form (2.10) of the perturbative $2n-$point functions, the loop-average $< W(C) >_{U_\theta(1)}$ is composed of in the $D = 2$ $U(1)$ theory (1.2). In section 3, it is sketched how these functions are modified under the two auxiliary (genus-preserving) deformations of a given diagram to be used for the derivation of the decomposition (1.8). To put the deformations into action, we also introduce a finite number of the judiciously selected elementary genus-one graphs so that any remaining non-elementary $G = 1$ perturbative diagram can be obtained through appropriate multiple application of the above deformations to one of thus selected elementary graphs. In section 4, we propose the $\gamma jrv-$parameterization of the latter graphs and discuss how they can be collected into certain subsets associated with the corresponding protographs. In turn, being parameterized by the $rv-$assignment, the protographs are obtained from the elementary graphs through elimination of some of their lines.

When a particular elementary diagram with a given $\gamma jrv-$assignment is dressed by all its admissible deformations, the corresponding perturbative $2n-$point function is replaced by the effective one endowed with the same assignment. As it is shown in section 5, the replacement is implemented in such a way that certain $n-v$ propagators of the elementary diagram are superseded by their effective counterparts (5.6). The integral representation of the effective $2n-$point functions, is completed in section 6.

In section 7, we express the $G = 1$ term $< W(\Box) >^{(1)}_{U_\theta(1)}$ of the expansion (1.4) as a superposition of the effective amplitudes (7.1) that are obtained when the arguments of the

effective $2n-$point functions are integrated over the rectangle $C = \Box$. The effective amplitudes can be collected into the three $rv-$superpositions $\mathcal{Z}_{rv}(\bar{A}, \bar{\theta}^{-1})$ associated with the corresponding protographs parameterizing the decomposition (1.8). The explicit expression (7.7) for $\mathcal{Z}_{rv}(\cdot)$ is then derived. It is observed that, for a fixed $rv-$specification, this expression can be deduced directly through the appropriate dressing of the $rv-$protograph. The derivation of the large θ representation (1.11) is sketched in section 8. Conclusions, a brief discussion of the perspectives, and implications for $D = 3, 4$ gauge theory (1.2) are sketched in section 9. Finally, the appendices contain technical details used in the main text.

2. Generalities of the perturbative expansion

Building on the integral representation of the $U_\theta(1)$ average, we begin with a sketch of the derivation of the relevant perturbative $2n-$point functions.

2.1 Average of the noncommutative Wilson loop

To this aim, consider the perturbative expansion of the average of the noncommutative Wilson loop [26]

$$W(C) = \mathcal{P} e_\star^{\,i \oint_C dx_\mu(s) \mathcal{A}_\mu(\mathbf{x}(s))} \,. \tag{2.1}$$

in the $U_\theta(N)$ noncommutative gauge theory on the 2D plane $\mathbb{R}^2$. For this purpose, it is sufficient to use the path-integral representation [14] of the $U_\theta(1)$ average

$$< W(C) >_{U_\theta(1)} = \left\langle exp\left(-\frac{1}{2} \oint_C dx_\mu(s) \oint_C dx_\nu(s') D_{\mu\nu}(\mathbf{x}(s) - \mathbf{x}(s') + \xi(s) - \xi(s')) \right) \right\rangle_{\xi(\tilde{s})} , \tag{2.2}$$

as it follows from the $N-$independence of the quantities $< W(C) >^{(G)}_{U_\theta(N)}$ which are, therefore, replaced by $< W(C) >^{(G)}_{U_\theta(1)}$ in eq. (1.4). In eq. (2.2), $D_{\mu\nu}(\mathbf{z})$ is the standard $D = 2$ photon's propagator in the axial gauge $\mathcal{A}_1 = 0$,

$$D_{\mu\nu}(\mathbf{z}) = < \mathcal{A}_\mu(\mathbf{z}) \mathcal{A}_\nu(\mathbf{0}) >_{U(1)} = -\frac{g^2}{2} \, \delta_{\mu 2} \delta_{\nu 2} \, |z_1| \, \delta(z_2) \,, \tag{2.3}$$

and the functional averaging over the auxiliary $\xi_\mu(s)$ field (parameterized by the proper time $s \in [0, 1]$ chosen to run clockwise starting with the left lower corner of $C = \Box$) is to be performed according to the prescription

$$\left\langle \mathcal{B}[\xi(s)] \right\rangle_{\xi(\tilde{s})} = \int \mathcal{D}\xi_\mu(s) \; e^{\frac{i}{2}(\theta^{-1})_{\mu\nu} \int ds ds' \xi^\mu(s) G^{-1}(s,s') \xi^\nu(s')} \; \mathcal{B}[\xi(s)] \,. \tag{2.4}$$

Here, $\mathcal{D}\xi_\mu(s)$ denotes the standard flat measure so that $< \xi^\mu(s) \xi^\nu(s') >= i\theta^{\mu\nu} \mathrm{sign}\,(s - s')/2$, where, prior to the regularization, we are to identify $G^{-1}(s, s') = \dot{\delta}(s - s')$.

Let us also note that eq. (2.4) is based on the integral representation

$$exp\left(-\frac{i}{2} \, \theta_{\mu\nu} \partial^{\mathbf{x}}_\mu \partial^{\mathbf{y}}_\nu \right) f_1(\mathbf{x}) \; f_2(\mathbf{y}) = \int e^{2i(\theta^{-1})_{\mu\nu} \xi_1^\mu \xi_2^\nu} f_1(\mathbf{x} + \xi_1) f_2(\mathbf{y} + \xi_2) \; \prod_{j=1}^{2} \frac{d^2 \xi_j^\mu}{w(\theta)} \tag{2.5}$$

of the star-product (1.1), where $w(\theta) = (\pi^2|\det\theta|)^{1/2}$. In consequence, the noncommutative Wilson loop (2.1) itself can be represented as [27],

$$W(C) = \left\langle exp\left(i \oint\limits_C dx_\mu(s) \mathcal{A}_\mu(\mathbf{x}(s) + \xi(s)) \right) \right\rangle_{\xi(\bar{s})} . \tag{2.6}$$

Finally, the coupling g^2 of the $U_\theta(N)$ noncommutative gauge theory is related to the string tension σ, entering eq. (1.6), by the formula

$$\sigma = g^2_{U_\theta(N)} N/2 \, . \tag{2.7}$$

2.2 Perturbative θ-dependent $2n-$point functions

Take any given nth order diagram of the weak-coupling expansion of the average (2.2) that, being applied to the $1/N$ series (1.4) can be rewritten in the form

$$< W(C) >^{(G)}_{U_\theta(N)} = \sum_{n=0}^{\infty} \lambda^{2n} \; < W(C) >^{(G,n)}_{U_\theta(N)} \tag{2.8}$$

with $\lambda = g^2 N$. For a particular $n \geq 2G$, $< W(C) >^{(G,n)}_{U_\theta(N)}$ is given by the multiple contour integral of the ξ-average applied to the corresponding product of n ξ-dependent propagators $D_{\mu\nu}(\mathbf{y}_l + \xi(s_l) - \xi(s'_l))$, where

$$\mathbf{y}_l = \mathbf{x}(s_l) - \mathbf{x}(s'_l) \, , \tag{2.9}$$

with $l = 1, 2, \ldots, n$, and $\mathbf{y}_l = (y^1_l, y^2_l)$, while y^1_l and y^2_l are associated with the vertical and horizontal axis respectively. Then, any diagram can be topologically visualized as the collection of the *oriented* (according to the proper-time parameterization) lines so that the qth propagator-line starts at a given point $\mathbf{x}(s'_q) \in C$ and terminates at the corresponding $\mathbf{x}(s_q) \in C$. When the ξ-averaging of the product is performed, the perturbative $2n-$point function can be rewritten [14] in the form

$$V^{(n)}_{U_\theta(1)}(\mathbf{y}_1, \ldots, \mathbf{y}_n) = o_n \prod_{1 \leq l < j}^{n} exp\left(\frac{i}{2} \, \mathcal{C}_{lj} \breve{\theta}_{\mu\nu} \partial^{\mathbf{z}_l}_\mu \partial^{\mathbf{z}_j}_\nu \right) D_{22}(\mathbf{z}_1) \; D_{22}(\mathbf{z}_2) \; \ldots \; D_{22}(\mathbf{z}_n)\Big|_{\{\mathbf{z}_k = \mathbf{y}_k\}} , \tag{2.10}$$

where[3] $o_n = (-1/2)^n/n!$, and the *intersection* matrix $\mathcal{C}_{lj} = -\mathcal{C}_{jl}$, being defined algebraically as

$$\mathcal{C}_{lj} = \frac{1}{2} \left(sign(s_l - s_j) + sign(s'_l - s'_j) - sign(s_l - s'_j) - sign(s'_l - s_j) \right) , \tag{2.11}$$

[3] In the computation of any $2n$th order perturbative diagram, the factor o_n disappears. The subfactor 2^{-n} is exactly cancelled by the symmetry factor responsible for the interchange of two different end-points of each of the n lines. By the same token, the subfactor factor $1/n!$ is precisely cancelled by the symmetry factor corresponding to all possible permutations of the n different (non-oriented) lines. Finally, $(-1)^{-n}$ is to be combined with the implicit factor $(-1)^{-n}$ that arises when one pulls the minus sign out of each propagator (2.3) entering $V^{(n)}_{U_\theta(1)}(\cdot)$.

counts the number of times the lth oriented line crosses over the jth oriented line (and, without loss of generality, we presume that $s_l \geq s'_l$ for $\forall l$). As for the relevant noncommutative parameter $\breve{\theta}_{\mu\nu}$, it is *twice* larger

$$\breve{\theta}_{\mu\nu} = 2\theta_{\mu\nu} \,, \tag{2.12}$$

compared to the parameter $\theta_{\mu\nu}$ defining the original star-product (1.1). Being rewritten in the momentum space, eq. (2.10) implies that, compared to the commutative case, a given $\theta \neq 0$ perturbative $2n-$point function is assigned with the extra $\theta-$dependent factor

$$\left\langle \prod_{k=1}^{n} e^{i\mathbf{p}_k\cdot(\xi(s_k)-\xi(s'_k))} \right\rangle_{\xi(\tilde{s})} = exp\left(-i \sum_{l<j} \mathcal{C}_{lj}\ \theta_{\mu\nu}\ p_l^{\mu}\ p_j^{\nu} \right) \,. \tag{2.13}$$

where the momentum $\mathbf{p}_l$ is canonically conjugated to the lth coordinate (2.9). In turn, the r.h. side of eq. (2.13) reproduces the existing formula [24, 37] obtained in the analysis of the partition function in the noncommutative field-theories.

Finally, the pattern of eqs. (2.13) and (2.11) suggests the natural definition of (dis)connected diagrams. Algebraically, a particular nth order graph is to be viewed as disconnected in the case when the associated $n \times n$ matrix $\mathcal{C}_{lj}$ assumes a *block-diagonal* form $\mathcal{C}_{lj} = \otimes_k \mathcal{C}^{(k)}_{l_k j_k}$, with $\sum_k n_k = n$, so that the nonvanishing entries of $\mathcal{C}_{lj}$ are reproduced exclusively by smaller $n_k \times n_k$ matrices $\mathcal{C}^{(k)}_{l_k j_k}$, where $n_k < n$ for $\forall k$. Conversely, when a nontrivial implementation of this decomposition of a particular $\mathcal{C}_{lj}$ is impossible, the corresponding diagram is called connected. As the rank $r[\mathcal{C}] = 2G(\{\mathbf{y}_l\})$ of the matrix $\mathcal{C}_{ij}$ is known to be equal to the doubled genus $G(\{\mathbf{y}_l\})$ of the diagram, one expects that the order n of a connected genus G graph complies with the inequality $n(\{\mathbf{y}_l\}) \geq 2G(\{\mathbf{y}_l\})$.

3. The two deformations and the irreducible diagrams

The aim of this section is to present the central elements of the exact resummation[4] of the weak-coupling series applied to the noncommutative Wilson loop average that, in turn, leads to the decomposition (1.8) introducing the parameters r and v. For this purpose, observe first that the complexity of the perturbative expansion of the considered average roots in the complexity of the perturbative $2n-$point functions (2.10) associated with the connected graphs (of an arbitrary large order) discussed in the end of the previous section. For a connected graph of order $m \geq 2G$, the $2m-$point function (2.10) can be expressed in the simplest cases as an irreducible star-product $f_1 \star f_2 \star \ldots \star f_m$ of multiplicity m, where the quantities $f_k(\cdot)$ are composed of the propagators (2.3). (In general, the pattern of the connected $2n-$point function can be deduced according to the prescription discussed in the beginning of subsection 3.3.) In particular, it can be shown that $2 \leq m \leq 3$ for $G = 1$, while eq. (2.10) for a generic $G = 1$ diagram can be represented in the form of an ordinary product of a single mth order star-product (or its generalization in the sense of the latter prescription) and a number of the propagators (2.3).

[4]The details of this resummation procedure will be published elsewhere.

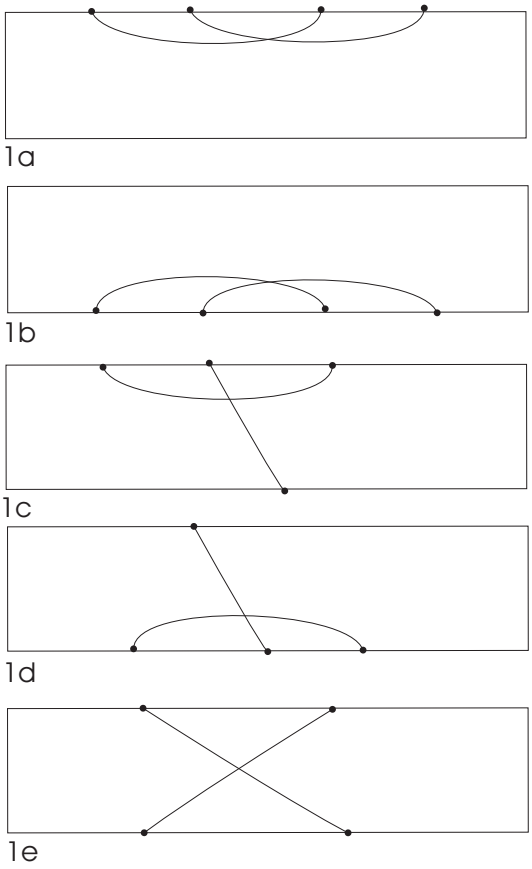

Figure 1: Connected $\mathcal{R}_a \times \mathcal{R}_b-$irreducible $n = 2$ diagrams.

To put this representation into use, we introduce the two *genus-preserving* deformations of any given diagram which are called $\mathcal{R}_a^{-1}-$ and $\bar{\mathcal{R}}_b^{-1}-$deformations. Increasing the order n of a $G \geq 1$ graph by one, they relate the corresponding pairs of functions (2.10) in a way that does *not* change the multiplicities of the irreducible star-products involved. Correspondingly, with respect to the inverse $\mathcal{R}_a-$ and $\bar{\mathcal{R}}_b-$deformations, one introduces $\mathcal{R}_a \otimes \bar{\mathcal{R}}_b-$irreducible Feynman diagrams.

The effectiveness of the construction is that nonvanishing functions (2.10) are associated only with the *finite* number of the irreducible diagrams depicted[5] in figures 1, 2, 7a, and 7e (which are postulated to fix the *topology* of the attachment of the lines' endpoints to the upper and lower horizontal sides of $C = \square$). Then, by construction, the $\bar{\mathcal{R}}_b^{-1}-$deformations does not change the number of connected components of a given irreducible diagram and may be applied separately to each line of the diagram. In consequence, the complete set of the *connected* genus-one diagrams can be generated applying all possible $\bar{\mathcal{R}}_b^{-1}-$deformations to all m lines of these $\mathcal{R}_a \otimes \bar{\mathcal{R}}_b-$irreducible diagrams. Given thus obtained set, the subsequent application of the $\mathcal{R}_a^{-1}-$deformations reproduces all the re-

[5]Actually, the diagrams in the figures 2a and 2b are irrelevant for the analysis as well.

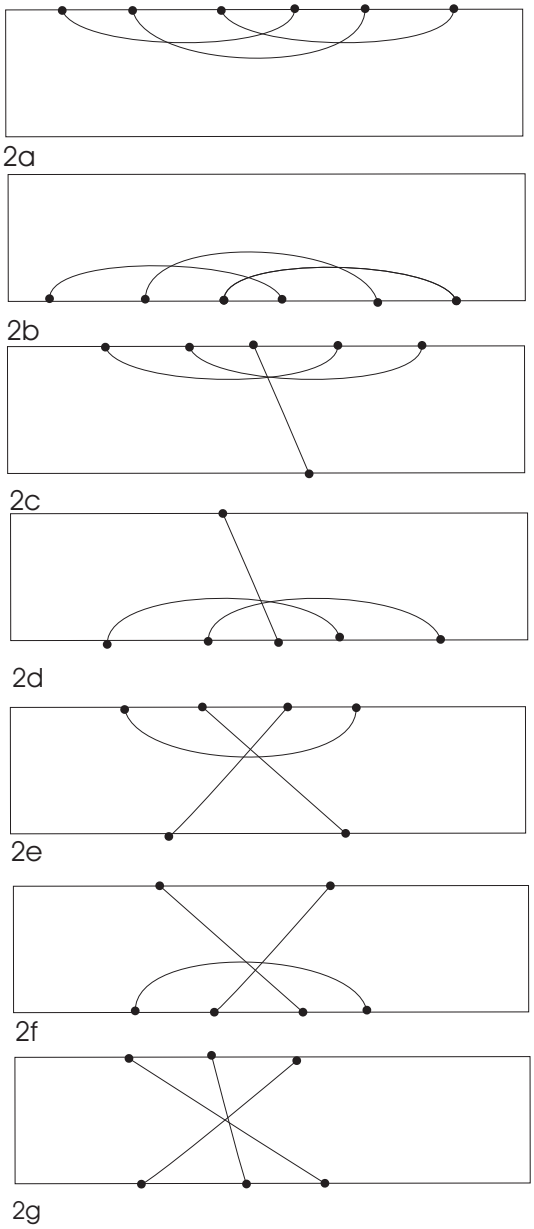

Figure 2: Connected $\mathcal{R}_a \times \mathcal{R}_b-$irreducible $n = 3$ diagrams.

maining disconnected $G = 1$ diagrams. In short, a composition of multiple $\mathcal{R}_a^{-1}-$ and $\bar{\mathcal{R}}_b^{-1}-$deformations, associated with some lines of an irreducible graph, is denoted as a $\mathcal{R}_a^{-1} \otimes \bar{\mathcal{R}}_b^{-1}-$deformation of this graph. Conversely, with any given a reducible graph, one can associate the corresponding irreducible diagram.

In the end of the section, we also discuss a reason for a further refinement of the resummation algorithm implemented via certain dressing of the lines of the so-called elementary (rather than irreducible) diagrams. The advantage of the refined algorithm is that, for any of the dressed lines of the a given elementary diagram, (in the relevant amplitude)

one merely *replaces* the perturbative propagator by a concise effective propagator to be introduced in subsection 5.3. In this way, the entire set of the genus-one Feynman diagrams (generated by the perturbative expansion of the average (2.2)) can be unambiguously decomposed into a finite number of subsets parameterized by the corresponding elementary graphs. In turn, each subset is described by the associated effective $2n-$point function that, therefore, accumulates the overall admissible $\mathcal{R}_a^{-1} \otimes \bar{\mathcal{R}}_b^{-1}-$dressing of the elementary $G = 1$ graph.

3.1 The $\mathcal{R}_a^{-1}-$deformations

After the $\mathcal{R}_a^{-1}-$deformation, a given elementary graph is modified by an addition of an extra ith propagator-line that does not intersect[6] any line in the original $\{k\}$-set of the elementary diagram:

$$\mathcal{C}_{ik} = 0 \qquad , \qquad \forall k \neq i \ . \tag{3.1}$$

Starting with a given $2n-$point function $V^{(n)}_{U_\theta(1)}(\cdot)$ and identifying $i = n+1$, one readily obtains that, modulo the numerical constant, the considered deformation of $V^{(n)}_{U_\theta(1)}(\cdot)$ merely multiplies it by the extra propagator,

$$V^{(n+1)}_{U_\theta(1)}(\mathbf{y}_1, \ldots, \mathbf{y}_n, \mathbf{y}_{n+1}) = -\frac{1}{2(n+1)} \ V^{(n)}_{U_\theta(1)}(\mathbf{y}_1, \ldots, \mathbf{y}_n) \ D_{22}(\mathbf{y}_{n+1}) \ . \tag{3.2}$$

Correspondingly, one defines the inverse of the $\mathcal{R}_a^{-1}-$deformation as the $\mathcal{R}_a-$deformation which eliminates such an ith line of a ($\mathcal{R}_a-$reducible) diagram that complies with eq. (3.1) for some k. In the absence of such a line (for any k), the graph is called $\mathcal{R}_a-$irreducible. Note that any connected diagram is necessarily $\mathcal{R}_a-$irreducible.

Concerning an $m-$fold application of the $\mathcal{R}_a^{-1}-$deformation, the corresponding generalization of eq. (3.2) is routine: the single factor $-D_{22}(\mathbf{y}_{n+1})/2(n+1)$ is replaced by the product $\prod_{k=1}^{m}(-1)D_{22}(\mathbf{y}_{n+k})/2(n+k)$. I.e., all of thus generated extra lines are assigned (as well as in the $\theta = 0$ commutative gauge theory) with the ordinary perturbative propagator (2.3). For example, a generic non-elementary $\mathcal{R}_a^{-1}-$deformation of the graph in figure 1a is described by the diagram in figure 3a. In the latter figure the additional lines are depicted by dotted straight lines. All these lines are necessarily vertical because the relative position of their end-points is characterized, owing to the pattern (2.3) of the propagator, by the vanishing relative times (associated with the horizontal 2−axis): $y^2_{n+k} = 0, \ \forall k \geq 1$. More generally, the vertical dotted lines in figures 5, 6, 8, and 9 are also generated by the admissible multiple $\mathcal{R}_a^{-1}-$deformations of the corresponding elementary graphs. Note also that, for a given elementary diagram, in the figures the temporal coordinates of the upper (or, equivalently, lower) end-points of the $\mathcal{R}_a^{-1}-$copies may span only the left- and rightmost time-intervals separated on the horizontal side of the rectangular contour C in the following way. While the leftmost interval is bounded from the right by the leftmost end-point of the lines[7] of the elementary diagram, the rightmost interval is bounded from the left by the rightmost end-point of the diagram.

[6] The condition (3.1) refers to such implementation of the decomposition $\mathcal{C}_{lj} = \otimes_k \mathcal{C}^{(k)}_{l_k j_k}$ when, except for a single factor $\mathcal{C}^{(q)}_{l_q j_q}$, all the remaining factors are one-dimensional.

[7] In each of the latter figures, the corresponding elementary diagram is depicted by solid lines.

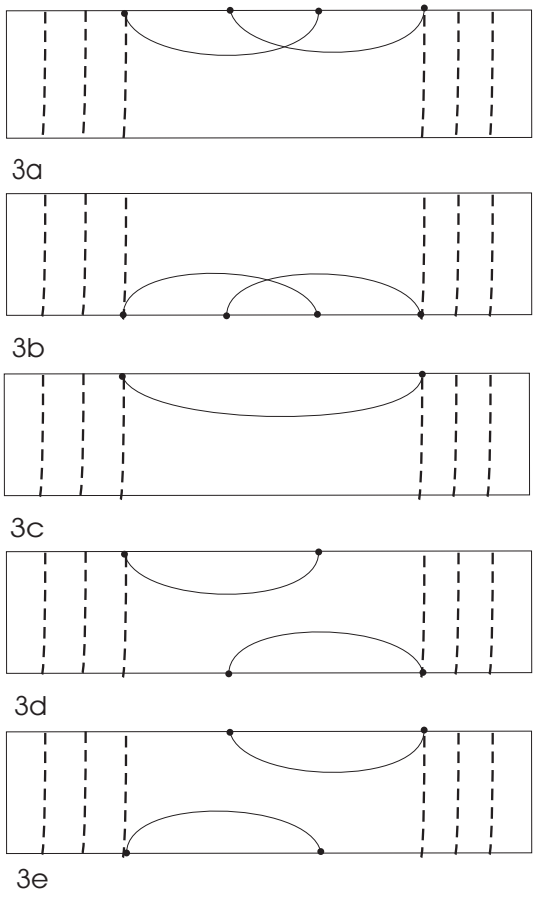

Figure 3: Examples of the $\mathcal{R}_a^{-1}-$deformations of the time-ordered protographs (represented by solid lines) in the case when (a),(b) $r = v = 0$, (c) $r = v - 1 = 0$ and (d),(e) $r = v = 1$. Dotted lines depict $\mathcal{R}_a^{-1}-$inclusions.

Finally, by the same mechanism as in the $\theta = 0$ case, the $\mathcal{R}_a^{-1}-$dressing of a given connected graph results merely in the multiplication of the amplitude, associated with this graph, by a factor (to be fixed in subsection 5.2).

3.2 The $\bar{\mathcal{R}}_b^{-1}-$deformations

The $\bar{\mathcal{R}}_b^{-1}-$deformation of a given kth line of a given elementary graph that introduces an extra line, labeled by i, so that the following twofold condition is fulfilled. Let the remaining lines of the latter graph are denoted as the $\{q\}_k-$set with $\forall q \neq k, i$. To begin with, one requires that the kth and the ith lines, being mutually non-intersecting (in the sense of eq. (2.11)), intersect the $\{q\}_k-$set in the topologically equivalent way (modulo possible reversion of the orientation). e.g. the $\bar{\mathcal{R}}_b^{-1}-$copies of the right and left solid horizontal lines in figure 1a are depicted by dotted lines in figures 4b and 4c respectively. In general, it can be formalized by the condition

$$\mathcal{C}_{ik} = 0 \quad , \quad \mathcal{C}_{iq} = \alpha_{ik}\, \mathcal{C}_{kq} \quad , \quad \forall q \neq k, i\,, \tag{3.3}$$

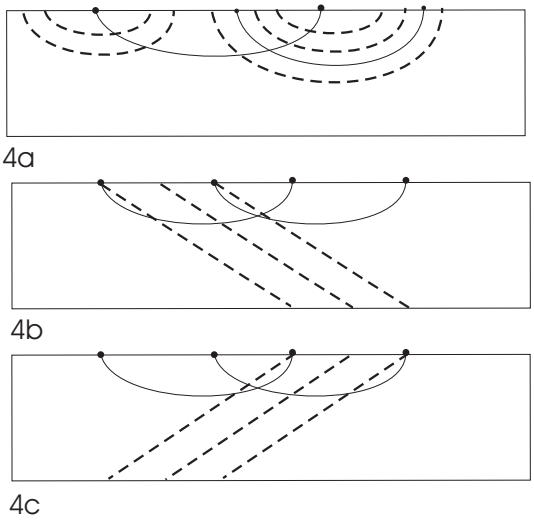

Figure 4: Examples of the $\mathcal{R}_b^{-1}-$deformations of the $\mathcal{R}_a \times \mathcal{R}_b-$irreducible diagram in figure 1a. Dotted lines depict: (a) horizontal $\mathcal{R}_b^{-1}-$copies of the right solid line of the diagram, (b) non-horizontal $\mathcal{R}_b^{-1}-$copies of this right line and (c) non-horizontal $\mathcal{R}_b^{-1}-$copies of the left solid line.

where, depending on the choice of the relative orientation of the ith line, the q-independent constant α_{ik} is equal to 1 or -1 (with $\alpha_{11} = 1$) while $\alpha_{ik} = \alpha_{ki}$. Additionally, it is convenient to impose that thus introduced extra line should *not* be horizontal, i.e., both its end-points are not attached to the same horizontal side (along the $2-$axis) of the rectangle C. As for the inverse transformation, the $\bar{\mathcal{R}}_b-$deformation deletes such an ith line of a diagram that eq. (3.3) holds true for some k. Correspondingly, any line of a $\bar{\mathcal{R}}_b-$irreducible graph has *no* $\bar{\mathcal{R}}_b^{-1}-$copies in the sense of the above twofold condition.

Next, identifying $\alpha_{np} \equiv \alpha_{21}^{(n)}$ with $p = n+1$ (while $\alpha_{nn} \equiv \alpha_{11}^{(n)} = 1$), one obtains that the $\bar{\mathcal{R}}_b^{-1}-$deformation of a diagram, described by eq. (2.10), results in the diagram described by the $2(n+1)-$point function

$$V^{(n+1)}_{U_\theta(1)}(\mathbf{y}_1,\ldots,\mathbf{y}_n,\mathbf{y}_{n+1}) = o_{n+1} \prod_{1\le l<j}^{n} e^{\frac{i}{2}\,\mathcal{C}_{lj}\breve{\theta}_{\mu\nu}\partial_\mu^{\mathbf{z}_l}\partial_\nu^{\mathbf{z}_j}} D_{22}(\mathbf{z}_1)\ \ldots D_{22}(\mathbf{z}_{n-1}) \times \quad (3.4)$$
$$\times \Big[D_{22}(\mathbf{z}_n)\ D_{22}((\mathbf{z}_n-\mathbf{y}_n)\alpha_{21}^{(n)}+\mathbf{y}_{n+1})\Big]\Big|_{\{\mathbf{z}_k=\mathbf{y}_k\}}\ .$$

which is expressed through the original $n \times n$ intersection matrix $\mathcal{C}_{lj}$. In view of the pattern (2.3) of the propagator, eq. (3.4) implies that

$$\alpha_{21}^{(n)} y_n^2 = y_{n+1}^2\ . \quad (3.5)$$

In turn, it entails that the $\bar{\mathcal{R}}_b^{-1}-$copy of a given line is characterized by *the same* modulus of the relative time (fixed by the second component y_l^2 of the relative distance (2.9)) as the line itself.

The multiple application of the $\bar{\mathcal{R}}_b^{-1}-$deformations (3.3) to a kth line, introduces an extra $\{l\}_k-$set of the lines which, intersecting neither each other nor the kth line, fulfill the

option of eq. (3.3) with $\mathcal{C}_{lq} = \alpha_{l1}^{(k)}\, \mathcal{C}_{kq}$, $\forall q \neq k, l$ (while $\alpha_{11}^{(k)} = 1$), where we have changed the notations introducing $\alpha_{l1}^{(k)}$ instead of α_{ik}. Then, generalizing the relation (3.5), the corresponding implementations of the $2n-$point function (2.10) enforce that

$$y_k^2 = \alpha_{l1}^{(k)} y_{k,l}^2 \quad , \quad \forall l = 2, \ldots, n_k \quad , \quad \forall k \,, \tag{3.6}$$

where $\mathbf{y}_{k,l}$ denotes the relative distance (2.9) corresponding to that $\bar{\mathcal{R}}_b^{-1}-$copy of the kth line (described by $\mathbf{y}_k \equiv \mathbf{y}_{k,1}$) which is endowed with the label l.

Let us also note another useful property[8] of the $\bar{\mathcal{R}}_b^{-1}-$deformations which enforces eq. (3.6). When applied to an elementary $G = 1$ graph, the (multiple) $\bar{\mathcal{R}}_b^{-1}-$deformations result in diagrams described by vanishing $2n-$point functions (2.10) unless they are constrained by a particular $\{\alpha^{(r)}\}-$assignment in the following sense. The quantity (2.10) may be nonvanishing only when, for any given rth line of the elementary graph, all its $\bar{\mathcal{R}}_b^{-1}-$copies (if being present) are assigned with *one and the same* value of the parameter

$$\alpha_{l1}^{(r)} = \alpha^{(r)} \quad , \quad \forall l \geq 2 \,, \ \forall r \,, \tag{3.7}$$

where $\alpha_{lk}^{(r)} = \pm 1$ enters the implementation of eq. (3.3) corresponding to the rth line.

Together with eq. (3.6), it guarantees the important property of any graph with a nonvanishing amplitude:

$$y_k^2 = \alpha^{(k)} y_{k,l}^2 \quad , \quad \forall l = 2, \ldots, n_k \quad , \quad \forall k \,, \tag{3.8}$$

i.e., *all* the $\bar{\mathcal{R}}_b^{-1}-$copies of a given line of the associated irreducible diagram are characterized by the same relative time. Diagrammatically, eq. (3.8) is implemented through the convention that, for $C = \square$, the latter copies are depicted by such straight dotted lines which are mutually *parallel*. An example is provided by figures 4b and 4c where the dotted lines depict the $\bar{\mathcal{R}}_b^{-1}-$copies of respectively the right and the left solid lines representing the $\mathcal{R}_a \times \bar{\mathcal{R}}_b-$irreducible diagram in figure 1a.

These figures exemplify another general rule: given a $\bar{\mathcal{R}}_b^{-1}-$dressing of a particular irreducible diagram, in the corresponding figure the temporal coordinates of the upper (or lower) end-points of the $\bar{\mathcal{R}}_b^{-1}-$copies may span only such time-interval that is bounded by the two specific end-points of this diagram: by a certain single end-point of the line, the copies are associated with, and by that end-point of some of the remaining lines which (in the sense of its temporal coordinate) is *adjacent to* the former end-point. E.g., in the case of figure 4b, these are the left end-points of the right horizontal solid line (dressed by $\bar{\mathcal{R}}_b^{-1}-$deformations) and of the left horizontal solid line. A more detailed prescription will be given in the next section.

3.2.1 Important topological selection-rule

The constraint (3.6) implies certain important *selection-rule* that underlies the considered resummation algorithm which implements the dressing of the $G = 1$ $\mathcal{R}_a \times \bar{\mathcal{R}}_b-$irreducible

[8] The proof of eq. (3.7), as well as of the selection-rule discussed in subsection 3.2.1, will be given in a separate publication.

diagrams. In particular, it is this rule which motivates the additional requirement that the extra line, introduced in the process of dressing of a given irreducible diagram according to eq. (3.3), is necessarily non-horizontal (in the sense formulated in the beginning of subsection 3.2). In turn, it allows to select easily those $\mathcal{R}_a \times \bar{\mathcal{R}}_b-$irreducible diagrams which are endowed with *nonvanishing* $2n-$point functions (2.10).

To briefly explain the point, let us first introduce the notion of the $\mathcal{R}_b^{-1}-$deformations. The definition of this type of the deformation can be obtained from the one of the $\bar{\mathcal{R}}_b^{-1}-$deformation omitting the latter additional requirement imposed on the extra line. Then, it is straightforward to verify that the $\mathcal{R}_a \times \bar{\mathcal{R}}_b-$irreducible Feynman diagrams of figures 1 and 2 represent all connected $\mathcal{R}_b-$irreducible (i.e., $\mathcal{R}_a \times \mathcal{R}_b-$irreducible) $G = 1$ diagrams. Although any $\mathcal{R}_b-$irreducible graph is evidently $\bar{\mathcal{R}}_b-$irreducible as well, the converse statement is not necessarily true. Furthermore, there are infinitely many $\mathcal{R}_a \times \bar{\mathcal{R}}_b-$irreducible connected graphs. E.g., any diagram of the type in figure 4a (with an *arbitrary* number of dotted horizontal lines) has to be included into the subset of the $\mathcal{R}_a \times \bar{\mathcal{R}}_b-$irreducible graphs which, being $\mathcal{R}_b-$reducible, are associated with the diagram in figure 1a (via the horizontal $\mathcal{R}_b^{-1}-$deformations of the right line of the latter diagram).

Fortunately, there is the selection-rule which guarantees that only a *finite* number of the $\mathcal{R}_a \times \bar{\mathcal{R}}_b-$irreducible graphs which, being $\mathcal{R}_b-$reducible, are assigned with a nonvanishing $2n-$point function (2.10). Therefore, it is convenient to enumerate relevant $\mathcal{R}_a \times \bar{\mathcal{R}}_b-$irreducible graphs (with a nonvanishing quantity (2.10)) combining the latter finite number of the $\mathcal{R}_b-$reducible diagrams with the $\mathcal{R}_a \times \mathcal{R}_b-$irreducible Feynman graphs of figures 1 and 2. Correspondingly, in the sector of connected diagrams, it proves the effectiveness of the proposed above prescription to include into the dressing only *non-horizontal* copies (of a given kth line) satisfying the condition (3.3).

As for the selection-rule, it states the following. The $2n-$point function (2.10), associated with a generic $\mathcal{R}_b-$reducible connected $G = 1$ diagram, is nonvanishing only when the diagram includes not more than *two* distinct $\mathcal{R}_b-$equivalent[9] horizontal lines. Furthermore, these two lines should be attached to different horizontal sides of the rectangle C. (To give an example of the reduction, consider various $\mathcal{R}_b^{-1}$-deformations of the right horizontal line in figure 1a, e.g., those depicted in figures 4a and 4b. Then, this rule guarantees in particular that the diagrams like in figure 4a are assigned with the vanishing amplitude.)

Finally, starting with the set of the $\mathcal{R}_a \times \mathcal{R}_b-$irreducible $G = 1$ graphs and employing thus implemented reduction, it is straightforward to reconstruct those $\mathcal{R}_b-$reducible $G = 1$ diagrams which, being $\mathcal{R}_a \times \bar{\mathcal{R}}_b-$irreducible, are described by a nonvanishing quantity (2.10). A direct inspection shows that these are only the Feynman diagrams[10] in figures 7a and 7e.

Let us also note another constraint to be used in the discussion below. Both the elementary graphs in the figures 2a and 2b and all their deformations are assigned with *vanishing* $2n-$point functions (2.10) and, therefore, can be excluded from the analysis. This

[9]Two lines are called $\mathcal{R}_b-$equivalent if, being endowed with labels i and k, they comply with the condition (3.3).

[10]As previously, the figures are postulated to fix the *topology* of the attachment of the lines' end-points to the upper and lower horizontal sides of $C = \square$.

property, which enforces the considered selection-rule, may be inferred from the general expressions discussed in subsection 6.1.

3.3 Refinement of the resummation algorithm

According to eq. (3.4), given a generic connected graph, the pattern of the corresponding $2l-$point function can be deduced from eq. (2.10) via the replacement $D_{22}(\mathbf{z}_k) \to f_k(\mathbf{z}_k, \ldots)$ performed in the $2n-$point function corresponding to the associated $\mathcal{R}_a \otimes \bar{\mathcal{R}}_b-$irreducible diagram. Here, $f_k(\mathbf{z}_k, \ldots)$ takes into account possible $\bar{\mathcal{R}}_b^{-1}-$dressing of the kth line of the irreducible diagram (described by the matrix $\mathcal{C}_{ij}$ of rank $n \geq l$) which is related to the connected graph in question via a sequence of $\bar{\mathcal{R}}_b-$deformations. Furthermore, once a kth line of the irreducible diagram may be dressed by conglomerates of $\bar{\mathcal{R}}_b^{-1}-$copies characterized by an *unambiguous* value of the corresponding parameter $\alpha^{(k)}$, (in the computation of the amplitude) the overall $\bar{\mathcal{R}}_b^{-1}-$dressing of this line can be accounted by a concise *exponentiation* prescription. This prescription results in the replacement of the associated perturbative propagator by its effective counterpart to be explicitly written in subsection 5.3.

The resummation algorithm, built on the $\mathcal{R}_a \otimes \bar{\mathcal{R}}_b-$deformations of the variety of the $\mathcal{R}_a \otimes \bar{\mathcal{R}}_b-$irreducible diagrams, still has a deficiency which is rooted in the following property. Some of these diagrams contain time-ordered components which possess a single line such that its $\bar{\mathcal{R}}_b-$deformations may be assigned with *different* signs of $\alpha^{(r)}$ introduced in eq. (3.7). In consequence, the concise replacement of the propagator can not be directly applied to such a line that renders a graphic interpretation of the computations rather murky. To circumvent this problem, we propose the following refinement of the algorithm to reproduce the complete set of the connected $G = 1$ diagrams. Instead of the $\mathcal{R}_a \otimes \bar{\mathcal{R}}_b-$irreducible Feynman diagrams, the idea is to introduce the larger set of the *elementary time-ordered* connected graphs which is postulated to include not only all time-ordered components of the $\mathcal{R}_a \otimes \bar{\mathcal{R}}_b-$irreducible Feynman diagrams in figures 1, 2, 7a, and 7e, but also a variety of a few connected $\bar{\mathcal{R}}_b-$*reducible* graphs. Correspondingly, the algorithm of the $\bar{\mathcal{R}}_b^{-1}-$dressing of the elementary graphs is different compared to the dressing of the irreducible diagrams (while the $\mathcal{R}_a-$dressing is not modified).

To begin with, a single line of some judiciously chosen subset of the elementary graphs is not dressed at all in the sense that the corresponding perturbative propagator is not modified. In turn, the overall $\bar{\mathcal{R}}_b^{-1}-$dressing of each of the remaining lines, being characterized by an *unambiguous* sign of the corresponding parameter $\alpha^{(r)}$, it does lead to the required replacement of the corresponding perturbative propagator by the effective one. As for the supplementary subset of the elementary graphs[11] where the dressing is applied to their lines, this dressing is characterized by an unambiguous $\{\alpha^{(k)}\}-$assignment for any such graph.

Concerning the variety of the elementary graphs with a single line without the $\bar{\mathcal{R}}_b^{-1}-$dressing, the prescription differs for its $\bar{\mathcal{R}}_b-$irreducible and $\bar{\mathcal{R}}_b-$reducible varieties. In particular, the variety of the $\bar{\mathcal{R}}_b-$irreducible graphs contains a certain specific subvari-

[11] All graphs in this variety are necessarily $\bar{\mathcal{R}}_b-$irreducible.

ety where this line coincides with the previously discussed line, the $\bar{\mathcal{R}}_b^{-1}-$copies of which may be endowed with both signs of $\alpha^{(k)}$. In the case of any given $\bar{\mathcal{R}}_b-$reducible elementary graph, there is exactly one pair of $\bar{\mathcal{R}}_b-$equivalent lines. The dressing is not to be assigned to one of the latter two lines so that the following fine-tuning takes place. The elimination of the remaining $\bar{\mathcal{R}}_b^{-1}-$copy of this line transforms the graph into such $\bar{\mathcal{R}}_b-$irreducible graph, where precisely the same line is to be devoid of the $\bar{\mathcal{R}}_b^{-1}-$dressing. Furthermore, there are precisely two distinct $\bar{\mathcal{R}}_b-$reducible elementary graphs which, being associated respectively with the options $\alpha^{(k)}=1$ and $\alpha^{(k)}=-1$, are transformed into a given irreducible graph in the above specific subvariety.

3.3.1 First look at the elementary graphs

To realize the above program, let us first select those of the irreducible diagrams that contain certain time-ordered components possessing a (single) line, the $\bar{\mathcal{R}}_b-$copies of which may be assigned with *different* signs of $\alpha^{(r)}$. A direct inspection verifies that these may be only diagrams with a *single* horizontal line (labeled by 1) associated with both signs of $\alpha^{(1)}$, i.e., the diagrams in figures 1c,1d and 2e,2f. Examples of the relevant components of the latter diagrams are given by the time-ordered graphs represented by the solid lines in figures 8a,b (corresponding to the diagram in figure 1c) and in figure 8c (corresponding to the diagram in figure 2e). The components, associated with both signs of $\alpha^{(1)}$, are geometrically selected by the condition that the lower end-point of each of the non-horizontal lines is located in *the interior* of the time-interval bounded by the end-points of the horizontal line. The extension to the case of figures 1d and 2f is routine.

Then, the proposal is threefold. First, with each of the above components, we associate the pair of the extra graphs obtained via the addition of such a single $\bar{\mathcal{R}}_b^{-1}-$copy of the horizontal line that is assigned with $\alpha^{(1)}=1$ and $\alpha^{(1)}=-1$ correspondingly (where $\alpha^{(1)}$ is to be identified with $\alpha_{21}^{(1)}$ in the sense of eq. (3.6)). For example, the considered components of the diagram in figure 1c are associated with those components of the Feynman diagrams[12] in figures 7b and 7c which are constrained by the following condition. The lower end-point of the non-horizontal line, traced back to figure 1c, is confined in the interior of the time-interval bounded by the end-points of the $\bar{\mathcal{R}}_b^{-1}-$copy of the horizontal line. Second, both in the considered components in figures 1c,d, 2e,f and in all thus associated with these components pairs of the extra graphs, the horizontal line is *not* to be endowed with any $\bar{\mathcal{R}}_b^{-1}-$dressing at all. As for admissible $\bar{\mathcal{R}}_b^{-1}-$deformations of the $\bar{\mathcal{R}}_b^{-1}-$copy of the horizontal line in the extra graphs, (in the sense of the $k=1$ option of eq. (3.6)) they are all described by *the same* parameter $\alpha_{l1}^{(1)}$ (with $l\geq 3$) equal to the corresponding value of $\alpha^{(1)}\equiv\alpha_{21}^{(1)}$ unambiguously characterizing a given extra graph. In this way, one evidently reproduces *the entire* pattern of the $\bar{\mathcal{R}}_b^{-1}-$dressing of the horizontal line originally formulated in the resummation-algorithm starting with the $\mathcal{R}_a\otimes\bar{\mathcal{R}}_b-$irreducible Feynman diagrams.

[12]Observe also that, in view of the condition (3.5), the geometry of these diagrams implies the additional constraint on the relative time-ordering of their end-points. E.g., in figure 7c the lower leftmost end-point (of the $\bar{\mathcal{R}}_b^{-1}-$copy of the horizontal line) must be to the right with respect to the upper leftmost end-point (of the horizontal line).

Third, to complete the proposal, it is convenient (see subsection 4.1) to apply the similar procedure not only to the time-ordered components of the diagrams in figures 1c,1d and 2e,2f but also to all the time-ordered graphs which may be related to the latter components via vertical reattachments applied to *the leftmost or rightmost* end-points of the lines these components. *Preserving* both the time-coordinates of the latter end-points and the intersection-matrix (modulo possible change of the sign of its entries), in this particular case the reattachments replace either one or both end-points of the single horizontal line from one horizontal side of C to another. E.g., in the case of figures 1c,1d, thus selected time-ordered graphs present those components of the diagram in figure 1e where *both* end-points of one line belong to the interior of the time-interval bounded by the end-points of the other line. Although both lines of the latter components are associated with a single value of $\alpha^{(r)}$, there is the following correspondence. Matching the pair of the $\alpha^{(1)} = \pm 1$ options of the $\bar{\mathcal{R}}_b^{-1}-$dressing of the horizontal line of the above components in figures 1c and 1d, there are two options of the topology of the considered components of the diagram in figure 1e. The options are differentiated by the property whether the lower end-point of the bounding line (obtained via a reattachment from the horizontal line of figure 1c or 1d) is to the left or to the right with respect to the upper end-point of this line.

Altogether, we arrive at the simple geometrical prescription to generate (in addition to figures 1, 2, 7a, and 7e) thus specified variety of the $\bar{\mathcal{R}}_b-$*reducible* connected graphs which possess exactly one pair of the lines that, being labeled by i and k, comply with the condition (3.3). These graphs can be obtained from the time-ordered components of the Feynman diagrams in figures 7a and 7e via the above vertical reattachments applied to the leftmost or/and rightmost end-points of each of these $\bar{\mathcal{R}}_b-$irreducible diagrams. Modulo the reflection interchanging the horizontal sides of $C = \square$, the additional Feynman diagrams are depicted in the remaining figures 7 so that the relevant time-ordered components are selected by the following topological conditions. In figures 7c,d and 7g,h, the lower rightmost end-point must be to the left with respect to the upper rightmost end-point. In turn, in figures 7b,f the lower leftmost end-point must be to the right with respect to the upper leftmost end-point. In particular, thus constrained diagram in figure 7d and its reflection-partner are associated with those components of the diagram in figure 1e where *both* end-points of one line are located in the interior of the time-interval bounded by the end-points of the other line.

4. The parameterization of the elementary graphs

To properly parameterize the elementary graphs introduced in the end of the previous section, we first discuss two types of the symmetry-transformations which relate these graphs so that they are combined into the corresponding symmetry-multiplets. By construction, the transformations do not alter the structure of the overall $\mathcal{R}_a^{-1} \otimes \bar{\mathcal{R}}_b^{-1}-$dressing which, therefore, characterizes a given multiplet as a whole. Then, both prior and after the overall $\mathcal{R}_a^{-1} \otimes \bar{\mathcal{R}}_b^{-1}-$dressing, the multiplets of the elementary graphs are parameterized by the

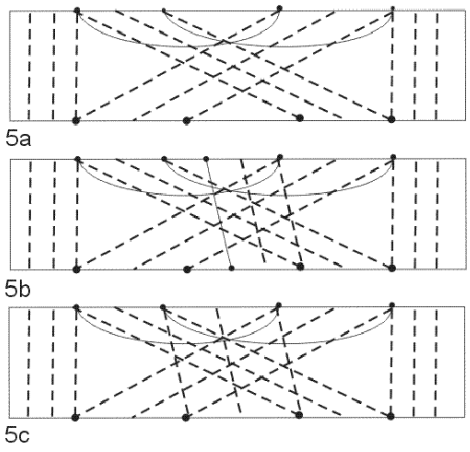

Figure 5: Examples of the $\mathcal{R}_a^{-1}\otimes\bar{\mathcal{R}}_b^{-1}-$dressing of (a) the elementary graph in figure 1a, (b) the elementary graph in figure 2c and (c) protograph in figure 3a. The dressed graphs are associated with the $\gamma-1=r=v=0$ effective amplitudes implemented as (a) $\mathcal{Z}^{(1)}_{100}$, (b) $\mathcal{Z}^{(1)}_{200}$ and (c) $\mathcal{Z}_{00}$.

appropriate $\gamma jrv-$assignment. In turn, within a given multiplet, its members are distinguished through certain supplementary $\{a_k\}_{rv}-$assignment.

We also discuss how the multiplets are naturally combined (with the help of the symmetry transformations) into the $rv-$varieties. Being associated with the decomposition (1.8), the latter varieties are labeled by the corresponding multiplets of the protographs parameterized by the same $\{a_k\}_{rv}-$assignment.

4.1 $S(4)-$symmetry and reflection-invariance

To introduce the required transformations, we are to postulate the following convention. When the elementary graphs are associated to one and the same time-ordered component of a given Feynman diagram, they are nevertheless considered to be *different*, provided the topology of the attachment of their lines' end-points (to the upper and lower horizontal sides of $C=\square$) is different. For example, the pairs of distinct graphs are depicted in figures 1a, 1b and figures 1c, 1d respectively.

Turning to the transformations of the elementary graphs, the first type is implemented through the vertical reattachments which, being introduced in subsection 3.3.1, can be combined to generate $S(4)-$*multiplets* of the latter graphs. Consisting of four graphs, each such multiplet implements the discrete space of the $S(4)-$group[13] of permutations. Since the reattachments involve only the rightmost or/and leftmost end-points of the graphs, thus implemented reattachments do *not* alter the modulus of the entries of the intersection-matrix $\mathcal{C}_{ik}$ associated to the graph used to generate the other three member of the $S(4)-$multiplet. An example of such multiplet is given by the graphs represented in figures 5c and 6a-6c by

[13]When applied simultaneously to this $4-$set of the graphs, the reattachments can be used to generate the 4! elements of the group itself.

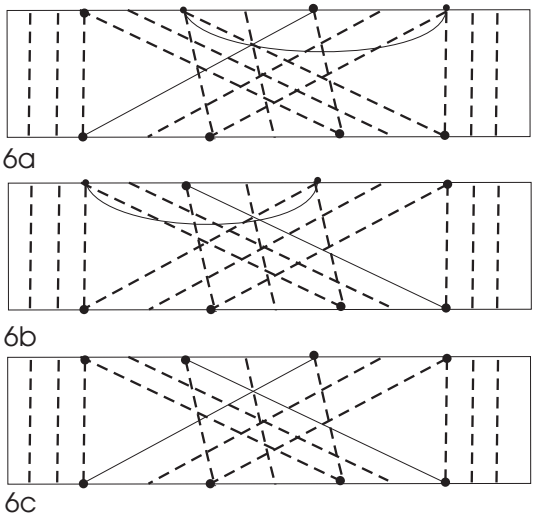

Figure 6: Examples of the $\mathcal{R}_a^{-1} \otimes \bar{\mathcal{R}}_b^{-1}-$dressing of the three protographs which are obtained from the protograph in figure 3a through the application of the vertical reattachments to its (a) leftmost end-point, (b) rightmost end-point and (c) both of the latter end-points.

the solid lines, where the reattachments replace (from one horizontal side of C to another) the single end-point of either one or both of the horizontal lines of the graph in figure 5c.

Furthermore, not only the elementary graphs but also their deformations, included into the subsets described by the corresponding effective amplitudes, are unambiguously split into a finite number of distinct (non-overlapping) $S(4)-$multiplets. As it is illustrated by the figures 5 and 6, the required symmetry of the dressing is maintained by the condition that, as well as the end-points of the $\mathcal{R}_a^{-1}-$copies, the positions of the end-points of all the $\bar{\mathcal{R}}_b^{-1}-$copies of any line (of a given elementary graph) are left intact under the reattachments. In this sense, the $\bar{\mathcal{R}}_b^{-1}-$dressing of each of the lines (including the ones involved into the $S(4)-$reattachments) is $S(4)-$*invariant*.

As for the second type of the transformations, the $S(4)-$multiplets of the elementary graphs may be related via the $S(2)-$reflection that (mapping the contour $C = \square$ onto itself) mutually interchanges the two horizontal sides of C. Leaving intact the $\mathcal{R}_a^{-1}-$dressing, this transformation is nontrivially applied not only to the lines of the elementary graph but also to all the $\bar{\mathcal{R}}_b^{-1}-$copies of these lines. To avoid double-counting, one is to consider only such reflections of the protographs which can not be alternatively reproduced as compositions of the vertical $S(4)-$reattachments.

Finally, one can implement the $S(4) \otimes S(2)-$transformations to combine the *dressed* (by all admissible $\mathcal{R}_a^{-1} \otimes \bar{\mathcal{R}}_b^{-1}-$deformations) elementary graphs into the $S(4) \otimes S(2)-$multiplets.

4.2 The $\gamma jrv-$parameterization of the $S(4) \otimes S(2)-$multiplets

Let us introduce the four integer numbers γ, j, r, and v which parameterize the $S(4) \otimes S(2)-$multiplets of the elementary graphs both prior and after their dressing by all

admissible $\mathcal{R}_a^{-1} \otimes \bar{\mathcal{R}}_b^{-1}-$deformations. Each such multiplet contains $h_{rv} = 2 + r - v = 1, 2$ $S(4)-$multiplets related via the $S(2)-$reflections discussed above. It is done so that the relevant geometry of the multiple deformations of the elementary graphs in all $S(4) \otimes S(2)-$multiplets is specified in the reflection- and reattachment-*invariant* way.

As a result, the algorithm of the resummation can be decomposed into the two steps. At the first step, for given values of γ, j, r, and v, one considers the dressing of certain $h_{rv} = 2 + r - v$ special elementary graphs related (when $h_{rv} = 2$) via the $S(2)-$reflections. In the corresponding $S(4)-$multiplet, each of the latter graphs has the *maximal* number (equal to h_{rv}) of the horizontal lines attached to $1 + r$ different horizontal sides of $C = \square$.

At the second step, the remaining three elementary graphs of each $S(4)-$multiplet can be then reproduced (together with their dressing) via the vertical reattachments of the leftmost or/and rightmost end-points of the above $2 + r - v$ horizontal lines. By construction, the intersection-matrix is invariant (modulo possible change of the sign of its entries) under these $S(4)-$transformations.

Similar procedure introduces the $rv-$parameterization of the associated $S(4)-$multiplets of the (dressed) protographs relevant for the decomposition (1.8). Consider a given $rv-$variety of the special elementary graphs which, sharing the same h_{rv} horizontal lines involved into the reattachments, are endowed with different values of γ and j. Then, the associated time-ordered protograph is represented precisely by these h_{rv} horizontal lines. As previously, the remaining three members of each $S(4)-$multiplet of the protographs are generated through the above vertical reattachments. Also, by the same token as in the case of the elementary graphs, the reflections are employed to generate $S(4) \otimes S(2)-$multiplets of the protographs.

Generalities of the proposed algorithm are discussed in subsections 4.2.1- 4.2.3 while the explicit construction is sketched in subsection 4.2.4.

4.2.1 The topological $jrv-$parameterization

Consider first the integers j, r and v which can be interpreted directly in terms of the relevant topological properties *common* for all the elementary graphs in a given $S(4)-$multiplet. To begin with, $r = 0, 1$ is equal to the number of the pairs of the $\mathcal{R}_b^{-1}-$equivalent (in the sense of subsection 3.2.1) lines available in a given elementary graph. Correspondingly, all the time-ordered graphs associated with figures 7 are assigned with $r = 1$, while the time-ordered components of the remaining Feynman diagrams in figures 1 and 2, are parameterized by $r = 0$.

Next, the number of the lines is equal to $n = 1 + j + r$ so that $j = 1, 2$. Therefore, the graphs of figures 1 and 7a-7d are assigned with $j = 1$, while the remaining elementary graphs are assigned with $j = 2$. It is also noteworthy that, for a given r, $j+1 = n-r = 2, 3$ yields the multiplicity of the irreducible star-product, the form of which (discussed in the beginning of section 3) assumes both the corresponding perturbative $2n-$point function (2.10), and its effective counterpart to be considered in subsection 6.1.

As for $v = 0, 1$ (with $0 \leq r \leq v \leq 1$ in compliance with eq. (1.8)), topologically it is determined employing the property that the nth order elementary graph has exactly $h_{rv} = 2 + r - v$ lines which may be involved into the vertical $S(4)-$reattachments *without*

changing (the modulus of) the entries of the intersection-matrix $\mathcal{C}_{ij}$. In other words, the rightmost and leftmost end-points of a given graph (which are the only its end-points such that the group of their reattachments do not alter $|\mathcal{C}_{ij}|$ for $\forall i,j$) belong to h_{rv} distinct lines of the graph. Correspondingly, *all* end-points of the remaining $n-h_{rv}$ lines (not involved into the reattachments) are located in the interior of the time-interval bounded by the leftmost and rightmost end-points of the h_{rv} reattached lines. Furthermore, only $h_{rv}-v$ of the reattached lines are to be dressed, together with all the remaining $n-h_{rv}$ lines not involved into the reattachments, by the $\bar{\mathcal{R}}_b-$copies so that the corresponding perturbative propagators are replaced by their effective counterparts.

4.2.2 The $rv-$parameterization of the multiplets of the protographs

The parameters r and v can be used to enumerate the protographs which are time-ordered as well. A particular protograph, can be reconstructed eliminating all the $n-h_{rv}$ lines of the corresponding elementary graph except for the $2+r-v$ lines affected by the $S(4)-$reattachments. Modulo the $S(4)-$reattachments, thus separated protographs are depicted by solid lines in figures 3a-3e for those protographs which, for a given $rv-$assignment possess the maximal number $2+r-v$ of the horizontal lines (attached to $1+r$ different horizontal sides of $C=\square$). The figures 3a,b and 3d,e are in one-to-one correspondence with the pairs of the $S(4)-$multiplets which, being related via the reflection (interchanging the horizontal sides of the contour C), are characterized by $r=v=0$ and $r=v=1$ respectively. In particular, the $r=v=0$ multiplet, associated with the protograph in figure 3a, is given by the protographs represented in figures 5c and 6a-6c by the solid lines. In turn, figure 3c refers to the single $r=v-1=0$ multiplet.[14]

In sum, there are precisely $h_{rv}=2+r-v$ $S(4)-$multiplets of the protographs which, being parameterized by a particular $rv-$assignment, are related via the $S(4)-$reflections.

4.2.3 The $\gamma-$parameterization

The necessity to complete the $jrv-$parameterization and introduce one more parameter γ, additionally specifying the $S(4)\otimes S(2)-$multiplets, is motivated by the geometry of the pairs of the *different* elementary graphs depicted by solid lines in figures 8a, 8b (both characterized by $j=r+1=v=1$) and 9a, 9b (both characterized by $j=r=v=1$). To distinguish between the graphs in each pair we introduce the additional label $\gamma=1,2$ so that figures 8a,9a and 8b,9b are parameterized by $\gamma=1$ and $\gamma=2$ respectively.

In general, with the help of the additional parameter $\gamma=1,\ldots,f_{jrv}$, one is to enumerate distinct $S(4)\otimes S(2)-$multiplets of the graphs which are singled out when one fixes the parameters j, r, and v. The previous discussion suggests that, to find the number f_{jrv}

[14]Recall that, in order to avoid double-counting, we take into account only those reflections of the protographs which can not be alternatively reproduced as compositions of the vertical $S(4)-$reattachments. Correspondingly, the $v=1$ protograph in figure 3c should *not* be accompanied by the reflection-partner which, being defined by the requirement that both end-points of the single line are attached to the lower side of C, can be alternatively obtained via the composition of the two vertical reattachments. Note also that the genus of the $v=1$ protographs is zero rather than one which explains why we have to start from the elementary graphs rather than directly from the protographs.

of such multiplets, it is sufficient to consider only the variety of those elementary graphs which, representing the corresponding multiplet, possess the *maximal* number h_{rv} of the horizontal lines for a particular $jrv-$specification. Then, f_{jrv} is equal to the number of distinct time-ordered $jrv-$components (of *the same* Feynman diagram) which, belonging to the latter variety, are not related via the $S(4)\otimes S(2)-$transformations. In turn, our aim is to prove that the latter number (being, in fact, $r-$independent) is equal to

$$f_{jv} = (1-v) + (3-j)v \quad , \quad f_{j0} = f_{2v} = 1 \ , \ \ \forall j, v \, , \tag{4.1}$$

which, in particular, implies that $f_{jv} = 1, 2$.

To this aim, for a particular $jrv-$specification, it is convenient first to fix generic positions both of the $2+r-v$ horizontal lines (involved into the $S(4)-$reattachments) and of the upper end-points of the remaining $n-(2+r-v) = j-1+v$ non-horizontal lines. Then, f_{jrv} can be identified with the number of different admissible $\left[\otimes_{i=1}^{j-1+v} Sign(y_i^2)\right]/S(j-1+v)-$assignments defined (when $j-1+v>1$) *modulo* possible $S(j-1+v)-$permutations of the labels i of the $j-1+v$ *non-horizontal* lines. Here, $Sign(y_i^2)$ denotes the sign-function depending on the relative time y_i^2 (i.e. the temporal component of the relative distance (2.9)) which, being associated with the ith non-horizontal line, may be different for different time-ordered components[15] of a given Feynman diagram.

To evaluate the number of such assignments, we first note that eqs. (3.5) and (3.3) guarantee that f_{jrv} is indeed $r-$independent, $f_{jrv} \equiv f_{jv}$. In turn, it allows to deduce f_{jv} restricting our analysis to the $r=0$ cases. Next, we should take into account that, among the $\delta-$functional constraints imposed by the $G=1$ effective $2n-$point function $\tilde{V}^{(n)}_{U_\theta(1)}(\{\mathbf{y}_k\})$, there are precisely $n-2 = j-1+r$ constraints which are the same as in the case of the perturbative $2n-$point function (2.10) of the associated elementary diagram,

$$\tilde{V}^{(n)}_{U_\theta(1)}(\cdot) \sim V^{(n)}_{U_\theta(1)}(\{\mathbf{y}_l\}) \sim \prod_{p=1}^{n-2G} \delta\left(\sum_{l=1}^{n} \lambda_l^{(p)} \, y_l^2\right) , \tag{4.2}$$

where the $n-2G$ n-vectors $\lambda_l^{(p)}$, depending only on the topology of the associated elementary graph, span the subspace of those eigenvectors of the intersection matrix $\mathcal{C}_{kl}$ which possess vanishing eigenvalue: $\sum_{l=1}^{n} \mathcal{C}_{kl}\lambda_l^{(p)} = 0$ for $p = 1, 2, \ldots, n-2G$. In consequence, among the $j-1+v$ lower end-points of the non-horizontal lines, only v points remain to be independent degrees of freedom (in addition to the $2h_{rv}|_{r=0} + (j-1+v)$ ones already fixed above) when $r=0$.

When $v=0$, obviously $f_{j0}=1$ for $j=1,2$. As for $v=1$, when we vary the position of the lower end-point of kth non-horizontal line representing the residual $v=1$ degree of freedom, the resulting time-ordered components of the transformed diagram are distinguished by the $\left[\otimes_{i=1}^{j} Sign(y_i^2)\right]/S(j)-$assignment. Therefore, $f_{j1} = (j-1)+2(2-j)$, where it is formalized that $f_{11} = (v+1)|_{v=1} = 2$, while $f_{21} = f_{11} - 1 = 1$. It follows from a direct inspection of the $v-1 = r = 0$ graphs represented by solid lines in figures 8a,b

[15] It is straightforward to observe that, once a particular $jrv-$specification is fixed, distinct (due to different assignments) $G=1$ elementary graphs are necessarily components of *the same* Feynman diagram.

(assigned with $j = 1$) and 8c (assigned with $j = 2$). Summarizing, one arrives at the formula (4.1) so that $1 \leq f_{jv} \leq 2$, and $f_{jv} = 2$ only when $j = v = 1$.

Note that, although the construction of the parameter f_{jv} is obviously reflection-invariant, the action of the reflections on the $S(4)-$multiplets of the elementary graphs is still nontrivial in the cases when $f_{jv} = 2$. The reflections, introduced in subsection 4.2.1, in these cases are postulated to relate those of the latter multiplets which, being endowed with the same $jrv-$assignment, are described by the two different values of γ. Summarizing, there are precisely $h_{rv} = 2 + r - v$ $S(4)-$multiplets of the elementary graphs which, being parameterized by a particular $\gamma jrv-$assignment, are related via the $S(4)-$reflections in the $j-$*independent* way.

4.2.4 Explicit construction of the elementary graphs and their deformations

To complete the discussion of subsection 4.2, for any given $jrv-$assignment let us explicitly separate the elementary graphs with the maximal amount $h_{rv} = 2+r-v$ of the horizontal lines and sketch the pattern of their $\bar{\mathcal{R}}_b^{-1}-$deformations. In particular, we discuss geometrical implications of the $n-2 = j-1+r$ specific constraints (4.2) imposed (on admissible combinations of y_l^2) both by the perturbative and by the associated effective $2n-$point $G = 1$ functions. Also, a direct inspection demonstrates that, in each such graph, the proposed pattern of the $\bar{\mathcal{R}}_b^{-1}-$dressing is characterized by a unique $\{\alpha^{(k)}\}-$assignment which matches the aim formulated in subsection 3.3. As for the $S(4)-$reattachments (generating the corresponding $S(4)-$multiplets which are combined, when $h_{rv} = 2$, into the pairs related via the reflections), it is verified that the proposed pattern of the $\bar{\mathcal{R}}_b^{-1}-$dressing can be implemented in the $S(4)-$invariant way.

In the $r = v = 0$ case when $f_{jv}|_{v=0} = 1$, the two $j = 1$ and the two $j = 2$ $S(4)-$multiplets can be generated from the graphs in figures 1a, 1b and 2c, 2d respectively so that, for each j, the two corresponding figures may be related via the reflection mutually interchanging the horizontal sides of $C = \square$. In the $j = 1$ case when $n - 2 = 0$, there are no any constraints (4.2). As for the $j = 2$ case when $n - 2 = 1$, eq. (4.2) implies that the relative times y_l^2 (associated with the three lines labeled by $l = 1, 2, 3$) are constrained by the condition

$$\mathcal{C}_{21} \cdot y_3^2 - \mathcal{C}_{31} \cdot y_2^2 + \mathcal{C}_{32} \cdot y_1^2 = 0 \tag{4.3}$$

which, geometrically, guarantees that the lower end-point of the third line is confined in the *interior*[16] of the time-interval bounded by the leftmost end-point of the first line and the rightmost end-point of the second line. It is this specific property which, being $S(4)-$*invariant*, implies that both of the latter end-points may be consistently involved into the $S(4)-$reattachments without changing $|\mathcal{C}_{ik}|$ with $i, k = 1, 2, 3$.

Concerning the $\bar{\mathcal{R}}_b^{-1}-$dressing, it applies to all $n = j + 1$ lines of the considered $r = v = 0$ elementary graphs since all these lines are associated with a unique $\alpha^{(k)}-$assignment.

[16] It matches the fact that both the elementary graphs in the figures 2a, 2b and all their $\mathcal{R}_a^{-1} \otimes \bar{\mathcal{R}}_b^{-1}-$deformations are assigned with *vanishing* amplitudes (2.10). A single $S(4)-$reattachment, applied to the latter figures, would otherwise generate configurations (with a nonvanishing amplitude) where the lower end-point of the third line is located *outside* the considered time-interval.

In turn, the uniqueness can be inferred from figures 5a and 5b which describe the $\mathcal{R}_a^{-1} \otimes \bar{\mathcal{R}}_b^{-1}-$dressing of the graphs in figures 1a and 2c correspondingly. The bunches of parallel dotted lines are vertical for the lines generated by the $\mathcal{R}_a^{-1}-$deformations, while $\bar{\mathcal{R}}_b^{-1}-$copies are collected into the varieties depicted by dotted lines parallel to the corresponding line of the elementary graph. Also, we presume the general (for $\forall r, v$) graphical prescription that, supplementing the discussion in the end of subsection 3.2, determines the time-interval spanned by the end-points of the $\bar{\mathcal{R}}_b^{-1}-$copies of a given line. For a horizontal line of an elementary graph, the upper/lower end-point of the rightmost and leftmost copies fixes respectively the rightmost and leftmost (solid) end-points of this interval on the upper/lower horizontal side of $C = \square$. As for the dressing of a non-horizontal line of an elementary graph, one end-point of the spanned interval is explicitly determined only by the associated end-point of the non-horizontal line itself. The remaining end-point of this interval is fixed by the appropriate (lower or upper) end-point of that $\bar{\mathcal{R}}_b^{-1}-$copy of the non-horizontal line which is furthest from this line. Next, from figures 5a and 5b, it is geometrically clear that, in view of eq. (3.8), the $\bar{\mathcal{R}}_b^{-1}-$dressing of each of the two reattached lines is indeed $S(4)-$invariant (e.g., compare figures 5c and 6a-6c). As for the parameterization of the lines of the elementary graphs, the left and the right horizontal lines in figures 1a and 2c are assigned with labels 1 and 2 respectively so that $\mathcal{C}_{21} = 1$. The remaining non-horizontal line in figure 2c attains the label 3.

In the $r = v - 1 = 0$ case, the graphs with the $h_{rv} = 1$ horizontal line are depicted by solid lines in figures 8a-8c, where the horizontal line is assigned with the label 1, with the non-horizontal line(s) being parameterized by the label(s) $2, 1 + j$ so that[17] $\mathcal{C}_{23} = 1$ when $j = 2$. The constraint, separating these $v = 1$ components, is that the $j + 1$ end-point at the lower side do belong to the time-interval bounded by the end-points of the remaining horizontal line attached to the upper side. The latter constraint merely separates those $f_{j1} = 3 - j$ time-ordered components of the Feynman diagrams in figure 1c and 2e which are not already included into the corresponding $r = v = 0$ $S(4)-$multiplets. Note also that, as well as in the $r = v = 0$ case, eq. (4.2) imposes a nontrivial constraint (represented by eq. (4.3)) only when $j = 2$ which results in the following geometrical property. Once the lower end-point of the second line is confined in the required time-interval,[18] the lower end-point of the third line is confined to the same interval too.

In turn, the construction of the $r = v - 1 = 0$ components of the diagrams in figure 1c and 2e enforces that only the two end-points of the single horizontal line are to be involved into the vertical $S(4)-$reattachments. The $S(4)-$transformations preserve the corresponding variant of the above geometrical property (see also subsection 3.3.1) so that the quantities $|\mathcal{C}_{ik}|$ are indeed kept intact. As for the $\bar{\mathcal{R}}_b^{-1}-$dressing, only non-horizontal lines are associated with a unique $\alpha^{(r)}-$assignment, while $\bar{\mathcal{R}}_b^{-1}-$copies of the horizontal line may assigned with $\alpha^{(1)} = \pm 1$ (as it clear from figures 7b,f and 7c,g associated with

[17] In other words, the label 2 is assigned to the non-horizontal line with the upper end-point located to the left with respect to the lower end-point.

[18] Otherwise, it would be impossible to reconcile the $S(4)-$symmetry with the fact that the elementary graphs in the figures 2a, 2b (as well as all their $\mathcal{R}_a^{-1} \otimes \bar{\mathcal{R}}_b^{-1}-$deformations) are assigned with vanishing amplitudes (2.10).

$\alpha^{(1)} = 1$ and $\alpha^{(1)} = -1$ respectively). Correspondingly, only the non-horizontal lines are to be dressed: see figures 8a, 8b (with $j = 1$) and 8c (with $j = 2$). As previously, the $\bar{\mathcal{R}}_b^{-1}-$dressing of a given solid line is depicted by the bunch of (non-vertical) dotted lines which are all parallel to this solid line. From figures 8a-8c, it is also geometrically clear that, in view of eq. (3.8), thus introduced $\bar{\mathcal{R}}_b^{-1}-$dressing is $S(4)-$invariant.

In the remaining $r = v = 1$ case, the graphs with $h_{rv} = 2$ horizontal lines are given by the entire decomposition of the Feynman diagrams in figures 7a (with $j = 1$) and 7e (with $j = 2$) into the time-ordered components parameterized by $j = 1, 2$ and $\gamma = 1, f_{j1} = 3 - j$. In turn, for a given j and γ, these components can be collected into the $S(2)-$multiplets. Each pair is comprised of the two graphs which, being related via the reflection mutually interchanging the horizontal sides of $C = \square$, differ from each other by the property (utilizing the condition (3.8)) whether the upper horizontal line is to the left or to the right with respect to the lower one. Correspondingly, the labels 1 and 4 are assigned to the left and right horizontal lines, while (in the case when the first line is attached to the upper side of C) the remaining two non-horizontal lines are parameterized similar to the corresponding figures 8a-8c.

In the $j = 1$ case, eq. (4.2) imposes the single condition (3.8) that can be written in the form $y_1^2 = -y_4^2$ which. When $j = 2$, in addition to the latter condition, eq. (4.2) imposes an implementation of the constraint (4.3) that leads to the following geometrical property exemplified by the pattern of figure 7e (which, therefore, is assigned with a nonvanishing amplitude). Namely, both the lower and the upper end-points of non-horizontal lines are located in the time-intervals bounded by the lower and the upper horizontal lines respectively. In turn, by construction of the components of the diagram in figure 7a and 7e, the $S(4)-$reattachments involve only the rightmost end-point of the right horizontal line and leftmost end-point of the left horizontal line. (In particular, the relevant components of figures 7b,f and 7c,g are related via the corresponding $S(4)-$transformations, to those components of the Feynman diagram in figure 7a,e where the upper horizontal line is respectively to the right and to the left with respect to the lower one.) This implementation of the $S(4)-$transformations is self-consistent since they preserve the corresponding variant of the latter geometrical property[19] that allows to keep intact the quantities $|\mathcal{C}_{ik}|$. Concerning the pattern of the $\bar{\mathcal{R}}_b^{-1}-$dressing, all lines possess their individual dressings except for the two horizontal lines (assigned with the labels 1 and 4 respectively). As it is clear from figures 9a, 9b (with $j = 1$) and 9c (with $j = 2$), there is an ambiguity in the assignment of $\bar{\mathcal{R}}_b^{-1}-$dressing to one of the latter two lines (in the sense of the replacement of the associated perturbative propagator by the effective one). For concreteness, we associate this dressing with the fourth line. Also, these figures demonstrate that (in view of eq. (3.8)) thus implemented $\bar{\mathcal{R}}_b^{-1}-$dressing, being characterized by a unique $\{\alpha^{(r)}\}-$assignment for any $r = v = 1$ elementary graph, is $S(4)-$invariant.

Summarizing the notations, in each $S(4)-$multiplet of the elementary graphs, the labels of the $\bar{\mathcal{R}}_b^{-1}-$dressed lines assume $n - v = r + j - v + 1$ different values in the

[19]The relevant variants are represented by the geometrical constraints imposed on the relevant components in figures 7b-7d and 7f-7h in the end of subsection 3.3.1.

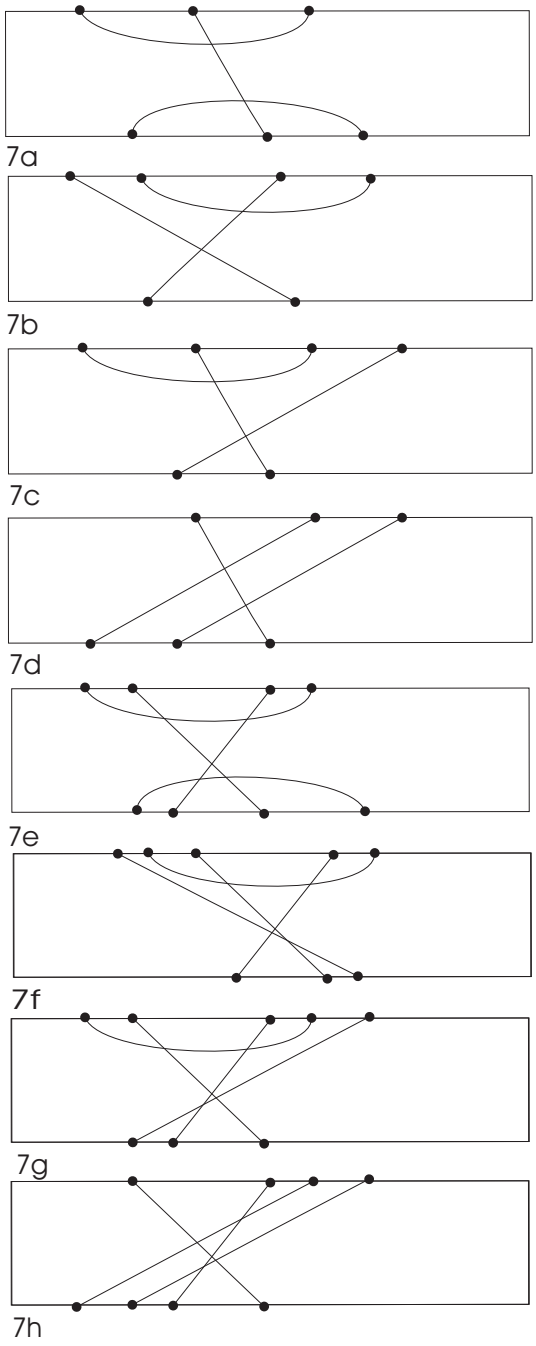

(a),(e) $\bar{\mathcal{R}}_b-$irreducible and (b)-(d),(f)-(h) $\bar{\mathcal{R}}_b-$reducible.

Figure 7: Connected $\mathcal{R}_b-$reducible elementary graphs:

set Ω_{jrv} obtained from the sequence $1+v,\ 2,\ 1+j,\ 2+2r$ via the identification of the $v+(2-j)+(1-r)=4+v-n$ coinciding entities (all being equal to 2) so that $n-v=\sum_{k\in\Omega_{jrv}}1$. Correspondingly, to parameterize the entire set of n lines, we introduce the set $\tilde{\Omega}_{jrv}$ obtained from the sequence $1,\ 2,\ 1+j,\ 2+2r$ via the identification of the

$(2-j)+(1-r)=4-n$ coinciding entities so that $n=\sum_{k\in\tilde{\Omega}_{jrv}}1$. In turn, the labels of the $2+r-v$ lines, involved into the $S(4)-$reattachments, assume values in the set $\mathcal{S}_{rv}$ obtained from the sequence 1, $c_{rv}=2+3r-v$ (with $c_{rv}=1,2,4$) via the identification of the $v-r$ coinciding entities.

4.3 The residual $\{a_k\}_{rv}-$parameterization

It remains to fix the residual parameterization to distinguish between the four different members of a given $S(4)-$multiplet endowed with a particular $\gamma jrv-$assignment. For each of the reattached lines, $1+(v-r)$ of its end-points are $S(4)-$transformed. Therefore, for cases other than $r=1-v=0$, the reattachments can be uniquely determined by the values of the spatial coordinates[20] $y^1_k=0,R$ of the $h_{rv}=2$ lines involved into the $S(4)-$transformations. In turn, the latter coordinates can be faithfully represented by the parameters $a_k=0,1$ so that $y^1_k=a_kR$, with k assuming the $h_{rv}=2$ different values ($k=1,2$ and $k=1,4$ in the $r=v=0$ and $r=v=1$ cases respectively).

In the $r=1-v=0$ case (when $h_{rv}=1$), in addition to a_1 we have to introduce the extra parameter $\tilde{a}_1$,

$$x^1(s'_1)=(1-a_1)\tilde{a}_1R \quad , \quad x^1(s_1)=\tilde{a}_1R+(1-\tilde{a}_1)a_1R\,, \tag{4.4}$$

which is equal to 1 and 0 depending on whether or not the reattachment involves the left(most) end-point of the solid horizontal line in figures 8a-c (while $x^1(s_1)-x^1(s'_1)=a_1R$). To simplify the notations, the pair of the parameters, used to represent the reattachments, is denoted as $\{a_k\}\equiv\{a_k\}_{rv}$ for all $0\leq r\leq v\leq 1$.

5. Dressing of the elementary graphs and protographs

To derive the representation (1.8), the first step is to express $<W(\Box)>^{(1)}_{U_\theta(1)}$ in terms of the $S(4)-$multiplets of the effective $2n-$point functions. Each of these functions describes the corresponding elementary graph together with all its admissible $\mathcal{R}_a^{-1}-$ and $\bar{\mathcal{R}}_b^{-1}-$deformations according to the algorithm sketched in the previous section.

In view of the factorization (3.2), for $C=\Box$ it is convenient to represent the effective functions as the product $\mathcal{I}^{(n)}(\{\mathbf{y}_k\})\tilde{V}^{(n)}_{U_\theta(1)}(\{\mathbf{y}_k\})$, where $\{\mathbf{y}_k\}$ denotes the set of the relative coordinates (2.9) characterizing the corresponding time-ordered elementary graph of a given order $2n$. In particular, the factor $\mathcal{I}^{(n)}(\cdot)$ (to be defined in eq. (5.5)) accumulates the overall $\mathcal{R}_a^{-1}-$dressing of the latter graph. As for $\tilde{V}^{(n)}_{U_\theta(1)}(\cdot)$, it describes a given elementary graph together with the entire its $\bar{\mathcal{R}}_b^{-1}-$dressing in the way consistent with the $S(4)\otimes S(2)-$symmetry. In turn, the quantity $\tilde{V}^{(n)}_{U_\theta(1)}(\cdot)$ can be introduced as the concise modification of the corresponding elementary $2n-$point function (2.10). For this purpose, the perturbative propagators of certain $n-v$ lines should be replaced by the effective ones defined by the $f_k=1$ option of eq. (5.6).

[20] One is to identify $R=x^1(s_l)-x^1(s'_l)$, $s_l>s'_l$, with the spatial component of the relative distance (2.9) such that $\mathbf{x}(s_l)$ and $\mathbf{x}(s'_l)$ belong respectively to the lower and upper horizontal sides of the contour $C=\Box$. In turn, in view of the proper time parameterization fixed prior to eq. (2.4), it implies that the vertical $1-$axis is to be directed from the upper to the lower horizontal side of the rectangle $\Box$.

Parameterizing the effective functions, the elementary graphs can be viewed as the *intermediate* collective coordinates which are useful in the computation of the corresponding individual effective amplitudes

$$\frac{1}{(2\pi\bar{\theta})^2}\ \mathcal{Z}^{(\gamma)}_{jrv}(\{a_k\},\bar{A},\bar{\theta}^{-1}) = \oint\limits_C \prod_{l=1}^{n} dx^2(s_l)dx^2(s'_l)\ \mathcal{I}^{(n)}(\{\mathbf{y}_k\})\tilde{V}^{(n)}_{U_\theta(1)}(\{\mathbf{y}_k\})\Big|^{\gamma}_{jrv} \tag{5.1}$$

where the vertical $S(4)-$reattachments of the $h_{rv} = 2 + r - v$ lines are described by the set of the parameters $\{a_k\} \equiv \{a_k\}_{rv}$ introduced in subsection 4.3. By construction, the $G = 1$ term $< W(\Box) >^{(1)}_{U_\theta(1)}$ of the expansion (1.4) can be represented as the superposition of the amplitudes (5.1) which, as we will see, should be combined into the $rv-$superposition $\mathcal{Z}_{rv}(\{a_k\},\cdot)$. These superpositions are obtained summing up the amplitudes (5.1) corresponding to all $\sum_{j=1}^{2} f_{jv}$ elementary graphs which are associated with a given $rv-$protograph according to the prescription discussed in subsection 4.2.2. Then, eq. (1.8) is reproduced provided

$$\mathcal{Z}_{rv}(\bar{A},\bar{\theta}^{-1}) = \sum_{\{a_l\}_{rv}} \mathcal{Z}_{rv}(\{a_k\},\bar{A},\bar{\theta}^{-1})\,, \tag{5.2}$$

$$\mathcal{Z}_{rv}(\{a_k\},\bar{A},\bar{\theta}^{-1}) = \sum_{j=1}^{2}\sum_{\gamma=1}^{f_{jv}} \mathcal{Z}^{(\gamma)}_{jrv}(\{a_k\},\bar{A},\bar{\theta}^{-1})\,,$$

where f_{jv} is defined in eq. (4.1), and the sum over $\{a_l\}_{rv}$ includes the contribution of the four terms related through the $S(4)-$reattachments applied to the end-points of those lines which, being associated with the corresponding protograph, are parameterized by the label $l \in \mathcal{S}_{rv}$ (where the set $\mathcal{S}_{rv}$ is introduced in the end of subsection 4.2.4). In this way, $\mathcal{Z}_{rv}(\bar{A},\bar{\theta}^{-1})$ yields the contribution of the $S(4)-$multiplet of the dressed protographs endowed with a given $rv-$assignment. (In view of the factor h_{rv} present in eq. (1.8), eq. (5.2) takes into account that, when $h_{rv} = 2$, the dressed elementary diagrams can be collected into the pairs related via the reflection which leaves the amplitudes $\mathcal{Z}_{rv}(\bar{A},\bar{\theta}^{-1})$ invariant, as it is verified in appendix D.)

Then, building on the pattern of the perturbative functions (2.10), the amplitude $\mathcal{Z}_{rv}(\{a_k\},\cdot)$ can be reproduced in a way which reveals the important reduction resulting in the final set of the collective coordinates that, in turn, supports the relevance of the protographs. We postpone the discussion of this issue till subsection 5.3.1.

5.1 Introducing an explicit time-ordering

To proceed further, it is convenient to reformulate both $\mathcal{I}^{(n)}(\{\mathbf{y}_i\})$ and $\tilde{V}^{(n)}_{U_\theta(1)}(\{\mathbf{y}_i\})$ in terms of a minimal amount of independent variable arguments instead of the $n-$set $\{\mathbf{y}_i\}$ of the relative distances (2.9). Consider a rectangular contour $C = \Box$ such that R and T denote the lengths of its vertical and horizontal sides which, in the notations of eq. (2.3), are parallel respectively to the first and the second axis. Then, the subset $\{y^1_i\}$ can be reduced to the variety $\{a_k\}$ of the parameters discussed in the context of eq. (5.2). Concerning the reduction of the remaining subset $\{y^2_i\}$, it is implemented by the constraints (4.2) imposed

on the temporal components y_l^2, In consequence, there are only $m = n+2$ independent *time-ordered* parameters $\tau_k \geq \tau_{k-1}$ which can be chosen to replace the set of the $2n$ temporal coordinates $x^2(s_l)$ and $x^2(s'_l)$ assigned to the line's end-points of a given elementary graph.

There is a simple geometrical prescription to introduce τ_k (with $\tau_0 = 0,\ \tau_{m+1} = T$) in such a way that fits in the purpose of the further description both of the $\mathcal{R}_a^{-1}-$ and of the $\bar{\mathcal{R}}_b^{-1}-$dressing. It is convenient to introduce this prescription in the two steps. First, it is performed for those graphs in a given $S(4)-$multiplet (with a particular $\gamma jrv-$assignment) which are characterized by the maximal number $h_{rv} = 2 - v + r$ of the horizontal lines. Second, combining the $S(4)-$reattachments and the reflection, this prescription can be generalized to deal with the entire $S(4)-$multiplets collected into h_{rv} reflection-pairs. Here, we restrict the discussion to the first step. A more detailed representation of the algorithm is given in appendix A where, in particular, explained how the proposed prescription can be formulated in the way invariant both under the $S(4)-$reattachments and under the reflection.

We proceed with the observation that there are $m - v$ parameters τ_i which are directly identified with the properly associated coordinates $x^2(\cdot)$ in the latter $2n-$set. Consider the simplest $r = v = 0$ cases of the elementary graphs in figures 1a and 2c endowed with $h_{rv} = 2$ horizontal lines. Then, the m parameters τ_i simply relabel, according to the relative *time-ordering*, the set of the m end-points (of the graphs) attached in these two figures to the upper horizontal side of $C = \square$. In the $v = 1$ cases (described by the solid lines in figures 8a-8c for $r = 0$ and in figures 9a-9c for $r = 1$), there are as well the $m - 1$ direct reidentifications associated with the following end-points of the elementary graphs with h_{rv} horizontal lines. These are the left- and rightmost end-points of the graph (belonging to $1+r$ its distinct horizontal lines) together with all the remaining $m-3$ end-points attached to the lower horizontal side of C. As for one more still missing parameter τ_{i_0}, we are to consider j extra non-horizontal lines introduced in the following way. Each such line, being $\bar{\mathcal{R}}_b^{-1}-$copy of one of j distinct non-horizontal lines of the elementary graph, assumes the furthest admissible position compared to the latter line of the graph in question. When $r = 0$, the variable τ_{i_0} is to be identified with the lower end-point of the single extra line. When $r = 1$, the condition (4.3) implies that the lower end-points of the pair of the extra lines *coincide*, being therefore both identified with τ_{i_0}.

Next, on the upper (or, alternatively, lower) horizontal side of the rectangle C, τ_q and τ_{q-1} can be viewed as the bordering points of the $n+3$ connected non-overlapping intervals

$$\Delta\tau_{k-1} = \tau_k - \tau_{k-1} \ \geq \ 0 \quad , \quad \sum_{k=0}^{m} \Delta\tau_k = T \quad , \quad m = n+2 = j+r+3\,, \tag{5.3}$$

the overall time T is split into. Consequently, the previously introduced relative times[21]

$$t_p^{(\gamma)} \equiv y_p^2\Big|_{jrv}^{\gamma} = (-1)^{s_p(\{a_k\})} \sum_{l=0}^{m} d_{jrv}^{(\gamma)}(p,l)\ \Delta\tau_l \quad , \quad d_{jrv}^{(\gamma)}(p,0) = d_{jrv}^{(\gamma)}(p,m) = 0\,, \tag{5.4}$$

can be represented as the superpositions of $\Delta\tau_k$, and for simplicity we omit the superscript jrv in the notation $t_p^{(\gamma)}$. In eq. (5.4), $d_{jrv}^{(\gamma)}(p,l) = 0, \pm 1$, while $s_p(\{a_k\})$ denotes an integer-valued $p-$dependent function[22] which additionally depends on the set $\{a_k\}$ of the variables introduced after eq. (4.4). E.g., the geometry of figures 8a and 8b implies that $t_2^{(1)} < 0$ and $t_2^{(2)} > 0$ respectively. Let us also note that the $S(4)-$symmetry of the dressing of the elementary graphs implies that the pattern of $t_p^{(\gamma)}$ is the same for all members of each $S(4)-$multiplet.

5.2 Accumulating the $\mathcal{R}_a^{-1}-$deformations

Given a particular effective amplitude, the associated $\mathcal{R}_a^{-1}-$deformations a given elementary graph are generated via *all* possible inclusions of such extra lines that, in accordance with eq. (3.1), intersect neither each other nor the original lines of the graph. In figures 3-9 the latter extra lines are depicted as vertical (due to the $\delta-$function in the perturbative propagator (2.3)) and dotted. In view of eq. (3.2), the inclusion of the deformations of this type merely multiplies the amplitude, describing the original elementary graph, by a factor $\mathcal{I}^{(n)}(\{\mathbf{y}_k\})$. To deduce this factor, we note that the temporal coordinates of the upper end-points of the $\mathcal{R}_a^{-1}-$copies may span only the first and the last intervals $\Delta\tau_0$ and $\Delta\tau_{n+2}$ respectively. Then, akin to the commutative case, it is straightforward to obtain that, when the superposition of all the admissible $\mathcal{R}_a^{-1}-$copies is included, it result in

$$\mathcal{I}^{(n)}(\{\mathbf{y}_k\}) = exp\left(-\sigma|R|\left[\Delta\tau_0 + \Delta\tau_{n+2}\right]\right)\,, \tag{5.5}$$

the τ_j-dependence of which matches the pair of the conditions (5.4) imposed on $d_{jrv}^{(\gamma)}(p,l)$.

5.3 The $\bar{\mathcal{R}}_b^{-1}-$deformations and the effective propagators

Next, consider the block $\tilde{V}^{(n)}_{U_\theta(1)}(\cdot)$ that results after the $\bar{\mathcal{R}}_b^{-1}-$dressing of a given elementary graph with n lines. The short-cut way to reconstruct this block is to specify those $n - v$ (with $v = 0, 1$) lines of the latter graph where the corresponding propagator (2.3) is replaced, in the relevant implementation of eq. (2.10), by its effective counterpart so that the $S(4)-$symmetry of the overall dressing is maintained. When the kth line is dressed by all admissible $\bar{\mathcal{R}}_b^{-1}-$deformations, the replacement is fixed by the $f_k = 1$ option of the substitution

$$D_{22}(\mathbf{z}_k) \longrightarrow \left(-\sigma|z_k^1|\right)^{f_k}\,\delta\left(z_k^2\right)\ exp\Big(-\sigma|R + (z_k^1 - y_k^1)\alpha^{(k)}|\Delta T_k^b(f_k,\gamma)\Big)\,, \quad k \in \Omega_{2rv}\,, \tag{5.6}$$

[21] As the temporal intervals y_l^2 are overlapping in general, it hinders a resolution the $G = 1$ constraints (4.2) directly in terms of these intervals. On the other hand, the $n > 2$ splitting (5.4) yields the concise form to represent, for any given time-ordered component of a Feynman graph, the latter resolution employing the *non-overlapping* intervals $\Delta\tau_k$.

[22] The explicit form of this function is fixed by eq. (D.5) in appendix D.

that reduces to the ordinary multiplication of the propagator $D_{22}(\cdot)$ by the $k-$dependent exponential factor (with the set Ω_{jrv} of the $n-v$ different labels being defined in the end of subsection 4.2.4). In this factor, the parameter $\alpha^{(k)} = \pm 1$ is traced back to eq. (3.8), and each elementary graph is unambiguously endowed with a single $\{\alpha^{(i)}\}-$assignment (with $i \in \Omega_{jrv}$).

Also,

$$\Delta T_k^b(f_k,\gamma) \,=\, \Delta\tau_{q(k)} + [1-f_k]\Delta\tau_{q(k)+2\omega_k^{(\gamma)}-1},$$
$$\Delta T_q^a \,=\, \Delta\tau_q \;\;,\;\; q = 0, n+2\,,$$

(i.e., $f_0 = f_{n+2} = 1$), while the extra subscripts a and b are introduced to indicate the type of the associated deformations. In turn, in the $f_k = 1$ case the interval $\Delta T_k^b(1,\gamma) = \Delta\tau_{q(k)}$ is spanned by the end-points of the $\bar{\mathcal{R}}_b^{-1}-$copies of the kth line (see subsection 4.2.4 for particular examples). As for the function $q(k)$ defining the label of the corresponding interval (5.3), it formally determines an embedding of an element of the $S(n-v)$ group of permutations into the $S(n+1)$ group: $0 < q(k) < n+2$ for all different $n-v$ values of $k \in \Omega_{jrv}$. In appendix A, we sketch a simple rule which allows to reconstruct $q(k)$ so that, for any given $S(4)-$multiplet, this function is the same for all four elementary graphs in this multiplet.

5.3.1 The completeness of the $\bar{\mathcal{R}}_b^{-1}-$dressing of the protographs

To explain the relevance of a certain $f_k \neq 1$ option of the replacement (5.6), we should take into account that, in the evaluation of the amplitude $\mathcal{Z}_{rv}(\{a_k\},\cdot)$ defined by eq. (5.2), there are important cancellations between the contributions of the individual effective amplitudes (5.1). To obtain $\mathcal{Z}_{rv}(\{a_k\},\cdot)$ for a particular $rv-$assignment, it is sufficient to take the *single* $j = 2$ elementary graph (unambiguously associated with the corresponding protograph) and apply, according to a judicious $\{f_k\}-$assignment, the replacement (5.6) to the same $n-v$ lines of this graph as previously. But, contrary to the computation of the amplitudes (5.1), the $f_k = 1$ variant of the replacement (5.6) remains to be applied only to the $2+r-2v$ lines involved into the $S(4)-$reattachments. The point is that $f_k = 0$ for all the $(v+j-1)|_{j=2}$ lines which, being not affected by the reattachments (while labeled[23] by $k \in \tilde{\Omega}_{2rv}/\mathcal{S}_{rv}$, i.e., $k = 3$ and, when $v = 1$, $k = 3-v$), therefore do *not* belong to the protograph. Furthermore, it is accompanied by such reduction of the measure that, implying the a specific completeness condition discussed below, retains relevant variable arguments which, at least in the simpler $r = v = 0$ case, are associated only with the corresponding protograph. It is further discussed in subsection 7.3, where a more subtle situation for other values of r and v is also sketched.

To interpret $\Delta T_k^b(0,\gamma)$ geometrically (for $k = 3-v, 3$), for a given elementary graph with the maximal number h_{rv} of horizontal lines, let us fix the positions of the end-points of the latter lines (involved into the $S(4)-$reattachments) and ,when $v = 1$, the value of $t_2^{(\gamma)}$. In view of the constraints (4.2), it leaves only the possibility to perform parallel transport of each of the $n - h_{rv}$ non-horizontal lines of the graph. Correspondingly, from

[23] Recall that the sets $\tilde{\Omega}_{jrv}$ and $\mathcal{S}_{rv}$ are introduced in the end of subsection 4.2.4.

figures 5b, 8a-c and 9a-c, we note that the intervals $\Delta\tau_{q(k)}$ are completely fixed for those k which label the $h_{rv}-v$ horizontal lines endowed with the individual $\bar{\mathcal{R}}_b^{-1}-$dressing. On the other hand, the value of each of the $n-h_{rv}$ remaining intervals $\Delta\tau_{q(k)}$, associated with the dressing of the non-horizontal lines, varies when one implements an admissible parallel transport of the kth non-horizontal line (with $k\in\tilde{\Omega}_{jrv}/\mathcal{S}_{rv}$). In turn, it implies that, with each of the latter $n-h_{rv}$ intervals $\Delta\tau_{q(k)}$, one necessarily associates the following *adjacent* interval $\Delta\tau_{q(k)+2\omega_k^{(\gamma)}-1}$ (with $2\omega_k^{(\gamma)}-1=\pm 1$) such that $0<q(k)+2\omega_k^{(\gamma)}-1<n+2$, (i.e., $\Delta T_k^b(f_k,\gamma)\cap\Delta T_0^a=\Delta T_k^b(f_k,\gamma)\cap\Delta T_{2+n}^a=0$, $\forall k\in\Omega_{jrv}$). Being *not* spanned by $\bar{\mathcal{R}}_b^{-1}-$copies of the lines of the graph (i.e., $q(p)\neq q(k)+2\omega_k^{(\gamma)}-1$ for $\forall k\in\Omega_{jrv}/\mathcal{S}_{rv}$, $\forall p\in\Omega_{jrv}$, $\forall\gamma$), this adjacent interval is bounded from one side by the appropriate end-point of the kth non-horizontal line. The coordinate of the latter end-point is equal to $\tau_{q(k)+\omega_k^{(\gamma)}}$ so that the parameter $\omega_k^{(\gamma)}$ is equal to 0 and 1 when thus introduced interval $\Delta\tau_{q(k)+2\omega_k^{(\gamma)}-1}$ is located respectively to the left and to the right with respect to $\Delta\tau_{q(k)}$. We refer to subappendix B.1 for more details.

Given the geometrical interpretation of $\Delta T_k^b(0,\gamma)$, the emphasized above cancellations (between the amplitudes (5.1)) result, for any admissible $\{f_k\}-$assignment, in the important completeness condition fulfilled by the $n-v=\sum_{k\in\Omega_{2rv}}1$ intervals[24] $\Delta T_k^b(f_k,1)$:

$$\sum_{k\in\Omega_{2rv}}\Delta T_k^b(f_k,1)=T-\Delta T_0^a-\Delta T_{n+2}^a\,,\qquad\qquad\sum_{k\in\Omega_{2rv}}f_k=2+r-2v\,,\tag{5.7}$$

where each $\Delta T_k^b(f_k,1)$ is spanned by the end-points of the $\bar{\mathcal{R}}_b^{-1}-$copies. As it will be verified in subsection 7.2, in a given $rv-$protograph these copies are associated with the kth line of the corresponding $j=2$ elementary diagram,

To explain the meaning of eq. (5.7) (to be verified in subappendix B.1), we first note that the residual time-interval $T-\Delta T_0^a-\Delta T_{n+2}^a$ results from the overall temporal domain T after the exclusion of its left- and rightmost segments ΔT_0^a and ΔT_{n+2}^a which (entering the factor (5.5)) are spanned by the end-points of the $\mathcal{R}_a^{-1}-$copies. Also, the $n-v$ open intervals $\Delta T_k^b(f_k,1)$ are mutually non-overlapping, $\Delta T_k^b(f_k,1)\cap\Delta T_q^b(f_q,1)=0$ for $\forall k\neq q$, which means that $q(p)\neq q(k)+2\omega_k^{(1)}-1$ $\forall k\in\Omega_{2rv}/\mathcal{S}_{rv}$, $\forall p\in\Omega_{2rv}$. Then, the completeness condition (5.7) geometrically implies therefore that, once a particular $rv-$protograph is fully dressed, the *entire* residual time-interval is covered by the $n-v=3+r-v$ mutually non-overlapping intervals $\Delta T_k^b(f_k,1)$. Examples are described by figures 5c (with $r=v=0$), 8f (with $r=v-1=0$), and 9f (with $r=v=1$).

On the other hand, in the evaluation of the individual effective amplitudes (5.1), the sum in the l.h. side of eq. (5.7) is replaced by the sum $\sum_{k\in\Omega_{jrv}}\Delta\tau_{q(k)}<T-\Delta T_0^a-\Delta T_{n+2}^a$ which generically is less than the residual time-interval. In turn, this inequality follows from the fact that the number $n+1$ of the relevant elementary intervals $\Delta\tau_k$ (the residual interval is decomposed into so that $\sum_{i=1}^{n+1}\Delta\tau_i=T-\Delta T_0^a-\Delta T_{n+2}^a$) is always less than the number $n-v=\sum_{k\in\Omega_{2rv}}1$ of the lines involved into the $f_k=1$ dressing (5.6). Examples are presented in the $j=2$ case by figures 5b, 8c, and 9c.

[24] One is to fix $\gamma=1$ owing to the $j=2$ option of eq. (4.1).

Finally, for the purposes of subsection 6.1, in the $v = 1$ cases it is convenient to define both $\omega_k^{(\gamma)}$ and $\Delta T_k^b(f_k, \gamma)$ not only for $j = 2$ but for $j = 1$ as well. As it is verified in subappendix B.1, the extension is fixed by the prescription:[25] $\omega_2^{(\gamma)}|_{j=1} = \omega_{4-\gamma}^{(1)}|_{j=2}$ with $\gamma = 1, 2$, while $\Delta T_k^b(f_k, \gamma)$ is to be defined by the same eq. (5.7).

It is also noteworthy that, together with the $\gamma-$dependence of $t_p^{(\gamma)}$ introduced in eq. (5.4), the $\gamma-$dependence of the auxiliary parameter $\omega_k^{(\gamma)}$ is the only source of the $\gamma-$dependence of the effective amplitude $\mathcal{Z}_{jrv}^{(\gamma)}(\cdot)$ in the $f_{jv} = 2$ case (see subsection 7.1) associated with the elementary graphs in a $S(4)-$multiplet with a given $\gamma jrv-$assignment. In turn, the $S(4)-$symmetry of the dressing of the elementary graphs guarantees that (as well as in the case of $t_p^{(\gamma)}$) the pattern of $\omega_k^{(\gamma)}$ is the same for all members of each $S(4)-$multiplet.

6. The structure of the effective amplitude $\tilde{V}^{(n)}_{U_\theta(1)}(\{\mathbf{y}_k\})$

The convenient representation (6.1) of the factor $\tilde{V}^{(n)}_{U_\theta(1)}(\cdot)$, describing a given $2n$th order elementary graph together with the entire its $\bar{\mathcal{R}}_b^{-1}-$dressing, can be deduced from the integral representation of the elementary $2n-$point function (2.10) through the simple prescription. For this purpose, the product of the concise exponential factors (6.3) is to be included under the integrand of such representation of the function (2.10) that generalizes eq. (2.5). In subsection 6.2, we present a brief verification that this prescription matches the result of the appropriate application of the $n - v$ replacements (5.6) with $f_k = 1$.

6.1 The $\bar{\mathcal{R}}_b^{-1}-$deformations of the elementary $2n-$point functions

Let us introduce the effective functions $\tilde{V}^{(n)}_{U_\theta(1)}(\{\mathbf{y}_k\})$ in a way that makes manifest the relations between those functions which are parameterized by the elementary graphs with a given $rv-$assignment. For this purpose, we first get rid[26] of the $n - 2 = r + j - 1$ $\delta(\cdot)-$functions (defined by the $G = 1$ eq. (4.2)), starting with the $(r + j - 1)-$fold integral

$$\int\limits_{-T}^{T} d^{j-1}t_3^{(\gamma)}\; d^r t_4^{(\gamma)}\; \tilde{V}^{(n)}_{U_\theta(1)}(\{\mathbf{y}_k\})\Big|_{jrv}^{\gamma} = J_{jrv}\left[\frac{(-1)^{\omega_3^{(\gamma)}-1}\partial}{\partial\tau_{q(3)+\omega_3^{(\gamma)}}}\right]^{j-1}\left[\frac{(-1)^{\omega_2^{(\gamma)}-1}\partial}{\partial\tau_{q(2)+\omega_2^{(\gamma)}}}\right]^{v}\times$$
$$\times\tilde{\mathcal{V}}_{jrv}^{(\gamma)}(\{a_i\},\{\Delta\tau_{q(k)}\}), \tag{6.1}$$

where $J_{jrv} = (-1)^{v+j-1}\sigma^{2+r-v}/(2\pi\theta)^2$, $\omega_k^{(\gamma)} = 0, 1$ is introduced in subsection 5.3.1 on the basis of eq. (5.7), and (for the sake of generality) we temporarily formulate the integration in terms of the relative times (5.4) (rather than $x^2(\cdot)$), postulating that $\int d^0x\tilde{V}(y) = \tilde{V}(y)$.

[25] It matches eq. (B.6).

[26] It is admissible because the effective amplitude (5.1) anyway involves the contour integrals over the $2n$ temporal coordinates $x^2(\cdot)$ of the lines' end-points which define the set $\{\mathbf{y}_k\}$. Also, the lines are labeled in subsection 4.2.4 so that the fourth line, being present only in the $r = v = 1$ cases, is the $\mathcal{R}_b^{-1}-$copy of the first line. As for the third line, being present only in the $j = 2$ cases, it is *not* involved into the $S(4)-$reattachments as well as the second line (present in all cases).

Then,

$$\tilde{\mathcal{V}}^{(\gamma)}_{jrv}(\{a_i\},\{\Delta\tau_{q(k)}\}) = \int d\zeta d\eta\; e^{i\left(\eta t_1^{(\gamma)}-\zeta t_2^{(\gamma)}\right)\mathcal{C}_{21}/\theta}\; \mathcal{K}_{rv}(\zeta,\eta,\{a_i\})\;\times \\ \times\left[\mathcal{F}(\alpha^{(1)}\zeta,\Delta\tau_{q(1)})\right]^{1-v}\mathcal{F}(\alpha^{(2)}\eta,\Delta\tau_{q(2)})\times \\ \times\left[\mathcal{F}(\alpha^{(3)}T_{\mathcal{C}_{ij}}(\eta,\zeta),\Delta\tau_{q(3)})\right]^{j-1}\left[\mathcal{F}(\alpha^{(1)}\zeta,\Delta\tau_{q(4)})\right]^{r}\,, \quad (6.2)$$

with[27] $\alpha^{(k)}$, $\mathbf{y}_k$, $\mathcal{C}_{ij}$, and $t_p^{(\gamma)}$ being given by eqs. (3.7), (2.9), (2.11), and (5.4) respectively, while

$$\tilde{\mathcal{K}}_{rv}(\zeta,\eta,\{a_i\}) = |a_1R+\zeta|\;|a_2R+\eta|^{1-v}|a_4R+\alpha^{(1)}\zeta|^{r} \quad , \quad y^1_k = a_kR\,, \\ \mathcal{F}(\eta,\Delta\tau_{q(k)}) = exp\left(-\sigma|R+\eta|\Delta\tau_{q(k)}\right)\,, \quad (6.3)$$

where $\Delta\tau_{q(k)}$ is the same $k\to q(k)$ option of the time-interval (5.3) as in the $f_k=1$ variant of eq. (5.6), and

$$T_{\mathcal{C}_{ij}}(\eta,\zeta) = (\mathcal{C}_{31}/\mathcal{C}_{21})\eta - (\mathcal{C}_{32}/\mathcal{C}_{21})\zeta\,, \quad (6.4)$$

with $|\mathcal{C}_{21}|=1$.

Next, eq. (6.1) is to be augmented by the $r+j-1$ constraints (imposed by thus resolved $\delta-$functions of eq. (4.2)) that results in the relations

$$(j-1)\left(t_3^{(\gamma)} - T_{\mathcal{C}_{ij}}(t_2^{(\gamma)},t_1^{(\gamma)})\right) = 0 \quad , \quad r\left(t_1^{(\gamma)}-\alpha^{(1)}t_4^{(\gamma)}\right) = 0\,, \quad (6.5)$$

where, the second condition yields (when $r=1$) the implementation of the general constraint (3.6), while the first one (imposed when $j=2$) merely reformulates the condition (4.3) (to be interpreted geometrically in appendix B). It also noteworthy that the r.h. side of eq. (6.1) depends on γ *only* through the $\gamma-$dependent quantities $\omega_p^{(\gamma)}$ together with the $\gamma-$dependent decomposition (5.4) of the parameters $t_1^{(\gamma)}$ and $t_2^{(\gamma)}$ entering eq. (6.2).

Finally, by construction of $\omega_k^{(\gamma)}=0,1$ (geometricall interpreted in subsection 5.3.1), in the r.h. side of eq. (6.1) the partial derivative $\partial/\partial\tau_{q(p)+\omega_p^{(\gamma)}}$ acts only on the pth factor (6.3) (with $p=3-v,3$) of the integrand in the expression (6.2). In consequence, these derivatives merely insert, under the integrand, the $r+j-1$ factors $-\sigma|R+\mathcal{G}_p(\zeta,\eta)|$ entering the exponent of eq. (6.3):

$$\left[\frac{(-1)^{\omega_3^{(\gamma)}-1}\partial}{\partial\tau_{q(3)+\omega_3^{(\gamma)}}}\right]^{j-1}\left[\frac{(-1)^{\omega_2^{(\gamma)}-1}\partial}{\partial\tau_{q(2)+\omega_2^{(\gamma)}}}\right]^{v} \quad\longrightarrow\quad (-\sigma)^{j-1+v}|R+T_{\mathcal{C}_{ij}}(\eta,\zeta)|^{j-1}|R+\eta|^{v}\,, \quad (6.6)$$

where we have used that $\alpha^{(2)}=1$ when $v=1$, while $\alpha^{(3)}=1$ when $j=2$. A formal proof of eq. (6.6) is sketched in appendix B

[27] Actually, the quantities $\alpha^{(k)}\equiv\alpha^{(k)}(\{a_k\})$, $\mathcal{C}_{ij}\equiv\mathcal{C}_{ij}(\{a_k\})$, and $t_p^{(\gamma)}\equiv t_p^{(\gamma)}(\{a_k\})$ implicitly depend (see appendix D) on the set $\{a_k\}$ of the variables introduced after eq. (4.4).

6.2 Relation to the elementary $2n-$point functions

Before we discuss how to reinterpret the partial integrand of the effective function (6.1) in compliance with the replacement (5.6), the intermediate step is to establish the relation between the latter function and its counterpart associated with the corresponding elementary graph. Also, we point out a preliminary indication of the relevance of the parameterization in terms of the protographs.

Once the replacement (6.6) is performed, the general rule states that, for any admissible $n = 1 + j + r$, the integral representations of a given elementary $2n-$point function $V^{(n)}_{U_\theta(1)}(\{\mathbf{y}_k\})$ can be deduced from the corresponding effective one $\tilde{V}^{(n)}_{U_\theta(1)}(\{\mathbf{y}_k\})$ through the replacement

$$\mathcal{F}(\cdot, \Delta\tau_{q(k)}) \longrightarrow 1 \ , \ \forall k \qquad \Longrightarrow \qquad \tilde{V}^{(n)}_{U_\theta(1)}(\{\mathbf{y}_k\}) \longrightarrow V^{(n)}_{U_\theta(1)}(\{\mathbf{y}_k\}) \,, \tag{6.7}$$

with $\mathcal{F}(\cdot)$ being defined by eq. (6.3). In particular, (provided $\mathcal{C}_{12} = -1$) the reduced option (6.7) of the $r = v = j - 1 = 0$ implementation of the function (6.1), being associated with the diagrams of figure 1, assumes the form of integral representation of the $f_k(\mathbf{z}) \to D_{22}(\mathbf{z}),\ k = 1, 2$ implementation of the star-product (2.5), where the propagator $D_{22}(\mathbf{z})$ is introduced in eq. (2.3). It is manifest after the identifications: $\zeta \to \xi^1_1,\ \eta \to \xi^1_2$. Correspondingly, the kth factor $(\mathcal{F}(\cdot, \Delta\tau_{q(k)}) - 1)$ accumulates the contribution of all admissible $\bar{\mathcal{R}}_b^{-1}-$copies of the kth line so that the interval[28] $\Delta\tau_{q(k)}$ is spanned by the temporal coordinates of the upper (or, equivalently, lower) end-points of the latter copies.

Altogether, in thus reduced eq. (6.1) the integral representation $V^{(n)}_{U_\theta(1)}(\{\mathbf{y}_k\})$ of a given $2n$th order elementary graph includes, besides the exponential factor $e^{i(\eta t_1 - \zeta t_2)\mathcal{C}_{21}/\theta}$ (inherited from eq. (2.5)) and the $G = 1$ product (4.2) of $n - 2$ different $\delta(\cdot)-$functions, the product

$$\tilde{\mathcal{K}}_{n+2}(\zeta, \eta, R) = \prod_{i=1}^{4} |a_i R + \mathcal{G}_i(\zeta, \eta)|^{w_i} \qquad , \qquad \mathcal{G}_k(\zeta, \eta) = \tilde{b}_k \zeta + \tilde{c}_k \eta \,, \tag{6.8}$$

composed of $n = 1 + j + r$ factors $|a_i R + \mathcal{G}_i(\zeta, \eta)|$ each of which represents (when[29] $w_i \neq 0$) the ith propagator of the latter graph so that $w_1 = w_2 = 1,\ w_3 = j - 1 = 0, 1,\ w_4 = r = 0, 1$ with $\sum_{i=1}^{4} w_i = n$. Here, a_k is defined in eq. (6.3), $\tilde{b}_q, \tilde{c}_q = 0, \pm 1$, while R is defined in the footnote prior to eq. (4.4), and $2 \leq n \leq 4$. In turn, it is the $\tilde{\mathcal{K}}_{rv}(\cdot)-$part (6.3) of $\tilde{\mathcal{K}}_{n+2}$ which, being associated with the $2 + r - v$ lines involved into the $S(4)-$reattachments (when a_k assumes both of the admissible values), refers to the protographs. The remaining $v + j - 1$ lines, corresponding to the $f_k = 0$ option of the replacement (5.6), are not affected by the reattachments so that the corresponding a_k are equal to unity which matches the $a_k = 1$ pattern of the exponents (6.3) *necessarily* associated with all these lines via the replacement (6.6).

In conclusion, it is routine to convert the inverse of the prescription (6.7) into the composition of the replacements (5.6). In view of eq. (6.6), the general pattern (6.1) is

[28] It is noteworthy that, underlying the solvability of the problem, the *local* in $\Delta\tau_{q(k)}$ pattern of the factor (6.3) is traced back to the specific constraints (3.6) imposed by the perturbative amplitudes (2.10).

[29] I.e., for $i \in \tilde{\Omega}_{jrv}$, with the set $\tilde{\Omega}_{jrv}$ being introduced in subsection 4.2.4.

such that any particular effective $2n-$point function $\tilde{V}^{(n)}_{U_\theta(1)}(\{\mathbf{y}_k\})$ can be deduced from the associated elementary one through the corresponding option of the replacement

$$\prod_{k=1}^{4}|a_kR+\mathcal{G}_k(\zeta,\eta)|^{w_k}\;\longrightarrow\;\prod_{k=1}^{4}|a_kR+\mathcal{G}_k(\zeta,\eta)|^{w_k}\;e^{-\sigma v_k|R+\mathcal{G}_k(\zeta,\eta)\alpha^{(k)}|\Delta\tau_{q(k)}}\,, \tag{6.9}$$

where $v_1=1-v=0,1$, $v_k=w_k$, for $k=2,3,4$ (with $v_k\neq 0$ only when $k\in\Omega_{jrv}$, where Ω_{jrv} is introduced in subsection 4.2.4) so that $\sum_{k=1}^{4}v_i=n-v$. In turn, it matches the pattern of eq. (6.2). Then, it takes a straightforward argument to verify that the substitution (6.9) is indeed equivalent to the $f_k=1$ prescription (5.6) applied, with the identification $\alpha^{(4)}=\alpha^{(1)}$, to the corresponding $\Omega_{jrv}-$subset of the $n-v$ perturbative propagators.

7. Integral representation of the effective amplitudes

At this step, we are ready to obtain the explicit form of the amplitude $\mathcal{Z}_{rv}(\bar{A},\bar{\theta}^{-1})$ which, being introduced in eq. (5.2), defines the decomposition (1.8) of the $G=1$ term $<W(\square)>^{(1)}_{U_\theta(1)}$ of the $1/N$ expansion (1.4). For this purpose, we first put forward the general representation (7.1) of the individual effective amplitudes (5.1) which, being parameterized by the corresponding elementary graphs, are evaluated *non-perturbatively* both in g^2 and in θ. The latter amplitudes arise when the $2n-$point function $\tilde{V}^{(n)}_{U_\theta(1)}(\{\mathbf{y}_k\})$, being multiplied by the factor (5.5), is integrated over the n pairs of the relative coordinates (2.9) (defining the set $\{\mathbf{y}_k\}$), all restricted to the contour $C=\square$.

Then, building on this representation, the superposition (5.2) of $\mathcal{Z}^{(\gamma)}_{jrv}(\cdot)$ is evaluated collecting together the contributions associated with all the elementary graphs endowed with the same $rv-$assignment. In turn, the specific cancellations, taking place between the different terms of the superposition, support the pattern of the relevant collective coordinates. In particular, it verifies the representation of $\tilde{V}^{(n)}_{U_\theta(1)}(\cdot)$ (discussed in subsection 5.3.1) formulated in terms of the properly dressed protographs. We also clarify the relation between the latter dressing and the structure of the collective coordinates.

7.1 General pattern of the individual effective amplitudes

Synthesizing the factors (5.5) and (6.1), one concludes that the individual effective amplitudes (5.1) assume the form

$$\begin{aligned}(-1)^{\sum_{l\in\mathcal{S}_{rv}}a_l}\;\mathcal{Z}^{(\gamma)}_{jrv}(\{a_k\},\bar{A},\bar{\theta}^{-1})=\bar{A}^{2+h_{rv}}\int d^{n+2}\bar{\tau}e^{-\bar{A}(\Delta\bar{\tau}_0+\Delta\bar{\tau}_{n+2})}\left[\frac{(-1)^{\omega_3^{(\gamma)}-1}\partial}{\partial\tau_{q(3)+\omega_3^{(\gamma)}}}\right]^{j-1}\times\\ \times\left[\frac{(-1)^{\omega_2^{(\gamma)}-1}\partial}{\partial\tau_{q(2)+\omega_2^{(\gamma)}}}\right]^{v}\mathcal{V}^{(\gamma)}_{jrv}(\{a_i\},\{\Delta\bar{\tau}_{q(k)}\}),\end{aligned} \tag{7.1}$$

where the sum in the l.h. side runs over the labels l of the $2+r-v$ lines involved into the $S(4)-$reattachments in the first relation of eq. (5.2) (with the set $\mathcal{S}_{rv}$ being specified

in the end of subsection 4.2.4), and we introduce the compact notation

$$\int\limits_{0\leq\bar{\tau}_k\leq\bar{\tau}_{k+1}}^{\bar{\tau}_m\leq 1}\prod_{l=1}^{m}d\bar{\tau}_l\ldots\equiv\int d^m\bar{\tau}\ldots\,, \tag{7.2}$$

for the integrations over the $m=n+2$ ordered times $\bar{\tau}_j$, and, for a rectangular contour $C=\square$ of the size $R\times T$, it is convenient to utilize the change of the variables

$$\tau_k=T\bar{\tau}_k\quad,\qquad t_k=T\bar{t}_k\quad,\qquad \zeta=R\bar{\zeta}\;,\quad \eta=R\bar{\eta}\,, \tag{7.3}$$

which introduces the dimensionless quantities $\bar{\tau}_k$ (with $\Delta\bar{\tau}_{k-1}=\bar{\tau}_k-\bar{\tau}_{k-1}\geq 0$), $\bar{\eta}$, $\bar{\zeta}$, and $\bar{t}_k$ so that $R^{4+r-v}\mathcal{V}_{jrv}(\{a_i\},\{\Delta\bar{\tau}_{q(k)}\})=\tilde{\mathcal{V}}_{jrv}(\{a_i\},\{T\Delta\bar{\tau}_{q(k)}\})$. In particular, this change makes it manifest that, besides the dependence on $\{a_i\}$ and $\bar{\theta}=\sigma\theta$, the considered effective amplitudes are certain functions of the dimensionless area of the rectangle C

$$\bar{A}=\sigma A(C)\Big|_{C=\square}=\sigma RT \tag{7.4}$$

rather than of R and T separately.

Note also that in the r.h. side of eq. (7.1) the $m=n+2$ species of the $d\bar{\tau}_j-$integrations reproduce,[30] according to the discussion of subsection 5.1, the $2n-$fold contour-integral (5.1) which runs over the time-coordinates $dx^2(s_l)$ and $dx^2(s'_l)$ constrained by the $G=1$ product (4.2) of the $\delta(\cdot)-$functions. Correspondingly, this transformation of the measure has the Jacobian which is equal to $(-1)^{n^-_{jrv}}$, where n^-_{jrv} and n^+_{jrv} denote the numbers of the line's end-points attached, for a given elementary graph, respectively to the lower and upper horizontal side of the rectangle $C=\square$ so that

$$(-1)^{n^-_{jrv}}=\prod_{i\in\tilde{\Omega}_{jrv}}(-1)^{a_i}\qquad,\qquad \frac{1}{2}(n^+_{jrv}+n^-_{jrv})=n_{jrv}\equiv n=\sum_{k\in\tilde{\Omega}_{jrv}}1\,, \tag{7.5}$$

where a_k is defined in eq. (6.3), while the set $\tilde{\Omega}_{jrv}$ is specified in the end of subsection 4.2.4. In turn, to justify the $\{a_k\}-$dependent sign-factor in the l.h. side of eq. (7.1), it remains to notice that $\sum_{k\in\tilde{\Omega}_{jrv}}a_k=v+j-1+\sum_{l\in\mathcal{S}_{rv}}a_l$ since $a_k=1$ for $\forall k\in\tilde{\Omega}_{jrv}/\mathcal{S}_{rv}$.

7.2 Derivation of the combinations $\mathcal{Z}_{rv}(\bar{A},\bar{\theta}^{-1})$

The effective amplitudes (7.1), parameterized by the individual elementary graphs, are still intermediate quantities. To say the least, for generic $\bar{A}$, they are *singular* for $\bar{\theta}^{-1}\to 0$. To arrive at amplitudes which are already continuous in $\bar{\theta}^{-1}$ in a vicinity of $\bar{\theta}^{-1}=0$, our aim is to evaluate the combinations (5.2) of the latter amplitudes entering the decomposition (1.8).

Then, to reveal the cancellations between different terms of the sum (5.2), in the r.h. side of eq. (7.1) one is to perform $v+j-1$ integrations to get rid of the corresponding number of the partial derivatives (employing that $0<q(k)<n+2$ for $\forall k=1,\ldots,n$). In

[30] To make use of eq. (6.1), we utilize the fact that, owing to the $G=1$ pattern (4.2), the integrations $\int d^{j-1}t_3\;d^rt_4$ can be reformulated as $r+j-1$ integrations with respect to the temporal coordinates $x^2(\cdot)$ of those end-points which are *not* involved into the definition of τ_k.

appendix B, it is shown that, matching the prescription (5.6) formulated in subsection 5.3.1, a straightforward computation yields

$$\mathcal{Z}_{rv}(\bar{A},\bar{\theta}^{-1}) = \bar{A}^{2+h_{rv}} \sum_{\{a_l\}_{rv}} (-1)^{\sum_{l\in\mathcal{S}_{rv}} a_l} \int d^{2+h_{rv}}\bar{\tau}\; e^{-\bar{A}(\Delta\bar{\tau}_0+\Delta\bar{\tau}_{2+h_{rv}})}\; \mathcal{V}_{2rv}(\{a_k\},\{\Delta\bar{T}^b_k\})\,, \tag{7.6}$$

where the sum over a_l is the same as in eq. (5.2), $\tilde{\mathcal{V}}_{2rv}(\cdot) \equiv \tilde{\mathcal{V}}^{(1)}_{2rv}(\cdot)$ is defined in eq. (6.2), and we have omitted the subscript $\gamma = 1$ since, in view of eq. (4.1), γ assumes the single value for $j = 2$ irrespectively of the values of r and v. Note that, in the exponent, $\Delta\bar{\tau}_{n+2}$ is replaced by $\Delta\bar{\tau}_{2+h_{rv}} \equiv T^{-1}\Delta T^a_{2+h_{rv}}$ while, in the quantity $\mathcal{V}_{2rv}(\cdot,\cdot)$, the set $\{\Delta\bar{\tau}_{q(k)}\}$ is superseded by $\{\Delta\bar{T}^b_k\} \equiv \{\Delta\bar{T}^b_k(f_k,1)\}$, where the intervals $\Delta\bar{T}^b_k(f_k,1) = T^{-1}\Delta T^b_k(f_k,1)$, being constrained by the condition (5.7), are introduced in eq. (5.7). Altogether, omitting the subscripts a and b, the relevant $3+h_{rv}$ intervals $\Delta\bar{T}_i = \bar{\tau}_{i+1} - \bar{\tau}_i \geq 0$ are expressed through $2+h_{rv}$ ordered quantities $\bar{\tau}_i$ characterized by the $m = 2+h_{rv}$ option of the measure (7.2).

Finally, according to appendices C and D, the r.h. side of eq. (7.6) can be rewritten in the form

$$\mathcal{Z}_{rv}(\bar{A},\bar{\theta}^{-1}) = \bar{A}^{2+h_{rv}} \int d^{2+h_{rv}}\bar{\tau} \int_{-\infty}^{+\infty} d\bar{\zeta}d\bar{\eta}\; e^{i\left(\bar{\eta}\bar{t}_1-\bar{\zeta}\bar{t}_2\right)\bar{A}/\bar{\theta}}\; \mathcal{K}_{rv}(\bar{\zeta},\bar{\eta})\; \mathcal{Y}_{rv}(\bar{\zeta},\bar{\eta},\{\Delta\bar{\tau}_k\}), \tag{7.7}$$

where $\bar{t}_p \equiv \bar{t}^{(1)}_p$, $p = 1, 2$,

$$\mathcal{Y}_{rv}(\cdot) = e^{-\bar{A}(\Delta\bar{\tau}_0+\Delta\bar{\tau}_{2+h_{rv}})}\; exp\left(-\bar{A}\left[(1+r-v)|1-\bar{\zeta}|\Delta\bar{\tau}_3+|1+\bar{\eta}|\Delta\bar{\tau}_{1+v}+|1-\bar{\zeta}+\bar{\eta}|\Delta\bar{\tau}_{2-v}\right]\right), \tag{7.8}$$

$\mathcal{K}_{rv}(\cdot)$ is given by eq. (1.12), and the sum over $\{e_k\}$ supersedes the one over $\{a_l\}_{rv}$ (combining four different implementations $\mathcal{Z}_{rv}(\{a_k\},\cdot)$) so that the dressing-weight $\mathcal{Y}_{rv}(\cdot)$ is manifestly $S(4)-$invariant, i.e., $\{e_k\}-$independent. For the particular $\{a_k\}-$assignments, $\mathcal{Z}_{rv}(\{a_k\},\cdot)$ is diagrammatically depicted in figures 5c ($a_1 = a_2 = 0$), 8f ($a_1 = 0$), and 9f ($a_1 = a_4 = 0$) which are associated with $r = v = 0$, $r = v-1 = 0$, and $r = v = 1$ respectively.

Let us also note that the representation (7.7) readily allows to demonstrate that, for $\forall\bar{A} > 0$, $\mathcal{Z}_{rv}(\bar{A},\bar{\theta}^{-1})$ is indeed continuous in $\bar{\theta}^{-1}$ in a vicinity of $\bar{\theta}^{-1} = 0$. This property, implied in the transformation of eq. (1.8) into eq. (1.10), will be explicitly derived in [25].

7.3 A closer look at the pattern of the collective coordinates

In conclusion, let us clarify the following subtlety concerning the pattern of the collective coordinates relevant for the dressing of the $rv-$protograph. The point is that, in the $v = 1$ eq. (7.7), both the measure $d^{2+h_{rv}}\bar{\tau}$ and the relative time $\bar{t}_2 \equiv \bar{t}^{(\gamma)}_2$ can not be fully determined only on the basis of the configuration of the $rv-$protograph itself (postulated to be constrained, in the $r = 1$ case, by the second of the conditions (6.5)). The general reason is traced back to the fact that the $v = 1$ protographs are not of genus-one and, therefore, their dressing necessarily encodes certain structure inherited from the associated $j = 2$ elementary diagrams.

In consequence, the above measure includes integration over one more parameter[31] $\bar{\tau}_{2+r}$ in addition to the $2h_{rv} - r = 2 - v + h_{rv}$ parameters which are directly identified (see appendices B and A for the details), with the independent temporal coordinates of the end-points of the protographs' lines:

$$\int d^{2+h_{rv}}\bar{\tau} \ \ldots = \int d^{2-v+h_{rv}}\bar{\tau} \int d^{v}\bar{t}_2 \ldots , \tag{7.9}$$

where we have used that $\bar{t}_2 = \bar{\tau}_{2+r} - \bar{\tau}_1$ (with $\tau_1 = x^2(s'_1)$ as it is depicted in figures 8f and 9f). Then, as it is discussed in appendix A, the presence of τ_{2+r} is tightly related to the first of the constraints (6.5) fulfilled by the three parameters t_p, $p = 1, 2, 3$. In turn, as it is sketched in appendix B, the latter constraints underlie the completeness condition (5.7) for $\forall r, v$.

Note also the reduction $\int d^{2+n}\bar{\tau} \ \ldots \to \int d^{4+r-v}\bar{\tau} \ \ldots$ of the relevant measure, formalized by the transition from the combination of the individual amplitudes (7.1) to eq. (7.6), entails the relevant $f_k = 0$ replacements (5.6) applied to the $j = 2$ eq. (7.1). Indeed, the latter replacements result after such integration over $n - (2 + r - v)|_{j=2} = v + 1$ parameters $\tau_{q(p)+\omega_p^{(\gamma)}}$ (with $p = 3 - v, 3$), in the process of which the corresponding intervals $\Delta\tau_{q(k)}$ vary in the domains $[0, \Delta T_k^b(0, \gamma)]$ (see appendix B for more details).

8. The large θ limit

At this step we are ready to put forward the prescription (8.1) to implement the large θ limit in eq. (7.7). By virtue of the $1/\theta^2$ factor in front of the sum in the r.h. side of eq. (1.10), the asserted large θ scaling $< W(\Box) >^{(1)}_{U_\theta(1)} \sim \theta^{-2}$ is a consequence of the important property of the combinations $\mathcal{Z}_{rv}(\bar{A}, \bar{\theta}^{-1})$. For any finite $\bar{A} \neq 0$, the relevant large θ limit (1.9) can implemented directly through the substitution

$$e^{i\left(\bar{\eta}\bar{t}_1 - \bar{\zeta}\bar{t}_2\right)\bar{A}/\bar{\theta}} \ \longrightarrow \ 1 \quad \Longrightarrow \quad \mathcal{Z}_{rv}(\bar{A}, \bar{\theta}^{-1}) \ \longrightarrow \ \mathcal{Z}_{rv}(\bar{A}, 0)\,, \tag{8.1}$$

to be made in the integrand of the representation (7.7) of the quantity $\mathcal{Z}_{rv}(\bar{A}, \bar{\theta}^{-1})$ that replaces the latter quantity by its reduction $\mathcal{Z}_{rv}(\bar{A}, 0)$. In turn, provided eq. (1.7) is valid, the prescription (8.1) yields the integral representation (1.10) for the next-to-leading term of the $1/\theta$ expansion (1.3) (with $< \mathcal{W}(\Box) >^{(1)}_N = 0$).

The self-consistency of the deformation (8.1) is maintained provided $\mathcal{Z}_{rv}(\bar{A}, \bar{\theta}^{-1})$ is continuous in $\bar{\theta}^{-1}$ in a vicinity of $\bar{\theta}^{-1} = 0$. Roughly speaking, for $\bar{A} \neq 0$ the latter property[32] is valid since this deformation does not violate the *convergence* of the $(m+2)-$dimensional integral over $\bar{\tau}_k$, $\bar{\zeta}$, and $\bar{\eta}$ defining the representation (7.7) of $\mathcal{Z}_{rv}(\bar{A}, \bar{\theta}^{-1})$, where $m = 2 + h_{rv}$. To demonstrate the convergence, it is convenient first to get rid of the explicit $m-$dimensional ordered integration over $\bar{\tau}_j$. For this purpose, it is useful to perform the

[31] This parameter supersedes, after the two integrations (over $\tau_{q(p)+\omega_p^{(1)}}$ with $p = 1, 2$), the parameter $\bar{\tau}_{3+r}$ defined by eq. (A.4) in the case of the $j = 2$ amplitude (7.1).

[32] A rigorous derivation of this property is presented in [25].

Laplace transformation of $\mathcal{Z}_{rv}(\bar{A},\bar{\theta}^{-1})$ with respect to the dimensionless area (7.4) that results in

$$\tilde{\mathcal{Z}}_{rv}(\beta,\bar{\theta}^{-1}) = \int_0^{+\infty} d\bar{A}\ \mathcal{Z}_{rv}(\bar{A},\bar{\theta}^{-1})\ e^{-\beta\bar{A}}\ . \tag{8.2}$$

The advantage of this trick is that, in the integral representation of the image $\tilde{\mathcal{Z}}_{rv}(\beta,\bar{\theta}^{-1})$, the $\bar{\tau}_j-$integrations can be easily performed using the general relation

$$\prod_{j=0}^{m}\frac{1}{\beta+B_j} = \int\limits_0^{+\infty} d\bar{A}\ e^{-\beta\bar{A}} \int\limits_{0\le\breve{\tau}_k\le\breve{\tau}_{k+1}}^{\breve{\tau}_m\le\bar{A}} \prod_{k=1}^{m} d\breve{\tau}_k \prod_{j=0}^{m} exp\left(-B_j\Delta\breve{\tau}_j\right)\ , \tag{8.3}$$

where $\breve{\tau}_j$ is to be identified with $\bar{A}\bar{\tau}_j$, while $\Delta\breve{\tau}_{j-1} = \breve{\tau}_j - \breve{\tau}_{j-1}$ with $\breve{\tau}_0 \equiv 0$ and $\breve{\tau}_{m+1} \equiv \bar{A}$. In particular, in this way one proves that the Laplace image $\tilde{\mathcal{Z}}_{rv}(\beta,0)$ of the large θ asymptote $\mathcal{Z}_{rv}(\bar{A},0)$ of the amplitude (7.7) assumes the form (1.11).

Then, the self-consistency of the prescription (8.1) can be reformulated as the requirement that $\tilde{\mathcal{Z}}_{rv}(\beta,\bar{\theta}^{-1})$ is continuous in $\bar{\theta}^{-1}$ in a vicinity of $\bar{\theta}^{-1}=0$. In turn, this property is traced back to the fact that the double integral (1.11) is convergent for $\forall\beta>0$ which is verified by a direct inspection.

Also, it should be stressed that, due to the infrared singularities of the propagators, the prescription (8.1) is not applicable directly to each individual perturbative diagram. This property may be inferred from the integral representations of the elementary amplitudes given by the reduction (6.7) of the effective amplitudes considered in subsection 6.1. Actually, even the individual effective amplitudes (7.1) still are not suitable for this purpose either that can be traced back to the violation of the completeness condition (5.7). It takes certain specific cancellations between the latter amplitudes that, resulting in the latter condition, makes the substitution (8.1) applicable to the combinations (7.7). We shall continue the discussion of this issue in [25].

9. Conclusions

In the present paper we obtain the exact integral representation (1.8) of the next-to-leading term $< W(\Box) >^{(1)}_{U_\theta(1)}$ of the $1/N$ expansion (1.4) of the average in the $D=2$ gauge theory (1.2). It provides the rigorous non-perturbative[33] computation made, from the first principles, in the noncommutative gauge theory.

The Laplace image (8.2) of the large θ asymptote of $< W(\Box) >^{(1)}_{U_\theta(1)}$ assumes the particularly concise form (1.10). In turn, the latter asymptote is argued to be directly related (1.7) to the next-to-leading term of the $1/\theta$ expansion (1.3) of $< W(C) >_{U_\theta(1)}$. It is noteworthy that the considered asymptote reveals the power-like decay which is in sharp contrast with the exponential area-law asymptote (1.6) valid in the leading order of the $1/N-$ (or, equivalently, $1/\theta-$) expansion. Furthermore, as the origin of the power-like decay can be traced back to the (infinite, in the limit $\theta\to\infty$) nonlocality of the

[33] It is specifically important in the large θ limit (1.9), where the truncated perturbative series of $< W(C) >^{(G)}_{U_\theta(1)}$ is shown [14] to result in the false asymptotical $\theta-$scaling that is supposed to take place not only for $D=2$ but for $D=3,4$ as well.

star-product, similar decay is supposed to persist for all $G \geq 1$ subleading[34] terms $< W(C) >^{(G)}_{U_\theta(1)}$ of the large θ $1/N$ expansion.

In consequence, it precludes an apparent extension of the stringy representation of the latter expansion in the spirit of the Gross-Taylor proposal [38] formulated for the commutative $D = 2$ gauge theories. Another subtlety, concerning possible stringy reformulation of the noncommutative observables, is that the noncommutative gauge invariance is also maintained [26] for certain combinations of the Wilson lines associated with the *open* contours $C = C_{xy}$ with $\mathbf{x} \neq \mathbf{y}$. Nevertheless, the optimistic point of view could be that all these subtleties may suggest a hint for a considerable extension of the stringy paradigm conventionally utilized in the context of two-dimensional gauge (or, more generally, matrix) systems.

As the developed here methods are general enough, we hope that our analysis makes a step towards a derivation of an arbitrary two-dimensional average $< W(C) >_{U_\theta(1)}$. Most straightforwardly, they can be applied to consider the $G = 1$ term of the average (2.2) for a generic rectangular contour $C = \Box$ with a nontrivial number $n \geq 2$ of windings. E.g., it would be interesting to adapt the pattern (7.1) to the case when $n >> 1$ and estimate its asymptotical dependence on n. Also, the $G \geq 2$ terms $< W(\Box) >^{(G)}_{U_\theta(1)}$ could be in principle evaluated akin to the $G = 1$ case that is expected to lead to a generalization of eq. (7.1). In particular, we expect that there should be $2G$ parameters ζ_q, η_q with $q = 1, \ldots, G$, while the factor in front of the integral becomes $\bar{A}^m/(\sigma\theta)^{2G}$.

More subtle open question is to generalize our approach to a (non-self-intersecting) contour of a generic geometry. In the commutative $\theta = 0$ case, the crucial simplification takes place by virtue of the invariance of the partition function under the group of (simplectic) area-preserving diffeomorphisms which guarantees that $< W(C) >_{U(1)}$ depends only on the area $A(C)$ irrespectively of the form of C. On the other hand, the representation (2.2) does not make manifest if there is a symmetry that relates the averages $< W(C) >_{U_\theta(1)}$ with different geometries of the contour C. Furthermore, the lowest order perturbative computation [14] indicates that the simplectic invariance may be lost in the non-commutative case. Nevertheless, the explicit $A(\Box)-$ (rather than twofold $R-$ and $T-$) dependence of the derived $G = 1$ term $< W(C) >^{(1)}_{U_\theta(1)}$ looks like a promising sign. Also, it would be interesting to make contact with the noncommutative Loop equations [28, 33] which might be an alternative approach to the above problems.

Finally, among other new questions raised by the present analysis, we would like to mention the following one important in the context of the $D = 4, 3$ noncommutative Yang-Mills theory (1.2). We conjecture that in this case the minimal area-law asymptote, presumably valid for a generic closed fundamental Wilson loop in the $N \to \infty$ limit, fades away at the level of the subleading $G \geq 1$ terms similarly to what happens in the $D = 2$ case.

[34] Contrary to the $G \geq 1$ terms, the leading $G = 0$ term is insensitive to the star-product structure that matches its $\theta-$independence (1.6).

Acknowledgments

This work was supported in part by the grant INTAS-00-390. The work of J.A. and Y.M. was supported in part by by the Danish National Research Foundation. A.D. and Y.M. are partially supported by the Federal Program of the Russian Ministry of Industry, Science and Technology No 40.052.1.1.1112 and by the Federal Agency for Atomic Energy of Russia.

A. The $\{\Delta\tau_{q(k)}\}$-assignment

By virtue of the $S(4)\otimes S(2)-$symmetry implemented in section 4, there is the following short-cut way to introduce the prescription that fixes the $\{\Delta\tau_{q(k)}\}-$assignment (entering eq. (5.6)) unambiguously for all the effective amplitudes collected into the $S(4)\otimes S(2)-$multiplets. For all inequivalent values of j, r, and v, we first fix the prescription[35] for a single graph in a particular $S(4)\otimes S(2)-$multiplet with given $\gamma jrv-$assignment. Then, it is verified that the pattern of the prescription is not changed when adapted to the remaining graphs obtained employing the $S(4)-$reattachments combined with the $S(2)-$reflections.

In turn, given an elementary graph representing such a multiplet, there are two steps to implement the $\{\Delta\tau_{q(k)}\}-$assignment. The first step, discussed in the present appendix, is to perform such a change of the variables that replaces $2n$ temporal coordinates[36] $x^2(s_l)$ and $x^2(s'_l)$, constrained by $G=1$ eq. (4.2), by $n+2$ independent parameters τ_i. At the second step, one is to determine the function $q(k):\ k\to q$. The latter step is established in appendix C.

A.1 The $r=v=0$ case

Both of the steps are most straightforward in the case of the $r=v=0$ multiplets when the realization of the two relevant symmetries of the assignment in question is routine as well. Presuming that $s_k\geq s'_k$ for $\forall k$, the first step can be formalized by the prescription

$$x^2(s'_k)=\tau_k\quad,\qquad x^2(s_k)=\tau_{k+j+1}\quad,\quad k=1,2\quad,\qquad (j-1)\left(x^2(s'_3)-\tau_3\right)=0\,,\quad \text{(A.1)}$$

where $x^\mu(s'_k)$, $x^\mu(s_k)$ are the end-points of the left ($k=1$) and right ($k=2$) lines in figure 1a ($j=1$) and 2c ($j=2$).

A.2 The $v=1$ cases

Concerning the $v=1$ cases,[37] consider first the $j=1$ graphs which, being depicted by solid lines in figures 8a, 8b and 9a, 9b, are associated with $r=0$ and $r=1$ respectively, where $\gamma=1$ and $\gamma=2$ are assigned to figures 8a,9a and 8b, 9b correspondingly. In all

[35] In certain cases, this assignment may be imposed in a few alternative ways without changing the corresponding effective amplitude. The prescription fixes this freedom in the $S(4)-$invariant way.

[36] Recall that l labels the lth line of a given graph, $s'_l<s_l$ for $\forall l$, and the proper-time parameterization goes clockwise starting with the left lower coner of $C=\square$.

[37] Recall that, in the $r=v-1=0$ case, one is to restrict the admissible positions of the lower end-points of those j non-horizontal lines which are not involved into the $S(4)-$reattachments. It is fixed by eq. (C.4).

figures, τ_1 and τ_{4+r} should be identified respectively with the temporal coordinates of the leftmost and rightmost end-points of the elementary graph, belonging to $1+r$ solid lines (defining the associated protograph). Next, the remaining $1+r$ end-points of the latter lines can be as well directly identified with the corresponding parameters τ_i so that it can be summarized by equations

$$x^2(s_1') = \tau_1 \ , \quad x^2(s_1)\delta_{1\gamma} + x^2(s_4')\delta_{2\gamma} = \tau_{4+r} \ , \quad x^2(s_2) = \tau_{1+r+\gamma} \quad , \quad \delta_{2r}\cdot\big(x^2(s_4) - \tau_2\big) = 0\,, \tag{A.2}$$

where δ_{nm} denotes the standard Kronecker delta-function with $\delta_{nn} = 1$ and δ_{nm} for $\forall n \neq m$.

For a given $n+2 = 3+j+r$, the direct reidentification (A.2) allows to define only $n+1$ parameters τ_i. The remaining $(n+2)$th parameter $\tau_{4+r-\gamma}$ has to be introduced via the following procedure which is also used to determined the corresponding interval[38] $\Delta\tau_{q(2)}$. The proposal is to identify $\tau_{4+r-\gamma}$ with the new position

$$\big(x^2(s_1)\delta_{1\gamma} + x^2(s_1')\delta_{2\gamma}\big) + (-1)^\gamma t_2 = \tau_{4+r-\gamma} \tag{A.3}$$

of the lower end-point of the second solid line resulting after the judicious *parallel transport* of this line. Namely, the line is transported, until its upper end-point hits the corresponding end-point of the first solid line, to the right in the $\gamma = 1$ case of figures 8a, 9a and to the left in the $\gamma = 2$ case of figures 8b, 9b. Note also that $\bar\tau_{4+r-\gamma}$ describes the collective coordinates defining the measure (7.9).

Turning to the $j = 2$ case of figures 8c and 9c (both assigned with $\gamma = 1$), we first note that the addition of the extra solid line (compared to figures 8a, 8b and 9a, 9b) results in the one more delta-function in the $G = 1$ factor (4.2). In consequence, compared to the associated $j = 1$ cases, only a single additional parameter τ_i is introduced which can be directly identified with the the temporal coordinate $x^2(s_3)$ of the lower end-point of this extra line (which, being non-horizontal, is not involved into the reattachments). As for the remaining $n+1 = 4+r$ parameters τ_k, they are defined in the way similar to the previous $j = 1$ discussion.

Actually, it can be reformulated in the more geometrically clear way. For this purpose, in all figures, τ_1 and τ_{5+r} should be identified correspondingly with the temporal coordinates of the leftmost and rightmost end-points of the elementary graph depicted by the solid lines. Additionally, the $2+r$ end-points (of the latter lines) can be as well directly identified with the corresponding parameters τ_i that can be summarized in the form

$$\begin{aligned} &x^2(s_1') = \tau_1\,, \qquad x^2(s_1)\delta_{1\gamma} + x^2(s_4')\delta_{2\gamma} = \tau_{5+r}\,, \\ &x^2(s_2) = \tau_{4+r}\,, \qquad\qquad x^2(s_3) = \tau_{2+r}\,, \qquad \delta_{1r}\big(x^2(s_4) - \tau_2\big) = 0. \end{aligned}$$

In this way, we define the $n+1$ parameters while the so far missing $(n+2)$th parameter τ_{3+r} can be determined through the following procedure utilizing the double parallel transport which, geometrically, can be visualized the triangle-rule (most transparent in figures 8f and 9f). The proposal is to identify τ_{3+r} with the position

$$\tau_1 + t_2 = \tau_{3+r} \tag{A.4}$$

[38] In turn, $\Delta\tau_{q(2)}$ is to be identified with the interval spanned by the lower end-point of the second solid line in the process of this parallel transport: $q(2) = 2+r$.

where the two lower end-points of the second and the third solid lines coalesce when these two lines are transported until their upper end-points *simultaneously* hit the corresponding end-points of the first (horizontal) solid line. In turn, it implies the algebraical fine-tuning maintained by the first of the conditions (6.5) which, geometrically, means that (when properly transported and reoriented) the three vector $\mathbf{y}_k,\ k=1,2,3$, can be combined into a triangle[39] in the $a_1=0$ case of figures 8c and 9c.

A.3 The $S(4)$- and reflection-invariance

Evidently, the proposed algorithm to introduce the $\{\Delta\tau_{q(k)}\}-$assignment is not changed after a generic combination of the $S(4)-$reattachments. Indeed, it readily follows from the fact that, keeping the temporal coordinates of the end-points intact, they are applied only to the right- or/and leftmost end-points of elementary graphs.

Concerning the reflection-invariance, consider first the $r=v=0$ case. Then the reflection (interchanging the horizontal sides of the rectangle C) is applied to the two $S(4)-$multiplets corresponding to the figures 1a (with $j=1$) and 2c (with $j=2$). In the reflection-partners represented by figures 1b and 2d respectively, the time-intervals $\Delta\bar{\tau}_k$ be associated to the lower horizontal side of C. In the latter two figures, we parameterize the left and the right horizontal lines by label 1 and 2 correspondingly (so that, in figure 2d, the remaining non-horizontal line is assigned with the label 3). Introducing the parameters τ_i by the same token as previously, it guarantees that the function $q(k)$ is reflection-invariant. Also, compared to the case of figure 1a and 2c, the figures 1b and 2d can be characterized via the replacements $t_p\to -t_p$, $\mathcal{C}_{il}\to -\mathcal{C}_{il}$ with $p=1,2$ and $i,l=1,2,3$. In turn, the latter replacements follow from the definitions (2.9) and (2.11) which are augmented by the convention to implement the proper-time parameterization (implying, in particular, that $s_l\geq s'_l$ for $\forall l$).

Finally, consider the remaining case of the three pairs of the $r=v=1$ $S(4)-$multiplets (assigned with $\gamma=1,2$ for $j=1$ and $\gamma=1$ for $j=2$) which, within a particular pair, are related through the reflection interchanging the vertical sides of $C=\Box$.

In each of the latter multiplets it is sufficient to consider the single elementary graph with the two horizontal lines. E.g., see figures 9g and 9h which are the reflection-partners of figures 9b and 9c respectively. For concreteness, we restrict[40] the discussion to figures 9c and 9h, associating the time-intervals $\Delta\bar{\tau}_k$ to the lower horizontal side of C. In the latter two figures, we parameterize the left and the right horizontal lines by label 1 and 4 correspondingly. Then, to maintain the reflection-covariance of the algorithm (introduced in the previous subappendix), in the case of figure 9h one is to perform the additional change of the variables $\bar{\tau}_k\to\bar{\tau}_{n+3-k}$ with $k=1,\ldots,n+2$ (possessing the Jacobian equal to unity) that results in the reidentification $\Delta\bar{\tau}_k\to\Delta\bar{\tau}_{n+2-k}$ applied to $k=0,\ldots,n+2$. (As previously, we require that $s_l\geq s'_l$ for $\forall l$.) This reidentification evidently implies the transformation $q(k)\to q(n+2-k)$, provided the labels 2,3 are assigned to the remaining non-horizontal lines so that $\mathcal{C}_{32}\to -\mathcal{C}_{32}$ (while $\mathcal{C}_{1p}\to -\mathcal{C}_{1p}$ for $p=2,3$). In turn, a

[39] A direct inspection of figure 5b and figures 6 reveals that, with a minor modification, a similar triangle-rule can be formulated in the $v=r=0$ case as well.

[40] The remaining two pairs, associated with figures 9a and 9b, are handled in a similar way.

direct inspection demonstrates that, after this transformation, the function $q(k)$ assumes the same form as in the case of figure 9c which verifies its reflection-covariance. As for the splitting (5.4), the reflection-partners can be characterized through the replacements $t_i \to -t_i$ for $i = 1, 2, 3, 4$.

B. Justifying eq. (7.6)

To transform the superposition (5.2) into the form of eq. (7.6), in the integral representation (7.1) of $\mathcal{Z}^{(\gamma)}_{jrv}(\cdot)$ one is to first perform (for each $v + j - 1 > 0$ term) the change of the variables

$$\int d^{2+n}\bar{\tau}\ \ldots \quad \longrightarrow \quad \int d^{2+h_{rv}}\bar{\tau}\ \int_{\bar{\tau}_{q_\gamma(3)-1}}^{\bar{\tau}_{q_\gamma(3)+1}} d^{j-1}\bar{\tau}_{q_\gamma(3)} \int_{\bar{\tau}_{q_\gamma(2)-1}}^{\bar{\tau}_{q_\gamma(2)+1}} d^{v}\bar{\tau}_{q_\gamma(2)}\ \ldots \tag{B.1}$$

that manifestly separates the $2+h_{rv}$ collective coordinates combined into the measure (7.9), provided $q_\gamma(p) = q(p) + \omega^{(\gamma)}_p$, where $\omega^{(\gamma)}_p = 0, 1$ is explicitly constructed in subappendix B.1 so that the prescription, formulated in the end of subsection 5.3.1, is valid. In turn, due to the presence of the corresponding number of the derivatives in the r.h.side of eq. (7.1), the remaining $v + j - 1$ integrations[41] (with respect to $\bar{\tau}_{q_\gamma(p)} \in [\bar{\tau}_{q_\gamma(p)-1}, \bar{\tau}_{q_\gamma(p)+1}]$) are readily performed. The computation is simplified by the fact[42] that, by construction of $\omega^{(\gamma)}_p$, both $\bar{t}^{(\gamma)}_1$, $\bar{t}^{(\gamma)}_2$ and $\Delta\bar{\tau}_{q(i)}$ are *independent* of $\bar{\tau}_{q_\gamma(p)}$ for $\forall i \neq p$, $\forall p = 3-v, 3$, and $\forall\gamma = 1, f_{jv}$, while $(-1)^{\omega^{(\gamma)}_3 - 1}\partial/\partial\bar{\tau}_{q_\gamma(p)}$ can be replaced by $\partial/\partial\Delta\bar{\tau}_{q(p)}$ when it acts on the $\Delta\bar{\tau}_{q(p)}-$dependent factor (6.3). In consequence, in the expression (6.2) for $\tilde{\mathcal{V}}^{(\gamma)}_{jrv}(\cdot)$, the dependence on $\tau_{q_\gamma(p)}$ is localized in the corresponding $k = p$ implementation of the factor (6.3). Furthermore, the interval $\Delta\bar{\tau}_{q(p)}$ varies in the domain $[0, \Delta\bar{T}^b_p(0,\gamma)]$ (where $T^b_p(0,\gamma) = \tau_{q_\gamma(p)+1} - \tau_{q_\gamma(p)-1}$ is defined in eq. (5.7)) when $\bar{\tau}_{q_\gamma(p)}$ spans the domain $[\bar{\tau}_{q_\gamma(p)-1}, \bar{\tau}_{q_\gamma(p)+1}]$.

Altogether, the amplitude (7.1) can be rewritten in the form which can be obtained from eq. (7.6) through the replacement

$$\mathcal{V}_{2rv}(\{a_k\}, \{\Delta\bar{T}^b_k\}) \longrightarrow \sum_{j=1}^{2}\sum_{\gamma=1}^{f_{jv}} \left[\sum_{\breve{\tau}_3=0}^{1}(-1)^{\breve{\tau}_3}\right]^{j-1} \left[\sum_{\breve{\tau}_2=0}^{1}(-1)^{\breve{\tau}_2}\right]^{v} \mathcal{V}^{(\gamma)}_{jrv}(\{a_i\}, \{\Delta\bar{\tau}_{q(k)}\})\Big|_{\{\breve{\tau}_p\}}, \tag{B.2}$$

where sum over $\breve{\tau}_p = (\Delta\bar{T}^b_p(0,\gamma) - \Delta\bar{\tau}_{q(p)})/\Delta\bar{T}^b_p(0,\gamma)$ reproduces the sum over the boundary values of the relevant intervals $\Delta\bar{\tau}_{q(p)}$, while $\mathcal{V}_{2rv}(\cdot,\cdot) \equiv \mathcal{V}^{(1)}_{2rv}(\cdot,\cdot)$ as well as in eq. (7.6).

Next, in the r.h. side of eq. (B.2), there are mutual cancellations (see eqs. (B.5) and (B.6) below) which, due to the $S(4)-$invariance of the $\bar{\mathcal{R}}^{-1}_b-$dressing, are maintained between the $j = 1$ and $j = 2$ terms considered *separately* for any admissible $\{a_l\}-$assignment. As a result, survives only the single $j = 2$ term

$$\mathcal{V}_{2rv}(\{a_i\}, \{\Delta\bar{\tau}_{q(k)}\})\Big|_{\{\Delta\bar{\tau}_{q(p)} = \Delta\bar{T}^b_p(0)\}} = \mathcal{V}_{2rv}(\{a_k\}, \{\Delta\bar{T}^b_k\}) \tag{B.3}$$

[41] Recall that these integrations are associated with those lines (of a given elementary graph) which, being non-horizontal, are *not* involved into the $S(4)-$reattachments.

[42] It is this fact that verifies the prescription (6.6).

(with $\bar{T}^b_p(0) \equiv \bar{T}^b_p(0,\gamma)|_{\gamma=1}$) characterized by the condition

$$\Delta\bar{\tau}_{q_\gamma(p)-1} = 0 \quad \Longrightarrow \quad \Delta\bar{\tau}_{q(p)} = \Delta\bar{T}^b_p(0,1), \qquad , \qquad \forall p = 3-v, 3\,, \tag{B.4}$$

that reduces the number $2+n$ of the original variables $\bar{\tau}_i$, entering eq. (7.1), to the smaller amount $2 + h_{rv}$ associated with eq. (7.7). In consequence, for fixed values of those $\bar{\tau}_k$ which define the collective coordinates entering the measure (7.9), it maintains the *maximal* value of $\sum_{p=3-v}^{3} \Delta\tau_{q(p)}$, where p labels those $v + j - 1$ lines of a given elementary graph which, being associated to $f_k = 0$ replacement (5.6), are not involved into the $S(4)-$reattachments. In turn, by virtue of the $j = 2$ constraints (6.5), it supports the completeness condition (5.7). Altogether, it verifies eq. (7.6).

As for the asserted mutual cancellations, the simplest situation takes place in the $r = v = 0$ case when the parameter γ, assuming the singe value (since $f_{j0} = 1$ according to eq. (4.1)), can be safely omitted. Therefore, for each admissible values of a_1 and a_2 (involved in the $v = 0$ summation in eq. (7.6)), the fine-tuning takes place between the pairs of effective amplitudes $\mathcal{Z}_{j00}(\{a_k\}, \bar{A}, \bar{\theta}^{-1})$ with $j = 1, 2$. In this case, due to the identity $\mathcal{F}(z, 0) = 1$ valid for $\forall z$ (as it is clear from the definition (6.3)), the very pattern (6.2) of $\mathcal{V}_{jrv}(\cdot)$ ensures the relation

$$\mathcal{V}_{200}(\{a_k\}, \{\Delta\bar{\tau}_{q(i)}\})\Big|_{\Delta\bar{\tau}_{q(3)}=0} = \mathcal{V}_{100}(\{a_k\}, \{\Delta\bar{\tau}_{q(i)}\}), \tag{B.5}$$

so that the reduction $\Delta\bar{\tau}_{q(k)} = 0$ converts the $6-$set $\{\Delta\bar{\tau}_k\}$ (associated with the $j = 2$ l.h. side of the identity) into its counterpart (in the $j = 1$ l.h. side) consisting of the 5 intervals $\Delta\bar{\tau}_k$. In turn, it proves the inverse of the $v = 0$ replacement (B.2) and, in consequence, the $v = 0$ option of the prescription (5.6) endowed with the $\{f_k\}-$specification in compliance with subsection 5.3.1. For the particular case of $a_1 = a_2 = 0$, $\mathcal{Z}_{00}(\{a_k\}, \cdot)$ (resulting from the cancellation between $\mathcal{Z}_{200}(\{a_k\}, \cdot)$, figure 5b, and $\mathcal{Z}_{100}(\{a_k\}, \cdot)$, figure 5a) is diagrammatically depicted by figure 5c. The remaining options of $\mathcal{Z}_{00}(\{a_k\}, \cdot)$ are represented by figures 6a-6c.

Concerning the $v = 1$ cases, the inverse of the $v = 1$ replacements (B.2) follow from the pair of the relations[43]

$$\mathcal{V}_{2r1}(\cdot, \{\Delta\bar{\tau}_{q(i)}\})\Big|_{\Delta\bar{\tau}_{q(p)}=0} = \mathcal{V}^{(p-1)}_{1r1}(\cdot, \{\Delta\bar{\tau}_{q(i)}\})\Big|_{\Delta\bar{\tau}_{q(2)}=\bar{T}^b_2(0,p-1)}, \quad p = 2, 3\,, \tag{B.6}$$

$$\mathcal{V}_{2r1}(\cdot, \{\Delta\bar{\tau}_{q(i)}\})\Big|^{\Delta\bar{\tau}_{q(3)}=0}_{\Delta\bar{\tau}_{q(2)}=0} = \mathcal{V}^{(\gamma)}_{1r1}(\cdot, \{\Delta\bar{\tau}_{q(i)}\})\Big|_{\Delta\bar{\tau}_{q(2)}=0} = 0\,, \tag{B.7}$$

where eq. (B.6) can be deduced essentially by the same token as eq. (B.5) (while eq. (B.7) is proved in [25]). The only new element is to take into account that, contrary to the $r = v = 0$ case (B.5), there are two $p = 2, 3$ options to implement the $j = 2 \to j = 1$ reduction (of the $(6 + r)-$set $\{\Delta\bar{\tau}_k\}$ into the corresponding $(5 + r)-$set) so that the pth option is associated with the $\gamma = p - 1$ implementation of $\mathcal{V}^{(\gamma)}_{1r1}(\cdot)$. Geometrically, for the

[43] In the derivation of eq. (B.6), we utilize that $\Delta T^b_2(0,\gamma)|_{j=1} = \Delta T^b_{4-\gamma}(0,1)|_{j=2}$ provided $t^{(\gamma)}_2|_{j=1} = t^{(1)}_{4-\gamma}|_{j=2}$.

particular $\{a_k\}-$assignments, the latter identification is clear from the comparison of the $j=2$ figures 8c and 9c with the $j=1$ pairs of the figures 8a, 8b and 9a, 9b respectively. (In the derivation of this representation of $\mathcal{Z}^{(1)}_{1r1}(\cdot)$, we also utilize the change of the variables $\bar{\eta} \to \bar{\eta}+\bar{\zeta}\ \bar{\zeta} \to \bar{\zeta}$ that, in the combination $\bar{\eta}\bar{t}^{(1)}_1 - \bar{\zeta}\bar{t}^{(1)}_2$ entering the relevant option of eq. (6.2), replaces $\bar{t}^{(1)}_2$ by $\bar{t}^{(2)}_2$.)

Finally, it is possible to diagrammatically visualize the $v=1$ replacement (B.2), in the form similar to the $r=v=0$ one. For simplicity, we as previously restrict the discussion to the case of the $\{a_k\}-$assignments with $a_1=0$ and, when $r=1$, $a_4=0$. Then, observe first that (in the $\gamma=1$ case) the relation (B.7) implies the equivalence of the effective amplitudes associated with figures 8a, 9a and 8d, 9d correspondingly. Next, the $p=3$ variant of the relation (B.6) guarantees that the superposition $\mathcal{Z}^{(2)}_{1r1}(\{a_k\},\cdot)+\mathcal{Z}^{(1)}_{2r1}(\{a_k\},\cdot)$ is diagrammatically represented by figures 8e and 9e when $r=0$ and $r=1$ respectively. As for $\mathcal{Z}_{r1}(\{a_k\},\cdot)$, being depicted in figures 8f and 9f when $r=0$ and $r=1$ correspondingly, it results after the residual cancellation which takes place, by the same token as in the $r=v=0$ case, between effective amplitudes of figures 8e (9e) and 8d (9d).

B.1 The choice of the $\{\omega^{(\gamma)}_k\}$-assignment

It remains to introduce the appropriate set of the parameters $\omega^{(\gamma)}_k$, where $k=3-v,3$ labels those $n-h_{rv}=v+j-1$ lines of the elementary graph which are *not* associated with the corresponding protograph, i.e., $k\in\mathcal{X}_{jrv}\equiv\tilde{\Omega}_{jrv}/\mathcal{S}_{rv}$ (where the sets $\tilde{\Omega}_{jrv}$ and $\mathcal{S}_{rv}$ are introduced in the end of subsection 4.2.4). For this purpose, we propose the following algorithm. First, we observe that the parameters $\bar{\tau}_{q_\gamma(k)}$ $(k=3-v,3,\ q_\gamma(p)=q(p)+\omega^{(\gamma)}_p)$ represent the temporal coordinates which remain dynamical when one fixes both the positions of the end-points of the corresponding protograph's line and, in the $v=1$ case, an admissible value of $t^{(\gamma)}_2$. In compliance with appendix A, for $v+j-1>0$ it leaves variable exactly $v+j-1$ independent temporal coordinates of either upper (when $v=0$) or lower end-points of the $v+j-1$ lines labeled by $k\in\mathcal{X}_{jrv}$. Correspondingly, each of thus introduced parameters $\bar{\tau}_{q_\gamma(k)}$ is associated with the two adjacent intervals $\Delta\bar{\tau}_{q_\gamma(k)-i}$ with $i=0,1$ so that $\sum_0^1\Delta\bar{\tau}_{q_\gamma(k)-i}=\Delta T^b_p(0,\gamma)$. Then, it is a matter of convention to choose one of the two possible values of $i=i_\gamma(k)$ in order to identify $q(k)=q_\gamma(k)-i_\gamma(k)$ for a given γ. Having fixed this freedom[44] according to the prescription of appendix C, one is led to the identification $\omega^{(\gamma)}_k=i_\gamma(k)$. Given this prescription, one obtains (in the $S(4)-$invariant and reflection-covariant way in the sense of subappendix A.3) that $\omega^{(1)}_3=0$ for $r=v=j-2=0$, $\omega^{(\gamma)}_2=\gamma-1$ for $v=j=1$ (and $\forall r=0,1$), while $\omega^{(1)}_p=3-p$ for $v=j-1=1$ (and $\forall r=0,1$). Also, it supports the prescription, formulated in the end of subsection 5.3.1.

Next, by construction, thus introduced $n-v$ intervals $\Delta T^b_k(f_k,\gamma)$ meet the important constraint (justified by a direct inspection of the relevant elementary graphs): these intervals are mutually *non-overlapping*. Furthermore, in the $j=2$ case, the very number

[44] A direct inspection of the elementary graphs verifies that this freedom is absent for the remaining h_{rv} lines which, being endowed with the $\bar{\mathcal{R}}_b^{-1}-$dressing, are assigned with $k\in\mathcal{S}_{rv}=\Omega_{jrv}/\mathcal{X}_{jrv}$, while $f_k=1$ in the sence of eq. (5.7), i.e., $\Delta T^b_k(1,\gamma)=\Delta\bar{\tau}_{q(k)}$ for $k\in\mathcal{S}_{rv}$.

$n - v$ of the intervals ensures that they comply with the completeness condition (5.7). (Among the $n+1$ intervals $\Delta\bar{\tau}_i$, comprising the residual temporal interval in the r.h. side of this condition, there are exactly $v+1$ pairs combined into the corresponding intervals $\Delta T_p^b(0,1),\ p = 3-v, 3$.) Also, the latter constraint guarantees that $\Delta\bar{\tau}_{q(i)}$ is independent of $\bar{\tau}_{q_\gamma(p)}$ for $\forall i \neq p$, $\forall p = 3-v, 3$. Finally, it is straightforward to argue that the same independence of $\bar{\tau}_{q_\gamma(p)}$ holds true for $\bar{t}_1^{(\gamma)},\ \bar{t}_2^{(\gamma)}$ as well. It is most transparent in the $r = v = 0$ case where these relative times are fully determined by the positions of the end-points of the $2 + r - v$ lines involved into the $S(4)-$reattachments. In the $v = 1$ case, this argument still applies to $\bar{t}_1^{(\gamma)}$, while the independence of $\bar{t}_2^{(\gamma)}$ is verified by the relation (A.3).

C. Explicit implementation of $\tilde{\mathcal{V}}_{2rv}(\{a_i\}, \{\Delta\tau_{q(k)}\})$

The aim of this appendix to explicitly determine the $\{a_l\}-$*dependent* parameters which define the relevant implementation of the pattern (6.2) of the quantity $\tilde{\mathcal{V}}_{2rv}(\cdot)$ entering eq. (7.6). In compliance with the discussion of subsection 4.2.4, our strategy is to introduce the required parameters for generic $\{a_l\}-$assignment as the $\{a_l\}-$dependent deformation of the parameters associated with a particular elementary graph in a given $rv-$variety of the elementary diagrams. In the next appendix, we will verify that, after an appropriate change of the variables $\bar{\zeta}$ and $\bar{\eta}$, one can rewrite this quantity in the form matching eq. (7.7).

C.1 The $r = v = 0$ case

Consider first the $a_1 = a_2 = 0$ contribution to the $r = v = 0$ superposition (7.6) which is determined by such implementation of $\tilde{\mathcal{V}}_{200}(\{a_i\}, \{\Delta\tau_{q(k)}\})$ that is parameterized by the $j = 2$ graph[45] 2c (when $\mathcal{C}_{12} = \mathcal{C}_{13} = \mathcal{C}_{23} = -1$), the deformations of which are described in figure 5b. Defining $\bar{\tau}_k$ and $\Delta\bar{\tau}_k$ according to the $j = 2$ eq. (A.1), the $\{a_l\}-$independent parameters $\bar{t}_p$ are determined by the $z = 0$ variant relations

$$(-1)^{a_1+z}\bar{t}_1 = \bar{\tau}_4 - \bar{\tau}_1 = \Delta\bar{\tau}_1 + \Delta\bar{\tau}_2 + \Delta\bar{\tau}_3 \quad , \quad (-1)^z\bar{t}_2 = \bar{\tau}_5 - \bar{\tau}_2 = \Delta\bar{\tau}_2 + \Delta\bar{\tau}_3 + \Delta\bar{\tau}_4 \, . \tag{C.1}$$

with $\bar{t}_1 - \bar{t}_2 + \bar{t}_3 = 0$, while the convention to fix the labels $k = 1, 2, 3$ is fixed in subsection 4.2.4. Correspondingly, it leads to the $a_1 = z = 0$ option of the identification

$$\begin{aligned} &q(2) = 1, && q(1) = 4\,, && q(3) = 3\ , \\ &\alpha^{(p)} = (-1)^z\mathcal{C}_{32} = 1\ , && -\alpha^{(1)} = (-1)^z\mathcal{C}_{p1} = (-1)^{a_1}\,,\ p = 2, 3\,, \end{aligned} \tag{C.2}$$

where, as it should, the function $q(k)$ is $\{a_l\}-$independent. Also, the $\omega_3^{(1)} = 0$ option of the $v = 0$ eq. (B.4) implies that the measure of the $r = v = 0$ representation (7.7) is obtained through the reidentification: $\bar{\tau}_i \to \bar{\tau}_i$ for $i = 1, 2$, while $\bar{\tau}_i \to \bar{\tau}_{i-1}$ for $i = 4, 5$ so that $\bar{\tau}_3$ disappears.

As for the remaining three contributions to the $r = v = 0$ superposition (7.6), they are associated with such implementation of the quantity $\tilde{\mathcal{V}}_{200}(\{a_i\}, \{\Delta\tau_{q(k)}\})$ that are parameterized by the $v = 0$ components of the diagrams 2e and 2g obtained through the vertical

[45] Recall that both the elementary and the effective amplitudes, associated with figures 2a and 2b, are vanishing due to the specific implementation of the $V^{(n)}_{U_\theta(1)}(\cdot) \to \tilde{V}^{(n)}_{U_\theta(1)}(\cdot)$ option of the $G = 1$ constraints (4.2).

reattachments applied to figure 2c. For this purpose, the leftmost or/and rightmost endpoint of the pair of the lines in figure 2c is/are replaced, keeping their time-coordinates $x^2(s'_1)$ and $x^2(s_2)$ intact, from the upper to the lower horizontal side of the rectangle C. Taking into account that the vertical 1−axis is directed from the upper to the lower horizontal side of the rectangle $\Box$, it is formalized by the relations

$$x^1(s'_1) = a_1 R \quad , \quad x^1(s_2) = a_2 R \quad , \quad x^1(s'_2) = x^1(s_1) = 0 \ . \tag{C.3}$$

When $a_1 + a_2 \geq 1$, it parameterizes the three different implementations of $\tilde{\mathcal{V}}_{200}(\cdot)$ which, being associated with figures 6a-6c, are described by the corresponding $\{a_k\}$−implementations of eqs. (C.2) and (C.1), where one is to put $z = 0$.

Finally, to compute the entire $r = v = 0$ contribution to the decomposition (1.8), it remains to include the contribution of such $r = v = 0$ superposition (7.6) that is associated with the $S(4)$−multiplet of the $j = 2$ elementary graphs specified by the graph in figure 2d. Alternatively, these graphs can be obtained from the previously constructed $j = 2$ $S(4)$−multiplet (specified by the graph in figure 2c) via the reflection interchanging the horizontal sides of the rectangle C. Then, introducing the $\{\Delta\bar{\tau}_k\}$−assignment according to the convention of subappendix A.3, one arrives at the $r = v = 0$ implementation of eq. (7.6) fixed by the $z = 1$ option of eqs. (C.1) and (C.2).

C.2 The $r = v - 1 = 0$ case

Next, consider the $a_1 = 0$ contribution to the $r = v - 1 = 0$ superposition (7.6) which is determined by such implementation of $\tilde{\mathcal{V}}_{201}(\{a_i\}, \{\Delta\tau_{q(k)}\})$ that is parameterized by the $v = 1$ component of the $j = 2$ diagram 2e (when $\mathcal{C}_{12} = \mathcal{C}_{13} = \mathcal{C}_{23} = -1$), the deformations of which are described in figure 8c. It is geometrically evident that there is the single $v = 1$ component (assigned with $\gamma = 1$) of the latter diagram which is constrained by the $p = 2, 3$ options of the condition

$$x^2(s_p) \in [x^2(s'_1), x^2(s_1)] \tag{C.4}$$

applied to both of the non-horizontal lines.

In this case, introducing $\bar{\tau}_k$ and $\Delta\bar{\tau}_k$ according to the $r = 0$ prescription of eqs. (A.4) and (A.4), the decomposition of the parameters $\bar{t}_p$ is determined by the $a_1 = \tilde{a}_1 = 0$ variant of the relations

$$(-1)^{a_1+\tilde{a}_1}\bar{t}_1 = \bar{\tau}_5 - \bar{\tau}_1 = \Delta\bar{\tau}_1 + \Delta\bar{\tau}_2 + \Delta\bar{\tau}_3 + \Delta\bar{\tau}_4 \quad , \quad \bar{t}_2 = \bar{\tau}_3 - \bar{\tau}_1 = \Delta\bar{\tau}_1 + \Delta\bar{\tau}_2 \, , \tag{C.5}$$

with $\bar{t}_1 - \bar{t}_2 + \bar{t}_3 = 0$, and the convention[46] to fix the labels $k = 1, 2, 3$ is sketched in subsection 4.2.4. Correspondingly, it yields the $a_1 = \tilde{a}_1 = 0$ option of the identification

$$\begin{aligned} q(2) = 3 \, , \qquad & q(3) = 2 \quad , \\ \alpha^{(3)} = \alpha^{(2)} = \mathcal{C}_{32} = 1 \quad , \quad & \mathcal{C}_{p1} = (-1)^{a_1+\tilde{a}_1} \, , \ p = 2, 3 \ . \end{aligned} \tag{C.6}$$

Also, the $\omega_p^{(1)} = 3 - p$ option of the $v = 0$ eq. (B.4) implies that the measure of the $r = v - 1 = 0$ representation (7.7) is obtained through the reidentification: $\bar{\tau}_1 \to \bar{\tau}_1$, $\bar{\tau}_3 \to \bar{\tau}_2$, while $\bar{\tau}_5 \to \bar{\tau}_3$ so that $\bar{\tau}_2$ and $\bar{\tau}_4$ disappear.

[46] Akin to figure 2c, the convention $\mathcal{C}_{23} = -1$ implies that $x^2(s_3) < x^2(s_2)$.

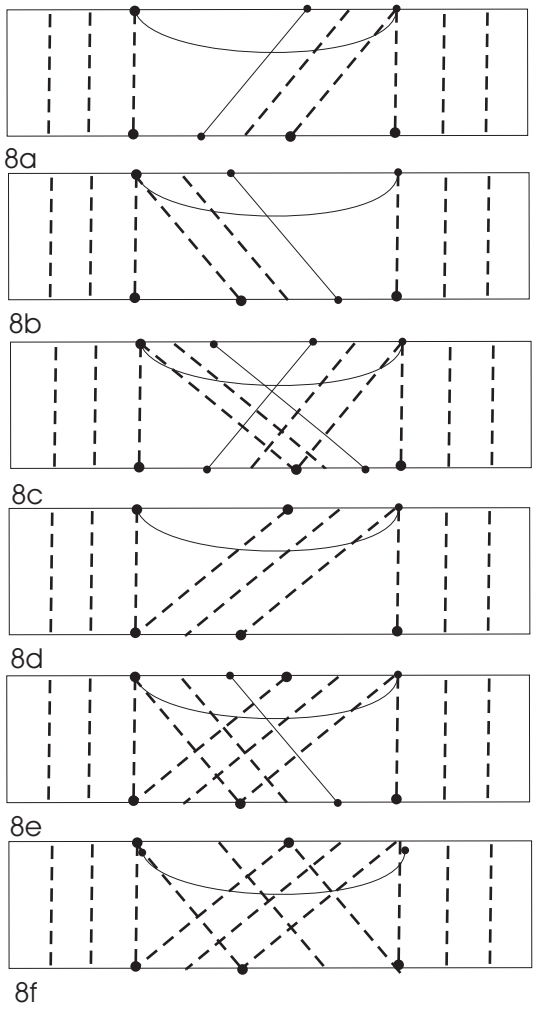

Figure 8: Dressed diagrams associated with (a) $\mathcal{Z}^{(1)}_{101}$, (b) $\mathcal{Z}^{(2)}_{101}$, (c) $\mathcal{Z}^{(1)}_{201}$, (d) the representation of $\mathcal{Z}^{(1)}_{101}$ built on the relation (B.7), (e) $\mathcal{Z}^{(2)}_{101} + \mathcal{Z}^{(1)}_{201}$, (f) $\mathcal{Z}_{01}$.

Then, the remaining three contributions to the $r = v - 1 = 0$ superposition (7.6) are associated with such implementation of the quantity $\tilde{\mathcal{V}}_{201}(\{a_i\}, \{\Delta\tau_{q(k)}\})$ that are parameterized by the $v = 1$ components of the diagrams 2f and 2g. In turn, the latter elementary graphs can be obtained from the $v = 1$ component of the diagram 2e through the vertical reattachments of the left or/and right end-point of its single horizontal line that is formalized by eq. (4.4). Together with the already considered $w = a_1 = 0$ case, it generates the four different implementations of $\tilde{\mathcal{V}}_{201}(\cdot)$ which are described by the corresponding $\{a_i\}-$dependent implementations of eqs. (C.5) and (C.6).

C.3 The $r = v = 1$ case

Consider the $a_1 = a_4 = 0$ contribution to the $r = v = 1$ superposition (7.6) which is determined by such implementation of $\tilde{\mathcal{V}}_{211}(\{a_i\}, \{\Delta\tau_{q(k)}\})$ that is parameterized by that

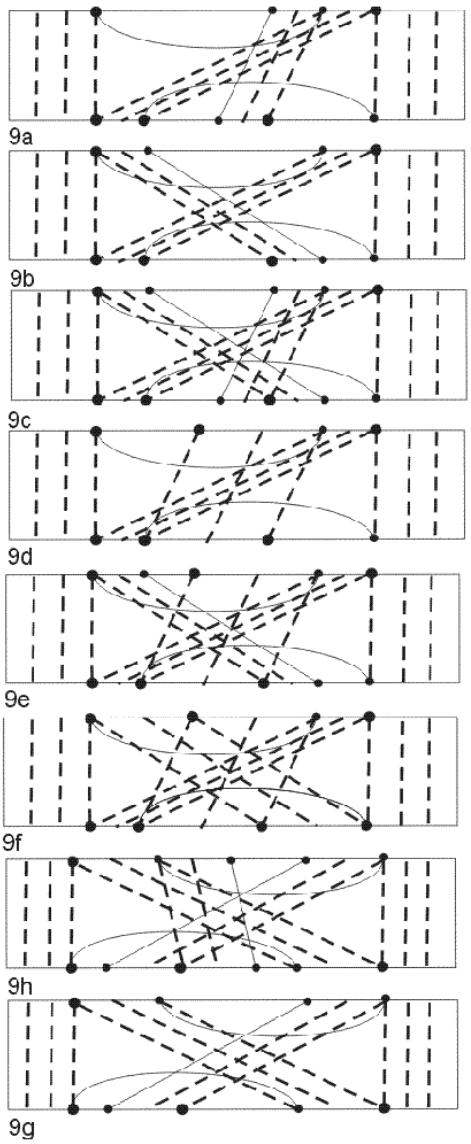

Figure 9: Dressed diagrams associated with (a) $\mathcal{Z}^{(1)}_{111}$, (b) $\mathcal{Z}^{(2)}_{111}$, (c) $\mathcal{Z}^{(1)}_{211}$, (d) the representation of $\mathcal{Z}^{(1)}_{111}$ built on the relation (B.7), (e) $\mathcal{Z}^{(2)}_{111} + \mathcal{Z}^{(1)}_{211}$, (f) $\mathcal{Z}_{11}$, (h) the reflection-partner of (c), and (g) the reflection-partner of (b).

component of the Feynman diagram in figure 7e (when $\mathcal{C}_{12} = \mathcal{C}_{13} = \mathcal{C}_{23} = -1$), where the upper horizontal line is on the left compared to the lower one. The $\bar{\mathcal{R}}_b^{-1}-$deformations of this components are depicted in figure 9c.

Defining $\bar{\tau}_k$ and $\Delta\bar{\tau}_k$ according to the $r = 0$ prescription of eqs. (A.4) and (A.4), the decomposition of the parameters $\bar{t}_p$ is determined by the $a_1 = z = 0$ relations

$$(-1)^{a_1+z}\bar{t}_1 = \bar{\tau}_6 - \bar{\tau}_2 = \Delta\bar{\tau}_2 + \Delta\bar{\tau}_3 + \Delta\bar{\tau}_4 + \Delta\bar{\tau}_5 \quad , \quad (-1)^z\bar{t}_2 = \bar{\tau}_4 - \bar{\tau}_1 = \Delta\bar{\tau}_1 + \Delta\bar{\tau}_2 + \Delta\bar{\tau}_3 \,, \tag{C.7}$$

with $\bar{t}_1 - \bar{t}_2 + \bar{t}_3 = 0$. In turn, the deformations of figure 7e, depicted in figure 9c, are described by the $a_1 = z = 0$ option of the identification

$$\begin{aligned} & q(2) = 4\,, \qquad q(3) = 3\,, \qquad q(4) = 1\ , \\ & \alpha^{(p)} = (-1)^z \mathcal{C}_{32} = 1\ , \qquad -\alpha^{(1)} = (-1)^z \mathcal{C}_{p1} = (-1)^{a_1}\ ,\ p = 2, 3. \end{aligned} \tag{C.8}$$

Also, the $\omega_p^{(1)} = 3 - p$ option of the $v = 1$ eq. (B.4) implies that the measure of the $r = v = 1$ representation (7.7) is obtained through the reidentification: $\bar{\tau}_i \to \bar{\tau}_i$ for $i = 1, 2$, $\bar{\tau}_4 \to \bar{\tau}_3$, while $\bar{\tau}_6 \to \bar{\tau}_4$ so that $\bar{\tau}_3$ and $\bar{\tau}_5$ disappear.

Concerning the remaining contributions to the $r = v = 1$ superposition (7.6), they are associated with the implementation of the quantity $\tilde{\mathcal{V}}_{211}(\{a_i\}, \{\Delta\tau_{q(k)}\})$ parameterized by the three elementary graphs. Being generated through the vertical reattachments applied to the leftmost or/and rightmost end-point of figure 7e. These graphs are depicted in figures 7g, 7h and the one obtained from figure 7f via the reflection interchanging the horizontal sides of $C = \square$. It is formalized by the relations

$$x^1(s_1') = a_1 R \quad , \quad x^1(s_4') = a_4 R \quad , \quad x^1(s_1) = x^1(s_4) - R = 0\ . \tag{C.9}$$

that, together with the above $a_1 = a_4 = 0$ option, yields the four different implementations of $\tilde{\mathcal{V}}_{211}(\cdot)$ described by the corresponding $\{a_k\}-$implementations of eqs. (C.7) and (C.8), where one is to put $z = 0$.

Finally, to compute the entire $r = v = 1$ contribution to the decomposition (1.8), it remains to include the contribution of such $r = v = 1$ superposition (7.6) that is associated with the $S(4)-$multiplet of the $j = 2$ elementary graphs specified by such component of figure 7e when the upper horizontal line is on the right compared to the lower one. Alternatively, it can be reproduced from the $S(4)-$multiplet, specified by the so far considered component of figure 7e, via the reflection interchanging the two vertical sides of $C = \square$. Then, introducing the $\{\Delta\bar{\tau}_{q(k)}\}-$assignment according to the convention of subappendix A.3 and performing the auxiliary change of the variables $\bar{\tau}_k \to \bar{\tau}_{n+3-k}$ (with $k = 1, \ldots, n+2$), by the same token as previously we arrive at the $r = v = 1$ implementation of eq. (7.6) fixed by the $z = 1$ option of eqs. (C.7) and (C.8).

D. Eq. (7.7): $S(4)$- and reflection-symmetry

As for the $\mathcal{R}_a^{-1}-$deformations, the vertical nature of the reattachments evidently implies both $S(4)-$ and reflection-symmetries of the parameters which determine the factor (5.5) (representing the latter deformations in eq. (7.7)). More generally, provided the prescription of subappendix A.3, these two symmetries hold true for the algorithm (presented in appendix A) to introduce the entire set $\{\Delta\tau_{q(k)}\}$.

Concerning the $\bar{\mathcal{R}}_b^{-1}-$dressing, the situation is a little bit more tricky as it is clear from the results discussed in the latter appendix. The relevant parameters, defining[47] the implementation (6.2) of $\tilde{\mathcal{V}}_{2rv}(\{a_i\}, \{\Delta\tau_{q(k)}\})$, may be changed by a particular reattachment

[47] In particular, it applies to the parameters $\alpha^{(i)}$ and y_i^1 which determine the implementations of the replacements (5.6).

or reflection. In consequence, the symmetries of the $\bar{\mathcal{R}}_b^{-1}-$dressing become manifest only *after* the appropriate change of the variables.

To explain this point, we first accept the convention that, for a given $rv-$specification, the $z-$ and $\tilde{a}_1-$dependent equations below are implemented according to the assignment fixed in the previous appendix. Then, a direct inspection (presented below) verifies that the quantity $\tilde{\mathcal{V}}_{2rv}(\cdot)$ is $z-$*independent*. Furthermore, after the corresponding implementation of the $z-$independent change of the variables,

$$\bar{\zeta} \;\longrightarrow\; (-1)^{a_1+m_{rv}(\tilde{a}_1)}\bar{\zeta} \quad , \quad \bar{\eta} \;\longrightarrow\; \bar{\eta} \qquad , \qquad m_{rv}(\tilde{a}_1) = v(1-r)\tilde{a}_1 \, , \tag{D.1}$$

the residual $\{a_i\}-$dependence (in the $r = v-1 = 0$ case including, by definition given after eq. (4.4), the $\tilde{a}_1-$dependence) of $\tilde{\mathcal{V}}_{2rv}(\cdot)$ arises only due to the corresponding dependence of the parameters[48]

$$e_1 = (-1)^{a_1+m_{rv}(\tilde{a}_1)}a_1 \quad , \quad e_2 = a_2 \quad , \quad e_3 = -a_4 \, , \tag{D.2}$$

in terms of which one formulates the quantity

$$\mathcal{K}_{rv}((-1)^{a_1+m_{rv}(\tilde{a}_1)}\bar{\zeta}, \bar{\eta}, (-1)^{a_1+m_{rv}(\tilde{a}_1)}\alpha^{(1)}, \{a_l\}) = \mathcal{K}_{rv}(\bar{\zeta}, \bar{\eta}, \alpha^{(1)}, \{e_l\}) \tag{D.3}$$

where $\mathcal{K}_{rv}(\bar{\zeta}, \bar{\eta}, \alpha^{(1)}, \{a_l\}) = R^{v-2-r}\tilde{\mathcal{K}}_{rv}(R\bar{\zeta}, R\bar{\eta}, \{a_l\})$ is obtained, from the factor (6.3) (implicitly depending on $\alpha^{(1)}$ when $r = 1$) via the change of the variables (7.3), and we take into account the transformation law

$$\alpha^{(1)} \;\longrightarrow\; (-1)^{a_1+m_{rv}(\tilde{a}_1)}\alpha^{(1)} \quad , \quad \alpha^{(k)} \;\longrightarrow\; \alpha^{(k)} \, , \; \forall k \neq 1 \, , \tag{D.4}$$

that unifies the particular implementations of this transformation which, being given in the previous appendix, directly follows from definition of $\alpha^{(k)}$ defined by eqs. (3.3) and (3.7).

Justifying the representation (7.7) of $\mathcal{Z}_{rv}(\cdot)$, we obtain that both the building block (7.8) and the exponential $e^{i\left(\bar{\eta}\bar{t}_1 - \bar{\zeta}\bar{t}_2\right)\bar{A}\mathcal{C}_{21}/\bar{\theta}}$ are manifestly $\{e_i\}-$independent (with $\bar{t}_p^{(1)} \equiv \bar{t}_p$ in the $j = 2$ case at hand). In turn, the relation (D.3) implies eq. (1.12). In particular, in the $v - 1 = r = 0$ case, $e_1 \equiv e_1(a_1, \tilde{a}_1)$ depends on the two independent parameters $\tilde{a}_1$ and a_1 which implies that the four members of the $j - 2 = v - 1 = r = 0$ $S(4)-$multiplet are specified by the three values of e_1 so that $e_1 = 0$ appears twice (for $a_1 = 0$, $\tilde{a}_1 = 0, 1$). In turn, it explains the origin of the factor $2^{(v-r)(1-|e_1|)}$ in eq. (1.12) which, being equal to unity unless $v - 1 = r = 0$, assumes the value 2 only when $e_1 = 0$.

To prove the asserted properties of $\tilde{\mathcal{V}}_{2rv}(\cdot)$, let us first verify the independence of the latter exponential. For this purpose, one is to utilize that, unifying eqs. (C.1), (C.5), and (C.7), the $\{a_i\}-$dependence of the splitting (5.4) is defined by the replacement

$$t_1 \;\longrightarrow\; (-1)^{a_1+k_{rv}(z)+m_{rv}(\tilde{a}_1)}t_1 \quad , \quad t_j \;\longrightarrow\; (-1)^{k_{rv}(z)}t_j \quad , \quad j = 2, 3, 4 \, , \tag{D.5}$$

[48] Eq. (D.2) unifies the $r = v = 0$ and $r = v = 1$ cases (characterized by $w = 0$) together with the $r = v - 1 = 0$ case. In particular, $m_{rv}(\tilde{a}_1) = 0$ for all $0 \leq r \leq v \leq 1$, except for $v - 1 = r = 0$ when $m_{rv}(\tilde{a}_1) = w$.

where[49] $k_{rv}(z) = ((1-v)+vr)z$. Therefore, modulo the sign factors, the splitting is $S(4)-$ and reflection-invariant. (In particular, the factor $(-1)^{a_1+m_{rv}(\tilde{a}_1)}$ arises due to the prescription formulated in the footnote after eq. (6.3).) Also, the previous appendix establishes variables, provided the transformation properties $\mathcal{C}_{kl} \to (-1)^{H_{kl}}\mathcal{C}_{kl}$ of the entries of the intersection-matrix,

$$\mathcal{C}_{p1} \longrightarrow (-1)^{a_1+k_{rv}(z)+m_{rv}(\tilde{a}_1)}\mathcal{C}_{p1}\,,\ \forall p \neq 1 \quad , \quad \mathcal{C}_{il} \longrightarrow (-1)^{k_{rv}(z)}\mathcal{C}_{il}\,,\ \forall i,l \neq 1\,, \tag{D.6}$$

where we take into account the definition (2.11) of $\mathcal{C}_{il}$ combined with the pattern of the reattachments (formalized by eqs. (C.3), (4.4), and (C.9)). Altogether, one concludes that (in the quantity (6.2)) the $\{a_i\}-$dependence of the factor $e^{i\left(\bar{\eta}\bar{t}_1-\bar{\zeta}\bar{t}_2\right)\bar{A}\mathcal{C}_{21}/\bar{\theta}}$ indeed disappears when eq. (D.5) is combined with the change (D.1) of the variables, provided the transformation law (D.6).

Next, let us turn to the $\{a_i\}-$dependence of the dressing weight (considered prior to the change of the variables) composed of the $n-v$ factors (6.3) entering the definition (6.2) of $\tilde{\mathcal{V}}_{2rv}(\cdot)$. In view of eq. (D.6), this dependence is determined by the transformation law (D.4) together with the replacement

$$T_{\mathcal{C}_{ij}}(\bar{\eta},\bar{\zeta}) \longrightarrow T_{(-1)^{H_{ij}}\mathcal{C}_{ij}}(\bar{\eta},(-1)^{a_1+m_{rv}(\tilde{a}_1)}\bar{\zeta}) = \bar{\eta}-\bar{\zeta} \tag{D.7}$$

of the arguments of the combination (6.4). As a result, after the change (D.1) of the variables, the considered weight assumes the $\{a_i\}-$independent implementation (7.8).

Finally, to deduce the relation (D.3), all what one needs is to apply the replacements (D.6) and (D.4) together with the change (D.1) of the variables. In particular, in the $r = v = 1$ case (characterized by $m_{11}(\cdot) = 0$), by virtue of eq. (D.4), the transformation yields $e_4 = (-1)^{-2a_1}a_4/\alpha^{(1)} = -a_4$, where $\alpha^{(1)} = -1$ is associated with figures 7a and 7e. Summarizing, it verifies that the decomposition (1.8), indeed assumes the form fixed by eq. (7.7).

References

[1] M.R. Douglas and N.A. Nekrasov, *Noncommutative field theory*, *Rev. Mod. Phys.* **73** (2001) 977 [hep-th/0106048].

[2] R.J. Szabo, *Quantum field theory on noncommutative spaces*, *Phys. Rept.* **378** (2003) 207 [hep-th/0109162].

[3] A. Bassetto, G. Nardelli and A. Torrielli, *Perturbative Wilson loop in two-dimensional non-commutative Yang-Mills theory*, *Nucl. Phys.* **B 617** (2001) 308 [hep-th/0107147].

[4] L. Griguolo, D. Seminara and P. Valtancoli, *Towards the solution of noncommutative $YM(2)$: Morita equivalence and large-N-limit*, *JHEP* **12** (2001) 024 [hep-th/0110293].

[5] W. Bietenholz, F. Hofheinz and J. Nishimura, *The renormalizability of $2D$ Yang-Mills theory on a non-commutative geometry*, *JHEP* **09** (2002) 009 [hep-th/0203151].

[49] In order to unify the three different $rv-$assignments, the function $k_{rv}(z)$ is chosen so that $k_{rv}(z) = z$ when $v = r = 0$ and $v = r = 1$, while $k_{rv}(z) = 0$ when $1 - v = r = 0$.

[6] L.D. Paniak and R.J. Szabo, *Instanton expansion of noncommutative gauge theory in two dimensions*, *Commun. Math. Phys.* **243** (2003) 343 [hep-th/0203166].

[7] A. Bassetto, G. Nardelli and A. Torrielli, *Scaling properties of the perturbative Wilson loop in two-dimensional non-commutative Yang-Mills theory*, *Phys. Rev.* **D 66** (2002) 085012 [hep-th/0205210].

[8] A. Bassetto and F. Vian, *Wilson line correlators in two-dimensional noncommutative Yang-Mills theory*, *JHEP* **10** (2002) 004 [hep-th/0207222].

[9] L.D. Paniak and R.J. Szabo, *Open Wilson lines and group theory of noncommutative Yang-Mills theory in two dimensions*, *JHEP* **05** (2003) 029 [hep-th/0302162].

[10] A. Bassetto, G. De Pol and F. Vian, *Two-dimensional non-commutative Yang-Mills theory: coherent effects in open Wilson line correlators*, *JHEP* **06** (2003) 051 [hep-th/0306017].

[11] E. Langmann, R.J. Szabo and K. Zarembo, *Exact solution of quantum field theory on noncommutative phase spaces*, *JHEP* **01** (2004) 017 [hep-th/0308043].

[12] H. Dorn and A. Torrielli, *Loop equation in two-dimensional noncommutative Yang-Mills theory*, *JHEP* **01** (2004) 026 [hep-th/0312047].

[13] W. Bietenholz, F. Hofheinz and J. Nishimura, *On the relation between non-commutative field theories at $\theta = \infty$ and large-N matrix field theories*, *JHEP* **05** (2004) 047 [hep-th/0404179].

[14] J. Ambjørn, A. Dubin and Y. Makeenko, *Wilson loops in 2D noncommutative euclidean gauge theory. I: perturbative expansion*, *JHEP* **07** (2004) 044 [hep-th/0406187].

[15] A. Bassetto, G. De Pol, A. Torrielli and F. Vian, *On the invariance under area preserving diffeomorphisms of noncommutative Yang-Mills theory in two dimensions*, *JHEP* **05** (2005) 061 [hep-th/0503175].

[16] M. Cirafici, L. Griguolo, D. Seminara and R.J. Szabo, *Morita duality and noncommutative Wilson loops in two dimensions*, *JHEP* **10** (2005) 030 [hep-th/0506016].

[17] A. Bassetto, G. De Pol, A. Torrielli and F. Vian, *Area preserving diffeomorphisms and Yang-Mills theory in two noncommutative dimensions*, *Nucl. Phys.* **161** *(Proc. Suppl.)* (2006) 21 [hep-th/0509114].

[18] J. Volkholz, W. Bietenholz, J. Nishimura and Y. Susaki, *The scaling of QED in a non-commutative space-time*, PoS(LAT2005)264 [hep-lat/0509146].

[19] N. Caporaso and S. Pasquetti, *Gauge-invariant resummation formalism and unitarity in non-commutative QED*, *JHEP* **04** (2006) 016 [hep-th/0511127].

[20] W. Bietenholz et al., *Numerical results for* U(1) *gauge theory on 2D and 4D non-commutative spaces*, *Fortschr. Phys.* **53** (2005) 418 [hep-th/0501147].

[21] H. Aoki, J. Nishimura and Y. Susaki, *The index theorem in gauge theory on a discretized 2D non-commutative torus*, *JHEP* **02** (2007) 033 [hep-th/0602078].

[22] H. Aoki, J. Nishimura and Y. Susaki, *Suppression of topologically nontrivial sectors in gauge theory on 2D non-commutative geometry*, hep-th/0604093.

[23] M. Riccardi and R.J. Szabo, *Wilson loops and area-preserving diffeomorphisms in twisted noncommutative gauge theory*, *Phys. Rev.* **D 75** (2007) 125022 [hep-th/0701273].

[24] T. Filk, *Divergencies in a field theory on quantum space*, *Phys. Lett.* **B 376** (1996) 53.

JHEP10(2007)079

[25] J. Ambjørn, A. Dubin and Y. Makeenko, *Large area asymptote of Wilson loops in* $2D$ *noncommutative euclidean gauge theory*, in preparation.

[26] N. Ishibashi, S. Iso, H. Kawai and Y. Kitazawa, *Wilson loops in noncommutative Yang-Mills*, *Nucl. Phys.* **B 573** (2000) 573 [hep-th/9910004].

[27] K. Okuyama, *A path integral representation of the map between commutative and noncommutative gauge fields*, *JHEP* **03** (2000) 016 [hep-th/9910138].

[28] J. Ambjørn, Y.M. Makeenko, J. Nishimura and R.J. Szabo, *Finite-N matrix models of noncommutative gauge theory*, *JHEP* **11** (1999) 029 [hep-th/9911041].

[29] J. Ambjørn, Y.M. Makeenko, J. Nishimura and R.J. Szabo, *Nonperturbative dynamics of noncommutative gauge theory*, *Phys. Lett.* **B 480** (2000) 399 [hep-th/0002158].

[30] S.-J. Rey and R. von Unge, *S-duality, noncritical open string and noncommutative gauge theory*, *Phys. Lett.* **B 499** (2001) 215 [hep-th/0007089].

[31] S.R. Das and S.-J. Rey, *Open Wilson lines in noncommutative gauge theory and tomography of holographic dual supergravity*, *Nucl. Phys.* **B 590** (2000) 453 [hep-th/0008042].

[32] D.J. Gross, A. Hashimoto and N. Itzhaki, *Observables of non-commutative gauge theories*, *Adv. Theor. Math. Phys.* **4** (2000) 893 [hep-th/0008075].

[33] M. Abou-Zeid and H. Dorn, *Dynamics of Wilson observables in non-commutative gauge theory*, *Phys. Lett.* **B 504** (2001) 165 [hep-th/0009231].

[34] M. Rozali and M. Van Raamsdonk, *Gauge invariant correlators in non-commutative gauge theory*, *Nucl. Phys.* **B 608** (2001) 103 [hep-th/0012065].

[35] A. Dhar and Y. Kitazawa, *High energy behavior of Wilson lines*, *JHEP* **02** (2001) 004 [hep-th/0012170].

[36] V.A. Kazakov and I.K. Kostov, *Nonlinear strings in two-dimensional u(infinity) gauge theory*, *Nucl. Phys.* **B 176** (1980) 199;
N.E. Bralić, *Exact computation of loop averages in two-dimensional Yang-Mills theory*, *Phys. Rev.* **D 22** (1980) 3090;
V.A. Kazakov, *Wilson loop average for an arbitrary contour in two-dimensional* U(N) *gauge theory*, *Nucl. Phys.* **B 179** (1981) 283.

[37] S. Minwalla, M. Van Raamsdonk and N. Seiberg, *Noncommutative perturbative dynamics*, *JHEP* **02** (2000) 020 [hep-th/9912072].

[38] D.J. Gross, *Two-dimensional QCD as a string theory*, *Nucl. Phys.* **B 400** (1993) 161 [hep-th/9212149];
D.J. Gross and I.W. Taylor, *Two-dimensional QCD is a string theory*, *Nucl. Phys.* **B 400** (1993) 181 [hep-th/9301068]; *Twists and Wilson loops in the string theory of two-dimensional QCD*, *Nucl. Phys.* **B 403** (1993) 395 [hep-th/9303046].

JHEP10(2007)079